Universidade do Minho
Escola de Engenharia

Renato Ferreira Gonçalves

High performance magnetoelectric nanocomposite morphologies for advanced applications

março de 2017

High performance magnetoelectric nanocomposite morphologies for advanced applications
Renato Ferreira Gonçalves
UMinho | 2017

Universidade do Minho
Escola de Engenharia

Renato Ferreira Gonçalves

High performance magnetoelectric nanocomposite morphologies for advanced applications

Tese de Doutoramento
Engenharia de Materiais

Trabalho efetuado sob a orientação de
Professor Senentxu Lanceros-Mendez
Professora Gabriela Botelho

março de 2017

STATEMENT OF INTEGRITY

I hereby declare having conducted my thesis with integrity. I confirm that I have not used plagiarism or any form of falsification of results in the process of the thesis elaboration.

I further declare that I have fully acknowledged the Code of Ethical Conduct of the University of Minho.

University of Minho, Braga, 10 de março, 2017

Full name: Renato Ferreira Gonçalves

Signature: 

Acknowledgments

First of all, I would like to express my gratitude to every person who somehow contributed for the development of this thesis.

The Foundation for Science and Technology (FCT), grant SFRH/BD/88397/2012, for the financial support to this project.

All the work at the thesis would not have been accomplished without the accompaniment and effort of my supervisors. In this sense, I would like to acknowledge the Professor Senentxu Lanceros-Mendez and Professora Gabriela Botelho for the opportunity, effort, scientific knowledge, sympathy, support, understanding and good vibes given to me.

To Professor Xavier Moya I would like to express my gratitude for the kind reception during the stay at Cambridge University - Department of Materials Science & Metallurgy. To Professors Harvey Amorín and Jesus Ricote I would like to thank all the kindness and support given to me at Materials Science Institute of Madrid, Consejo Superior de Investigaciones Científicas (CSIC).

To the Electroactive Smart Materials group (ESMG), I would like to thank all the great team spirit, encouragement and friendship given by all group. A special thanks to the Doctors Vitor Sencadas, Pedro Martins and Carlos Costa due to all the help, effort and support given to me. To the Magnetoelectric Group for all the hours at the laboratory searching and pursuit what sometimes appeared impossible.

I would like to acknowledge all my friends and Claudia Teixeira for unconditional support, good moments and for being present at good and difficult times. At last and more important I would like to thank my sister and parents for the unconditional love, support and for always believing in my capability.

Thank you all for keeping up with me on this good and happy journey!!

“The important thing is not to stop questioning. Curiosity has its own reason for existing.”

Albert Einstein

Abstract

The magnetoelectric (ME) effect is characterized by the variation of the electrical polarization of a material with an applied magnetic field and the variation of the magnetization of a material with an applied electric field. Single-phase materials with intrinsic ME effect are not generally used for practical applications since they typically show weak ME coupling at room temperatures. Such problem has been overcome by the development of ME composites. Strong ME effect at room temperature has been obtained, particularly in those composed by a piezoelectric and a magnetostrictive phase. In such materials, a strain is induced on the magnetostrictive phase once a magnetic field is applied to the composite. This strain is transmitted to the piezoelectric constituent, which undergoes a change in the electrical polarization. In an analogous way, the reverse effect can occur.

The main objective of the thesis was the development of high performance polymer-based ME materials, that were characterized, optimized and their potential applications evaluated. Particulate ME composites were produced from materials with strong piezoelectric - poly(vinylidene fluoride) (P(VDF)) - and magnetostrictive - Cobalt iron oxide ($CoFe_2O_4$ - CFO) - responses in the form of film, membrane, fibers, and spheres. Related piezoelectric materials, such as the copolymer of P(VDF), poly(vinylidene fluoride-trifluoroethylene) (P(VDF-TrFE)), and magnetic nanoparticles, such as magnetite (Fe_3O_4), goethite (δ-FeO(OH)) and CoFeO(OH), were also used. All developed morphologies show the presence of the ME effect.

The studies on film morphology addressed the relevance of the magnetostrictive filler dispersion on ME composite response, suggesting that the use of surfactants or ultrasounds to improve the dispersion leads to the same ME response. The filler size and shape shows an important role on the ME measurements. Studies with Fe_3O_4 nanoparticle with sizes of 9, 30 and 50 nm within a P(VDF-TrFE) matrix show that the largest α_{31} = 0.97 $mV.cm^{-1}Oe^{-1}$ is obtained for the lowest nanoparticle size. The shape of the same filler was studied and the results shows that a rod shape, comparing with a spherical, nucleate the β-phase of P(VDF), due to the high interface interaction between the polymer and the filler. Anisotropic nanosheet fillers of δ-FeO(OH) and CoFeO(OH)

were synthetized and evaluated for the preparation of ME composites. Thus, δ-FeO(OH) /P(VDF-TrFE) composites lead to a maximum ME response of 0.4 $mV.cm^{-1}.Oe^{-1}$, which depends on filler content, alignment state as well as on both incident magnetic field direction and magnitude. A new ME effect is proposed based on the magnetic rotation of the nanosheets inside the piezoelectric polymer matrix. New CoFeO(OH) highly magnetostrictive (λ = 507 ppm) and anisotropic nanostructures were synthesized by a coprecipitation method using a modified gas-slugs microfluidic system. CoFeO(OH) /P(VDF-TrFE) composites reveal an interfacial ME coupling strongly dependent on the angle between H_{DC} and filler length direction, with a maximum α_{31} = 5.10 $mV.cm^{-1}.Oe^{-1}$.

ME membranes were also produced in CFO/P(VDF-TrFE) composites. The porous morphology and ME response were evaluated. The porous composite shows piezoelectricity with an effective piezoelectric coefficient (d_{33}) of -22 $pC.N^{-1}$, a maximum magnetization of 12 $emu.g^{-1}$ and a maximum ME coefficient of 9 $mV.cm^{-1}.Oe^{-1}$.

ME nanofibers and microspheres of CFO/P(VDF) produced by electrospinning and electrospray technique, respectively, were studied and evaluated. The average diameter of the nanofibers is ≈325 nm, independently of filler content, and the amount of crystalline polar β-phase was strongly enhanced when compared to pure P(VDF) polymer fibers, due to the introduction of the magnetostrictive fillers. The piezoelectric response of these electroactive nanofibers was modified by an applied magnetic field, thus evidencing the ME character of the CFO/P(VDF) composites. The CFO nanoparticles content in the ME microspheres (3-7 μm diameter) reached values up to 27 wt.%, despite their concentration in the starting solution reaching values up to 70 wt.%. No relevant effect on β-phase content (≈60 %), crystallinity (40 %) and onset degradation temperature (460-465 °C) of the polymer matrix was observed. The ME microspheres show a maximum $|d_{33}|$≈30 $pC.N^{-1}$, leading to a ME response of $\Delta|d_{33}|$≈5 $pC.N^{-1}$ obtained when a 220 mT DC magnetic field was applied. Its also shown that the interface between CFO and P(VDF) (0-55 %) has a strong influence on the ME response of the microspheres.

The simplicity and the scalability of the processing methods used in the present work as well as the excellent ME response in a large variety of composite morphologies suggest a large application potential of the developed polymer-based ME composites in areas such as sensors and actuators and tissue engineering, among others.

Resumo

O efeito magnetoelétrico (ME) é caraterizado pela variação da polarização elétrica do material na presença de um campo magnético e pela variação da magnetização do material quando um campo elétrico é aplicado. Os materiais de fase única com o efeito ME intrínseco não são usualmente utilizados em aplicações uma vez que possuem fraco acoplamento ME à temperatura ambiente. Este problema é então ultrapassado com o desenvolvimento de compósitos MEs. Nestes, verifica-se um forte efeito ME obtido à temperatura ambiente, particularmente quando constituídos por uma fase piezoelétrica e outra magnetostritiva. Nestes materiais, a deformação é induzida na fase magnetostritiva quando um campo magnético é aplicado ao compósito. Essa deformação é transmitida ao constituinte piezoelétrico que provoca uma mudança na polarização elétrica do material. O efeito contrário pode ser também observado.

O objetivo principal desta tese foi o desenvolvimento de materiais ME de base polimérica com alta performance, caracterização, otimização e avaliação para potencial aplicação. Foram produzidos compósitos ME particulados a partir de materiais com uma forte resposta piezoelétrica – poli(fluoreto de vinilideno) (P(VDF)) – e magnetostritiva – $CoFe_2O_4$ (CFO) – em forma de filme, membrana, fibras e esferas. O polímero piezoelétrico como o copolimero do P(VDF), poli(fluoreto de vinilideno-trifluoretileno) (P(VDF-TrFE)), e nanopartículas como Fe_3O_4, δ-FeO(OH) e CoFeO(OH) foram também estudados. Todos as morfologias desenvolvidas mostram a presença do efeito ME.

Os estudos realizados na morfologia de filmes mostram a relevância da dispersão do material de reforço nos compósitos ME. Estes sugerem que tanto o uso de surfactantes como do ultrassons, para dispersar, têm a mesma influência nas medidas ME dos compósitos. O tamanho e a forma do material de reforço têm um papel importante nas medidas ME. Estudos com nanopartículas de Fe_3O_4 com tamanhos de 9, 30 e 50 nm no interior da matriz polimérica de P(VDF-TrFE), mostram que o maior α_{31} (0.97 $mV.cm^{-1}Oe^{-1}$) é obtido para a nanopartícula de menor tamanho. A influência da forma do material de reforço foi estudada e os resultados mostram que a forma de bastão, comparada com a esférica, nucleiam a fase β do P(VDF) devido à alta interação na interface entre o polímero e o material de reforço. Foram também sintetizadas e avaliadas as nanofolhas anisotrópicas de δ-FeO(OH) e CoFeO(OH) para a preparação de

compósitos ME. Compósitos de δ-FeO(OH)/P(VDF-TrFE) com um máximo de ≈0.4 $mV.cm^{-1}.Oe^{-1}$, variam consoante a concentração do material de reforço, alinhamento e a direção e intensidade dos dois campos magnéticos incidentes. Um novo efeito ME é proposto baseado na rotação magnética das nanofolhas no interior da matriz polimérica. Sintetizou-se uma nova nanoestrutura anisotrópica de CoFeO(OH) com alta magnetostrição (λ = 507 ppm), pelo método de coprecipitação, com uma modificação no sistema microfluídico "gas-slugs". Nanocompósitos de CoFeO(OH) /P(VDF-TrFE) revelam um acoplamento ME fortemente dependente do ângulo entre o H_{DC} e o comprimento do CoFeO(OH), com um máximo α_{31} de 5.10 $mV.cm^{-1}.Oe^{-1}$.

Membranas ME foram igualmente produzidas em compósitos CFO/P(VDF-TrFE). A morfologia porosa e a resposta ME foram avaliadas. O compósito poroso apresenta uma resposta piezoelétrica com um coeficiente piezoelétrico efetivo (d_{33}) de -22 $pC.N^{-1}$, uma magnetização máxima de 12 $emu.g^{-1}$ e um coeficiente ME máximo de 9 $mV.cm^{-1}.Oe^{-1}$.

Foram estudadas e avaliadas nanofibras e microesferas de CFO/P(VDF) produzidas por electrospinning e electrospray, respetivamente. O diâmetro médio das nanofibras foi de ≈325 nm, independentemente da quantidade de material de reforço e da quantidade da fase polar β, que é fortemente aumentada com a introdução do material de reforço magnetoestritivo quando comparada com as fibras puras de P(VDF). A resposta piezoelétrica das nanofibras eletroativas é modificada com a aplicação de um campo magnético, evidenciando assim o carácter ME do compósito CFO/P(VDF). Microesferas ME (3-7 μm de diâmetro) com nanopartículas de CFO foram preparadas com concentrações que chegam aos 27 % em peso, apesar de a solução inicial ter 70 %. Não foram verificadas alterações de fase β (≈60 %), cristalinidade (40 %) e temperatura de degradação onset (460-465 °C) do polímero. As microesferas ME apresentam um máximo $|d_{33}|$≈30 $pC.N^{-1}$, com a uma resposta ME de $\Delta|d_{33}|$≈5 $pC.N^{-1}$ quando um campo magnético DC (220 mT) é aplicado. Verificou-se que a interface entre as nanopartículas de CFO e o P(VDF) (0-55 %) tem uma forte influência na resposta ME das microesferas.

A simplicidade e a escalabilidade dos métodos de processamento apresentados neste trabalho, assim como a distinta resposta ME numa ampla variedade de morfologias, sugerem uma potencial aplicabilidade dos compósitos ME de base polimérica, em áreas como sensores e atuadores, engenharia de tecidos, entre outros.

Table of content

List of figures

List of tables

List of symbols

A_α	Absorbance of P(VDF) α-phase
A_β	Absorbance of P(VDF) β-phase
d_{33}	Piezoelectric coefficient
E_Y	Young's modulus
F(β)	β-phase
H_{DC}	DC magnetic field
K_α	Absorption coefficients of P(VDF) α-phase
K_β	Absorption coefficients of P(VDF) β-phase
$M_{(H)}$	Magnetization
$m(x)_{IO}$	Mass of the composite that has not degraded at the temperature at which the mass loss rate of the pristine polymer is maximum
ME_E	Magnetoelectric effect when electrical field is applied
ME_H	Magnetoelectric effect when magnetic field is applied
m_I	Mass fraction of the polymer located at the interface
m_{IO}	Mass of the pristine polymer at the temperature at which the mass loss rate is maximum
M_S	Saturation magnetization
tan δ	Dielectric loss
wt.%	Weight percentage
X_c	Crystallinity content
α	Magnetoelectric coefficient
ΔE	Variation of the electric field
ΔH	Variation of magnetic field
ΔH_α	Melting enthalpies of P(VDF) α-phase
ΔH_β	Melting enthalpies of P(VDF) β-phase
ΔM	Variation of the magnetization
ΔP	Variation of the electric polarization
λ	Magnetostriction
ρ	Density
ε'	Dielectric constant

List of abbreviations

AC	Alternating current
CFO	$CoFe_2O_4$ – Cobalt iron oxide
DC	Direct current
DMF	N,N-dimethylformamide
DSC	Differential Scanning Calorimetry
EDS	Energy-dispersive detector
ES	Electrospinning
FTIR	Fourier transformed infrared spectroscopy
ME	Magnetoelectric
MF	Multiferroic
MNPs	Magnetic nanoparticles
NFO	Nickel ferrite
NIPS	Nonsolvent induced phase separation
NRs	Nanorods
P(VDF)	Poly(vinylidene fluoride)
P(VDF-HFP)	Poly(vinylidene fluoride-hexafluoropropylene)
P(VDF-TrFE)	Poly(vinylidene fluoride-trifluoroethylene)
PEI	Polyethyleneimine
PP	polypropylene
PPM	Polarized porous membrane
PTFE	Polytetrafluoroethylene
PU	Polyurethane
PVP	polyvinylpyrrolidone
PZT	Lead zirconate titanate
SQUID	Superconducting quantum interference device
TBA	Tert-butyl alcohol
TD	Terfenol-D
TEM	Transmission electron microscopy
TGA	Thermo Gravimetric Analysis
TIPS	Thermally induced phase separation

VIPS	Vapor induced phase separation
XRD	X-ray diffraction
ZFC-FC	Zero-field-cooled field-cooled

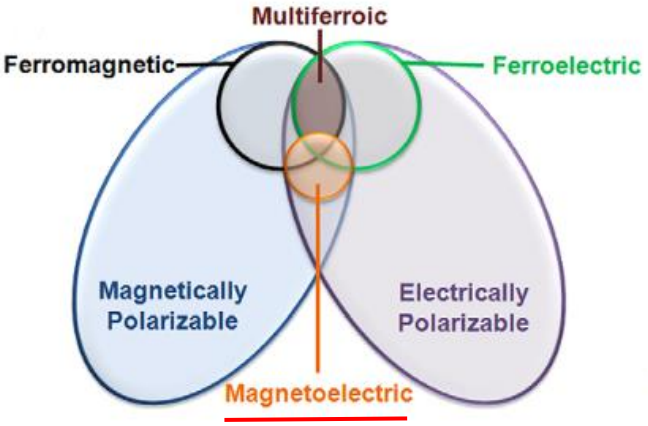

Chapter 1

Introduction

The main concepts related to magnetoelectric (ME) materials and structures are presented, together with the state of the art indicating the relevance and advantages of polymer-based ME novel morphologies. The selection of piezoelectric and magnetostrictive materials is also discussed in this chapter and novel application areas are introduced. Finally, the main objectives and the structure of the thesis are presented.

1.1. Introduction

The magnetoelectric (ME) effect, defined as the variation of the electric polarization (ΔP) in response to an applied magnetic field (ME_H) or the variation of the magnetization (ΔM) under an applied electrical field (ME_E), is a scientifically interesting and technological useful phenomenon, with an increasing range of applications in areas such as computer memories, smart sensors, actuators, high frequency microelectronic devices and biomedical materials [1-5]. It can be described as direct effect (1.1) or inverse effect (1.2):

$$\boldsymbol{ME_H} \rightarrow \Delta P = \alpha \Delta H \tag{1.1}$$

$$\boldsymbol{ME_E} \rightarrow \Delta M = \alpha \Delta E \tag{1.2}$$

where α represent the ME coefficient, ΔH the variation of magnetic field and ΔE the variation of the electric field [6].

A single phase multiferroic (MF) is a material that simultaneously possesses two or more 'ferroic' order parameters (ferroelectricity, ferromagnetism and ferroelasticity). A small subgroup of all magnetically and electrically polarizable materials are either ferromagnetic or ferroelectric. In this subgroup, fewer still simultaneously exhibit both order parameters (multiferroic). In some of these materials, electric fields cannot only reorient the polarization, but also control magnetization; similarly, a magnetic field can change electric polarization (figure 1.1) [7].

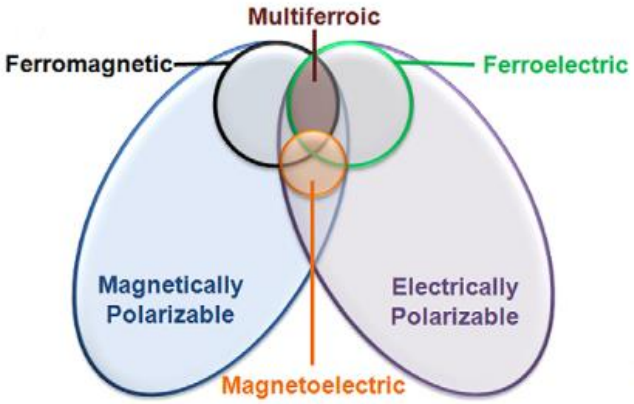

Figure 1.1. Relationship between multiferroic and magnetoelectric materials [7].

The ME effect can occur in single-phase materials or in composites. In the later, the ME effect can be achieved by the combination of magnetostrictive and piezoelectric responses [8]. Single-phase ME materials, typically show very low ME coupling at low temperatures, hindering their implementation into technological applications [2, 9, 10].

Nanocomposites are multi-phasic materials where the matrix material incorporates units with at least one dimension in the size range below 100 nm. They combine both the properties of the matrix material and the nanosized filler resulting in novel functional materials, which match the needs of a given application. In general, the range of host materials used in nanohybrids is vast, including organic polymers, silica or even liquid media. Host materials, that display tunable properties which respond to an external stimulus, are of particular interest. In this context, the use of magnetic fields as external stimulus has attracted increasing interest due to their several advantages [11] and applications in medical therapy and diagnosis, separations, catalysis and actuation (e.g., the relatively large penetration depth). To produce a response to an external magnetic field, the matrix host is loaded with magnetic nanoparticles, which can be well dispersed in different materials and show peculiar properties when exposed to static or alternating magnetic fields. The interaction between a magnetic field gradient and the magnetic moments of the particles induces magnetomechanical forces, which may be employed to change the shape of the host materials or to move the material [11].

ME composites emerged as an interesting possibility for device applications as in those composites, consisting on the combination of magnetostrictive and piezoelectric phases. The ME effect is the result of a product property, i.e., the mechanical deformation induced by a magnetic field, due to the magnetostriction of one of the phases, results in a dielectric polarization variation due to the piezoelectric effect of the other phase, allowing large ME effects at room temperature [3, 6, 9]. The large ME effect at room temperature is the main characteristic of these composites that leads to the use of these materials in new applications.

1.2. Types of magnetoelectric film composites

The ME composites can be classified in two ways: material based and structure based. The materials that can be used as ME composites have to possess piezoelectric

and magnetostrictive phases. These properties are mandatory for composites. ME composites structures have an important role due to the different interactions between the piezoelectric and magnetostrictive materials. The contact area and orientation between the materials are the key issue to reach a high ME effect.

1.2.1. Material based magnetoelectric composites

ME composite materials can be ceramic or polymer-based. Ceramic- and alloy-based ME materials exhibit ME coefficients three orders of magnitude higher than the polymer-based ME materials, but they are limited by reactions at the interface regions which lead to high dielectric losses, hindering sustainable device applications [2]. Alloys ME composites are commonly formed by magnetostrictive Terfenol-D (TD) or Metglas, due to their high ME effect. Figure 1.2 shows the different ME susceptibility of diverse materials [12].

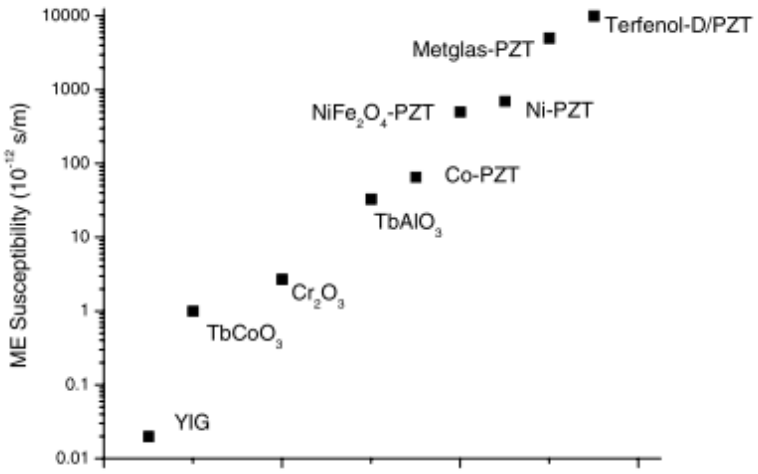

Figure 1.2. Maximum ME susceptibility of diverse materials [12].

TD together with some piezoelectric materials have been applied in different laminated ME composites. Yang Zhu and Jean W. Zu, for example, prepared one ME generator for energy harvesting application with laminated lead zirconate titanate (PZT) and TD. The 3 – layer laminated ME composite shows a TD/PZT/TD structure [13]. However, ME composites that have TD in their composition, cannot be used in low magnetic fields due their low permeability, high saturation field and mechanical hysteresis [14, 15]. One of the disadvantages is also the high cost. As an alternative,

others alloys, such as Metglas, have been explored and studied for ME composites. The Metglas is a commercial amorphous alloy formed by a fast solidification process, that is responsible for the magnetic properties of the composite. Comparing with the TD, Metglas shows a higher piezomagnetic coefficient (at low magnetic fields) and higher magnetic permeability. The high ME coefficients obtained with Metglas raised scientific interest, leading to the development of new materials. ME composites with Metglas are often used in magnetic sensors (AC and DC magnetic fields). J. Gao et al, confirmed that a high sensibility for DC field is verified with the application of different frequencies (1 kHz and 10 kHz), showing the potential application of those materials as location and navigation devices [16].

A rich combination of ferroelectric and magnetic oxides (mainly ferrites) can be used for the development of ceramic-based ME composites. Ceramic-based ME composites are synthetized at high temperatures. Theoretically, these composites show a high ME effect, however, this ME effect is lower than the predicted due the inherent preparation problems, such as thermal expansion and atomic interfacial interdiffusion reactions [14]. Giap V. Duong at al, claimed that laminate ME composites with 50 % of $CoFe_2O_4$ (CFO) and 50 % of barium titanate ($BaTiO_3$) shows a better magnetostrictive and piezoelectric coupling than the same materials in particulate structures [17]. Jing Ma et al., also indicated that laminate ME composites exhibit higher ME coefficients due to the reduction of dielectric losses, when compared with particulate ME composites. The author also affirmed that, in laminates, the ferrite layer is not sufficiently conducting itself. To solve that, the addition of metals as nickel and silver is necessary [14]. In these kind of composites, the major problem is related with the functional properties. These properties are complex and affected by various factors such as magnetic and ferroelectric properties of the materials, preparation method, structure, defects originated by the coupling of the materials and the interfaces between the layers, among others [18].

Polymer-based ME composites have attracted increasing interest from the industrial point of view as they can solve the abovementioned application problems. Further, in polymer-based ME composites strain coupling does not deteriorate with operation, as the magnetostrictive material is in direct contact with and completely

surrounded by the piezoelectric polymer matrix. They show simple and scalable production methods, a flexible structure, without large leakage currents, can be fabricated by conventional low-temperature polymer processing into a variety of forms (such as thin sheets or molded shapes) and can exhibit tailored mechanical properties, flexibility, lightweight, versatility, low cost and biocompatibility [2, 3].

Comparing the polymeric-based with the ceramic-based ME composites, less studies have been devoted to particulate structures in the last decade. Polymers such as poly(vinylidene fluoride) (P(VDF)) and polyurethane (PU) have been used due to their good piezoelectric and mechanical responses [19]. Several studies have been carried out with these polymers [20]: Rabah Belouadah et al., used P(VDF) and PU as polymers in ME composites together with magnetite (Fe_3O_4) and TD at different percentages (2 and 50 %) and different polymer combinations. The model and the experimental data shows that the mechanical losses in the magnetostrictive materials play a key role, since they induce magnetostrictive losses and ME losses on the ME response [21]. MF composites composed by P(VDF) and CFO, $Ni_{0.5}Zn_{0.5}Fe_2O_4$ and $NiFe_2O_4$ were studied. P(VDF) shows different phases, however the α phase processing was used in this study. It was verified that with the addition of the nanoparticles previously mentioned, the P(VDF) crystalizes in the β-phase. For a ME composite, it is essential that the P(VDF) possesses the β-phase due to its piezo-, pyro- and ferroelectric properties, contrary to the α-phase. The study also concluded that the concentration and the type of ferrite influences the interaction and the interface between the polymer and the ferrite. The β-phase percentage increases with the addition of the ferrites. For the CFO ferrite, the β-phase reaches around 90 %. It was also concluded that the addition of the ferrite induces a decrease of the thermal stability of the polymer [22]. The addition of different quantities of nanoparticles, such as CFO and $NiFe_2O_4$, in P(VDF) was investigated. It was verified that, for the P(VDF) composite to reach 90 % of the β-phase, it is necessary to add 5 weight percentage (wt.%) of CFO and 50 wt.% of $NiFe_2O_4$. These results Indicate that different nanoparticles promote the β-phase at different crystallization rates [23, 24]. The nanoparticles surface charge also has a strong influence on the nucleation of the P(VDF). The electrical interaction, due to the presence of negative nanoparticle surfaces, will interact with the polymeric CH_2 groups that have positive charge density. This

interaction induces the polymer chains to align on the surface of the nanoparticle resulting in the P(VDF) β-phase nucleation [25]. The main issue of the ME composites is to understand and control all the processing variables. Polymer-based ME composites are prepared to be applied in devices due the high ME effect above room temperature and the low cost [14].

1.2.2. Structures

The ME composites are divided in three main structures: particulate (0-3), laminate (2-2) and pillar (1-3). The particulate structure 0-3 means that magnetic particles (0) are embedded in a ferroelectric film matrix (3). The laminate structure 2-2 consists in horizontal structures with alternating ferroelectric (2) and magnetic (2) layers, or simply a ferroelectric (or magnetic) thin film grown on a magnetic (or ferroelectric) substrate. The pillar structure 1-3 are fabricated by vertical structure with one-phase nanopillars (1) embedded in a matrix of another phase (3) [26]. Figure 1.3 illustrates these main structures.

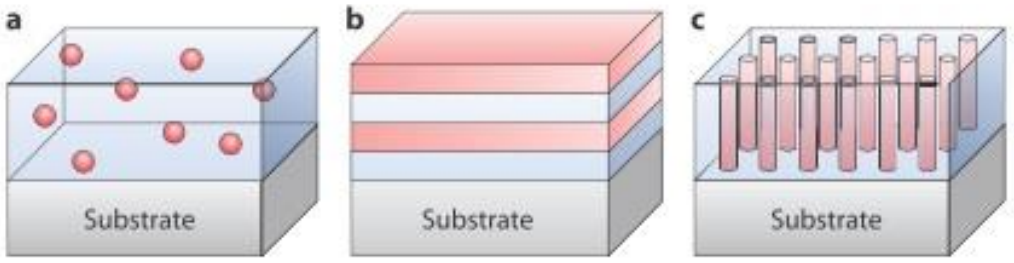

Figure 1.3. Main structures for ME composites; a) particulate, b) laminate and c) pillar [26].

In order to produce particulate ME composites, different materials such as ferrites, piezoelectric ceramics and polymers have been investigated. Similar materials have been investigated in laminate and pillar ME composites, but alloys as TD and Metglas are the most often used in these structures [27].

1.3. Possible novel morphologies of particulate magnetoelectric composites

In the last decade, many studies have been carried out in the area of ME and MF nanostructured materials in order to reach and fill future technological needs [28]. Across the interface of such nanostructured ME materials, the electric polarization can be coupled to the magnetization, based on the interplay among the lattice, charge, spin, and orbital degrees of freedom realized usually by the exchange of certain type(s) of potential energy, such as mechanical, electric, and magnetic. Such coupled polarization and magnetization can be exploited to significantly improve the performance of many devices such as memories, tunable radio-frequency/microwave devices, and magnetic sensors [29]. Such structures, can optimize the ME coupling once is possible to control of the size, interface and epitaxial strain of the nanostructures [30].

The low dimensionality opens a new road of opportunities and challenges [31]. At the nanoscale some materials present new interesting effects that should be studied and understood. The nanostructured materials present a great potential functionality due to the large surface to volume ratio when compared with the bulk. With the miniaturization of the ME materials size, applications on medical and biomedical engineering could be then explored. Different morphologies with different connectivities between the magnetostrictive and piezoelectric materials have been produced allowing to obtain innovative structures. In this subchapter, the low dimensionality of polymer-based ME composites will be presented, challenges that need to be addressed in pursuing practical applications of ME devices will be discussed and promising future for research and technology in this field evaluated.

1.3.1. Morphologies

Low dimensional materials can be prepared with different morphologies such as: film, membrane, fiber, sphere (Figure 1.4), and some unconventional structures.

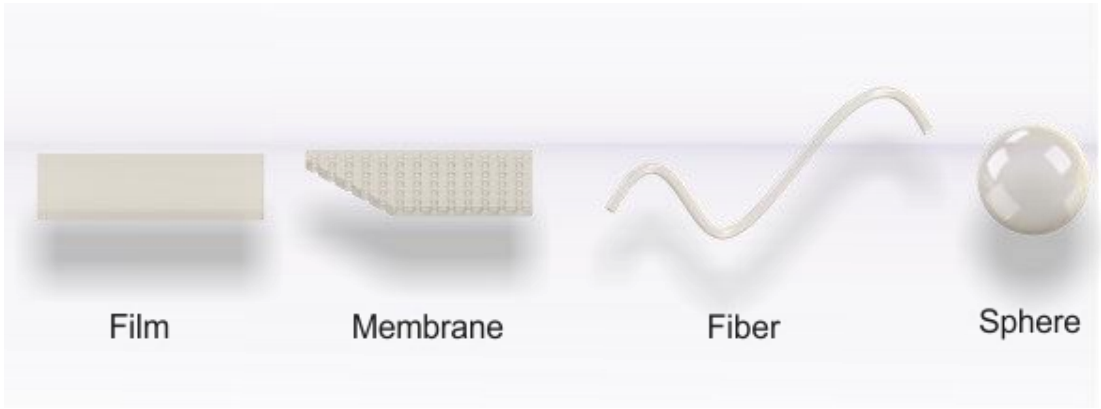

Figure 1.4. Different ME morphologies: film, membrane, fiber and sphere.

Polymer-based nanostructures can be produced by different techniques according to the possibilities and limitations of each of them. The physical-chemistry properties of the composite material are central factors that will determine which method will be adapted.

Phase inversion, also denoted as polymer precipitation or phase separation method, is a demixing process that transforms a polymer solution into solid form through the solvent removal. This method is the mostly used process to obtain polymer structures due to its versatility and scalability. During the process, the polymer solution is separated into a polymer rich and polymer lean phase. The membrane and film morphology can be reached by controlling parameters as solution thermodynamics and demixing kinetics. Different methods can be used to perform the phase inversion process: vapor induced phase separation (VIPS), nonsolvent induced phase separation (NIPS) and thermally induced phase separation (TIPS). TIPS is a method based on the fact that the solvent quality usually decreases with temperature decrease. After demixing is induced, the solvent is removed by extraction, evaporation or freeze drying. A membrane is formed from the homogeneous solution, where phase separation is induced by removal of the thermal energy. Research in this method was raised due to the simplicity of the method, high reproducibility, low defects produced in the polymer structure, high porosity and the ability to produce narrow pores with good distribution [32, 33].

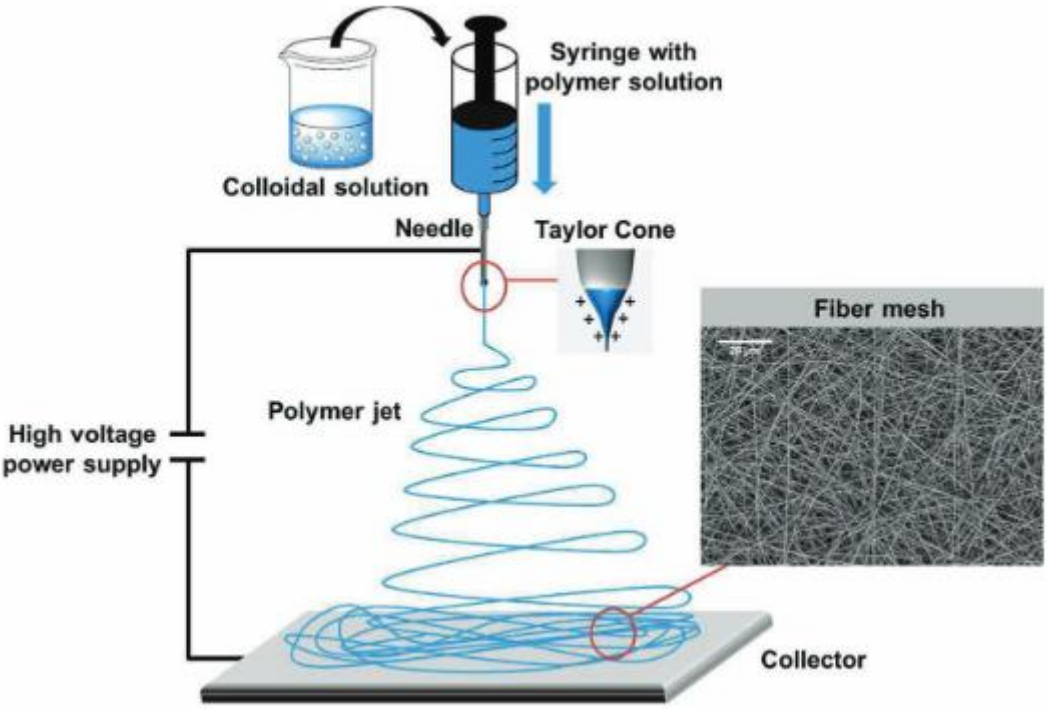

Figure 1.5. Electrospinning set-up [34].

Electrospinning (ES) (figure 1.5) and electrospray techniques allow the production of fibers or spheres, respectively. Beyond that, membranes can be easily fabricated by these techniques. Both techniques depend on the complex interplay of surfaces, shapes, rheology and electrical charge. Those phenomena interact in different ways to create charged jets of polymer solutions and molten polymers. The charges are usually carried by ions, which may move through the fluid faster, commensurate with, or slower than the shape of the fluid changes. For a fixed quantity of fluid, the Coulomb repulsion between the charged ions promote the creation of shapes such as a jet, while the surface tension of the fluid favors sphere-like shapes with smaller surface area per unit mass [35]. When the electrical potential of the surface is increased to a sufficiently high value, the electrical forces act in opposition to, and dominate the surface tension of the fluid. A charged jet of fluid is then ejected (Taylor cone). During the travel between the needle and the collector most of the solvent is evaporated, leaving the polymer dry and stack in the collector. A typical ES apparatus contains a high voltage supplier, pump system and the collector [35]. The electrospray, self-dispersing in space of the spheres due to the highly charged of droplets prevent spheres agglomeration and coagulation.

If the solution concentration is high, the jet from the Taylor cone is stabilized, and elongation takes place [36]. Among these techniques processing parameters, solution properties and ambient conditions are the key for controlling the polymer morphology. Molecular weight, concentration, viscosity, solvent volatility, applied voltage, flow rate, needle diameter, temperature and humidity are the main parameters that influence the obtained microstructure.

ME films are the most studied morphologies by the scientific community, due to their easy processability and fabrication. Since the thesis is focused on new ME morphologies, the state of art on ME membranes, nanofibers and microspheres will be highlighted.

1.3.1.1. Membranes

Membranes and porous films have a central role on different areas such as environment, energy, chemical and medical industries. Pores based morphologies are one of the most promising functional materials due to the outstanding properties and their applicability. As porosity provides a great tool to strain engineer nanostructured materials and the high surface area of porous materials opens new ways of opportunity for ME composites (pores can host several kinds of materials), ME porous materials can be an added-value on the ME area. Nevertheless, just few studies [37-40] are devoted to this subject.

Quickel et al. [37] created ME porous structures, based on nanoporous Bismuth ferrite ($BiFeO_3$) through epitaxy-free wet chemical methods. By comparing porous materials with non-porous films (produced using analogous methods), it was found that the porous ones reveal large changes in saturation magnetization – M_S - (0.04 to 0.84 μb) as a result of the application of an electric field.

A different study on nickel ferrite-PZT bulk composites performed by Petrov et al. [38] has shown by theoretical and experiment methods, that porosity has influence on ME response. The changes made on ferrite included Co substitution and Fe deficiency that resulted in a high resistivity for the ferrite and an improvement in the ME voltage. Results shown that the ME coefficient (at low frequency) decreases linearly (from 50 to 10 $V.cm^{-1}Oe^{-1}$) as the sample (60 vol.% ferrite and 40 vol.% PZT) porosity increases from

5 to 40 %. Experimental data were in good agreement with the theoretical calculations allowing to produce composites with the desired and tailored ME parameters.

Using the same piezoelectric material, PZT, but changing the magnetostrictive one, CFO, Xu et al. [39] reported a new method for fabrication of ME porous composites. In such work, a combination of methods as tert-butyl alcohol (TBA)-based freeze-casting technique, a chemical solution deposition method, and an impregnation process were used, leading to composites with different volume fractions of PZT, with stable and excellent dielectric behaviors, good ferroelectricity and ferromagneticity. The ME effect of the composite was dependent on the PZT and CFO content, namely the composite with PZT volume fraction of 0.5 and CFO mass fraction of 0.2 presented a maximum ME coefficient of 2.2 $mV.cm^{-1}.Oe^{-1}$. The study also indicated that the ME coefficient of the composites saturate at 3 kOe, suggesting that samples are applicable for relatively weak magnetic fields application devices. However, the samples present low ME coefficient. The lower response observed in such porous structures, compared with other ME composite structures, was due to the leakage current caused by the 3-1 structure. The authors stated that a better coupling between the CFO nanoparticles and PZT matrix is necessary, as well as the decrease of the influence of low resistance of ferromagnetic phase on depolarization of the piezoelectric phase. One of the most innovative approaches to solve this problem is the use of a polymer matrix. Following this line, novel multifunctional porous membranes suitable for advanced applications, ranging from biomedical to water treatment, have been established by the integration of magnetic CFO nanoparticles into P(VDF-TrFE), taking advantage of the interactions between the magnetostrictive filler and the piezoelectric polymer. The porous membranes showed a piezoelectric response with an effective piezoelectric coefficient (d_{33}) coefficient of ≈20 $pC.N^{-1}$, a maximum magnetization of ≈10 $emu.g^{-1}$ and a maximum ME coefficient of ≈10 $mV.cm^{-1}$ Oe^{-1}.

A high-voltage corona discharge system (point-to-plane type) has been constructed by Zhang et al. [40] aiming to improve the ME response of porous polypropylene (PP) and polyvinyl chloride (PVC) composites. As a result of the 30 kV voltage, electrical charges are induced due to the Parson Breakdown during the corona discharge procedure. Furthermore, the ME responses between discharged and non-

discharged porous PP and PVC have been measured and compared, being found that the porous PP shows better charge storage ability, leading to fine ME effect response. A higher ME current was generated in the corona discharged porous PP than in the discharged PVC, which was subjected to 0.1 mT AC magnetic field and 0 mT DC magnetic field, while frequency was in the range 0-4000 Hz. The main result of this work was the suggestion that charges injected in the polymers can induce ME responses on porous structures.

Despite these promising studies, that open the door for innovative applications ranging from biomedical or drug delivery systems to water treatment, more works are needed in this area in order to validate their added value.

1.3.1.2. Fibers

The diameter of electrospun polymer fibers span more than four orders of diameter, with nanofibers that have cross-sections containing fewer than 10 elongated polymer macromolecules at one end of the range, and conventional textile fibers at the other. Polymer nanofiber technology continues to evolve rapidly as the usefulness of nanofibers becomes apparent to a growing number of applications [35]. Additionally, fiber structure allows a good demonstration of intrinsic ME coupling without the substrate clamping such as the one obtained with thin films. Once the aspect ratio is enhanced, the mechanical displacement can be amplified by the piezoelectric or magnetostrictive effect leading to an improved ME coupling [41].

As in the case of ME membranes, the first reports on ME fibers were related with piezoelectric ceramic-based materials. Zhao et al. [42] produced Aurivillius $Bi_5Ti_3FeO_{15}$ (BTF) MF nanofibers using ES with further calcination. In order to provide fiber structure, the polymer polyvinylpyrrolidone (PVP) was used and removed by one calcination step, being obtained fibers with ≈ 400 nm. For ME measurements the MF sample was pressed in a pellet and fixed in a rigid sample shelf. The ME coefficient was then measured in a DC magnetic field of 300 Oe and frequencies ranging between 0.5 and 126 kHz. Such ME coefficient reached a maximum of 14 $mV.cm^{-1}.Oe^{-1}$ at 16 kHz. It was also observed that the phase remains almost unchanged as a function of frequency. From the technological applicability point of view, the phase information near the resonance frequency is very

important when ME elements are joined together. One of best innovations achieved in this field was the study of the weak coupling behavior of macro-ferroelectric and ME due the non-sintering and pressing process and the filled air. Nevertheless, the results offer new comprehensions into the design and application of promising lead-free MF materials for novel devices [42].

In the case of the fiber structure, no studies were reported on polymer-based ME. This shows that a new area of innovation and opportunities are open to be explored. The applicability of fiber morphology is vast and the expected ME effect is high due the large surface area of magnetostrictive nanoparticles within the piezoelectric polymer fibers.

1.3.1.3. Spheres

The sphere coating with a different material is a relatively new and a promising research area. The coating not only changes the surface of the sphere but also its interaction and properties, such as catalytic, optical, magnetic and others. In this way, new functionalities can be added to a material only depending on the coating used.

Ceramic-based ME spheres are the most studied, due to their high ME coefficient when compared with the polymeric analogues. Particles like BCZT/CFO, BTO/ nickel ferrite (NFO), CFO/$BaTiO_3$, SiO_2/Ni, SiO_2/Fe_3O_4, $BaTiO_3$/Fe_3O_4, PZT/Fe_3O_4 are some examples of ceramic-based ME spheres. The techniques used for the preparation of these particles vary between sol-gel, hydrothermal, solid state and others.

Kumar et al. [43] synthetized a core-shell BCZT/CFO composite by a co-sol-gel technique. In this study, it was demonstrated that the sample revealed a ferromagnetic ordering at room temperature with a M_S of 14.93 $emu.g^{-1}$ and a remnant magnetization of 6.93 $emu.g^{-1}$. The composite exhibited a ME coefficient of 12.15 $mV.cm^{-1}.Oe^{-1}$ and presented highly sensitivity to the AC magnetic field [43].

In another study, Srinivasan et al. [44] reported a magnetic-field-assisted-assembly of barium titanate (BTO)/NFO core-shell particles (BTO/NFO) produced by chemical self-assembly. Linear chains were formed at low particle concentrations, evolved into 2D and 3D arrays at high particle concentrations. One of the studies estimated the ME coefficient for a free- standing BTO-NFO core-shell particle and then

extended the model to include an array of linear chains of the particles. One of the main results obtained predict a reduction in ME coefficient for the array compared to isolated core-shell particle. This decrease is due to dipole-dipole interactions and demagnetization and depolarizing effects [44].

Chaudhuri et al. [45] synthetized CFO/$BaTiO_3$ nanocomposites by hydrothermal and sol-gel techniques. A comparative study with CFO, CFO-BTO mixture and CFO-BTO core-shell particle was performed. It was proved that the magnetostriction of the CFO-BTO core-shell nanocomposite is higher than the CFO-BTO mixture; there results that are theoretical reinforced once the microstrain of the core-shell nanoparticles was much higher (≈2 times) than the CFO-BTO mixture. As expected, the ME coefficient for the core-shell was higher (8.13 $mV.cm^{-1}.Oe^{-1}$) than the mixture (0.10 $mV.cm^{-1}.Oe^{-1}$). This substantial difference between the ME coefficient is also explained by the aggregation and irregular form which act as conductive channels to disable the poling effort [45].

The main problems in the production of the abovementioned ceramic spheres are the agglomeration, the high temperatures needed for the processing and the use of reagents with high toxicity and vapor pressure. This agglomeration can reach 20 µm of diameter in the worst cases. The use of a polymer as piezoelectric phase, instead of a ceramic, is a good way to avoid such issues. Since the polymer can be more easily functionalized, further properties may be added beyond the ME response.

1.3.2. Materials for polymer-based composites

According to chapter 1.1.1. different materials can be used to obtain a ME composite. The piezoelectric polymer P(VDF) is one of the most promising materials for the development of polymer-based ME composites. On the other hand, the CFO nanoparticles are one of the most studied particles in ME composites. These two materials were intensively studied due to their outstanding properties. As each material in particular presents high piezoelectric (P(VDF)) and magnetostrictive (CFO) responses, the combination of these two materials is expected to provide a suitable polymer-based ME composite.

1.3.2.1. Poly(vinylidene fluoride)

Poly(vinylidene fluoride) - P(VDF) - and its copolymers offer unique advantages over piezoelectric ceramic, like flexibility and therefore can be formed easily on to the curved surfaces. Further, P(VDF) is chemically inert, tough, creep resistant and has good stability when exposed to radiation [46]. In addition, it has a low density along with low dielectric permittivity resulting in a very high voltage coefficient [47]. P(VDF) is a semicrystalline polymer which exists in five different phases: α, β, γ, δ and ε. Those five distinct crystalline phases are related to different chain conformations designed as all trans (TTT) planar zigzag for the β-phase, trans-gauche–trans-gauche (TGTG') for the α and δ phases and T3GT3G' for γ and ε phases [46]. Of the five distinct phases that P(VDF) can assume, α and β phase are the most common (mechanical drawing contributes to the transition of the original α structure into β-phase – Figure 1.6); nevertheless β-phase and δ-phase are the only ones exhibiting a spontaneous polarization, thus piezoelectricity, being for such reason the most suitable for ME applications.

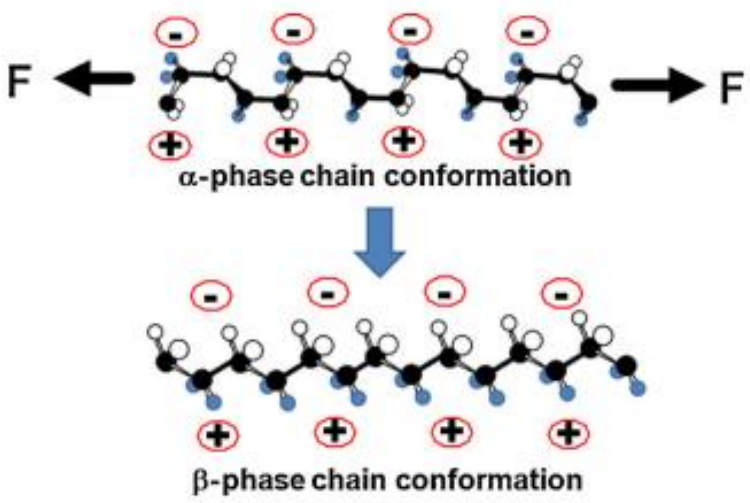

Figure 1.6. Conversion of α-crystalline conformation into β-crystalline conformation [48].

In order to improve the P(VDF) properties and to adapt it to the increasing technological demands, different copolymers of P(VDF) such as poly(vinylidene fluoride-trifluoroethylene) (P(VDF-TrFE)) and poly(vinylidene fluoride-hexafluoropropylene) (P(VDF-HFP)) have been developed. P(VDF-TrFE), is the most studied copolymer on ME laminates. Contrary to P(VDF), and in precise molar ratios, it always presents the

ferroelectric crystalline β-phase, since the addition of the third fluoride in the TrFE monomer unit, with a large steric hindrance, favours the all-trans conformation and therefore prompts the ferroelectric β-phase, independently of the used processing procedure: melting or solution casting. This situation occurs when the monomer vinylidene fluoride (VDF) content is between 50 and 80 %, corresponding also to the ferroelectric behavior of the copolymer [46]. Moreover, the high degree of crystallinity and the preferred orientation of the well grown crystallites explain the higher remnant polarization (~110 $mC.m^{-2}$) present when compared with P(VDF), which, in turn, gives rise to a larger electromechanical coupling factor, k, that is translated into a higher efficiency in mechanical to electrical transformation, that is very useful for use in ME composites.

1.3.2.2. Cobalt Ferrite

Ferrite properties can be improved with the incorporation of divalent metallic ions inside their structure. One element that promotes that improvement is cobalt. Cobalt increases the coercivity due the growth of magnetocrystalline anisotropy resultant from the coupling of the spins of the cobalt and iron ions. Cobalt ferrite has as molecular formula $CoFe_2O_4$, is a cubic ferrite with an inverse spinel structure. The anisotropy constant of CFO is higher than that of the common ferrites as magnetite and maghemite [49]. The M_S changes with size and temperature. The M_S values vary between 53 and 79.5 $emu.g^{-1}$. For CFO the maximum value was 79.5 $emu.g^{-1}$ for 48 nm nanoparticles close to the bulk value of 80.8 $emu.g^{-1}$ (figure 1.7) [50].

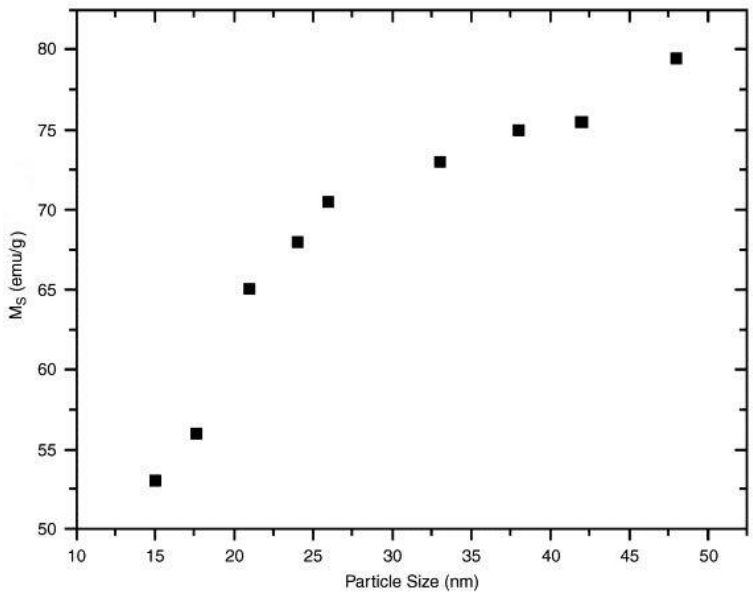

Figure 1.7. M_S as function of CFO nanoparticle size (nm) at maximum applied field of 15 kOe [50].

A decrease in nanoparticle size results in a decrease in coercivity and M_S, whereas the susceptibility and anisotropy constant have been reported to increase. Due to high value of magnetostriction, high Curie temperature (520 °C), low cost and easy processability, polycrystalline CFO can be a better alternative for magnetostrictive material against the currently used alloy-based magnetostrictive material [51]. Furthermore, CFO nanoparticles show large chemical stability, mechanical hardness, wear resistance and are easy to synthetize [52].

1.4. Novel application perspectives

ME materials in general, and polymer-based ME materials in particular, are interesting for an increasing number of technological applications, in particular, for sensors and actuators. Polymer-based ME nanocomposites have attracted considerable attention in recent years. Such structures are a current and future topic of interest for studies on the physics of ME interactions and application from micro to nanoelectronics. Innovative techniques, methodologies and procedures need to be developed and optimized for measurements of accurate direct and inverse ME effects in those structures [2]. Some of the applications of the ME polymer-based composites are: magnetic field sensors, transducers, filters, oscillators, phase shifters, memory devices and biomedical materials [5, 12, 14].

Novel areas of application are emerging in the biomedical field. In particular, controlling the functions of the biological macromolecules has become one of the areas with more study efforts in biology, biomedical and biotechnology. In order to stimulate cell functions, approaches as using heat generated by hysteresis losses of magnetic nanoparticles placed in high magnetic field frequency and mechanical agitation of the nanoparticles attached to the cells using external low magnetic field frequency.

A few existing articles [53-55] of ME nanoparticles do not report the ME coefficient. The extrapolation of the ME coefficient is based on laminated ME composites. At the present, the polymer-based ME composite with higher ME coefficient is a laminated ME obtained by Jin et al. with a cross-linked P(VDF-TrFE)/Metglas 2605 with 383 000 $mV.cm^{-1}.Oe^{-1}$ [53]. Nanoparticles under the 50 nm are estimated to possess a ME coefficient of 5 $V.cm^{-1}.Oe^{-1}$, and thus generate 25 mV under 100 Oe of magnetic field. This voltage is sufficient to trigger action potential in nerves and to control ion transport through ion channels. Further, it is expected that by increasing particle size to 1 µm, the voltage generated can be increased by 2 orders of magnitude [54]. The literature does not possess enough available data on polymer-based ME composites but these materials are intriguing for reasons such as: the capacity of no particles agglomeration in the absence of an external field (due to polymer functionalization) and the biocompatibility of some polymers that allows the bioapplications of these materials [54].

One example of applicability of a polymer-based ME composites was performed with P(VDF-TrFE) with TD in order to study the ME effect on tissue growth. Through an external AC magnetic field, the poled composite in contact with the cell culture provides the cell growth when compared with a non-poled composite. The study shows that the mechanical and electrical stimulus play an important key role on pre-osteoblast cell growth, which was enhanced up to 25 % [55].

With polymer-based ME spheres new applications areas can be opened and solve some of the drawbacks reported before. The use of these kind of materials as biomaterials for cell culture, drug delivery, and others, is expected to increase when suitable materials are available. The low size ME nanoparticles can be million times smaller than the size of a typical mammalian cell, allowing them to easily accommodate

inside the cells. They can also propagate through the bloodstream, reaching the vascular system. These properties will allow the possibility to direct the particles to a specific organ. The addition of magnetostrictive materials into the piezoelectric spheres allows the improvement of the applications of the polymer spheres as magnetic nanosensors and actuators, and also, to take advantage of the induced ME phenomenon. The main drawback of the polymer-based ME is the time-consuming ME voltage coefficient determination. It can be theoretically predicted using simulation software or using other equipment as Piezoelectric Force Microscopy (PFM) with an applied magnetic field. These kind of materials present a vast applicability in low size devices and biotechnology.

1.5. Objectives

In the present thesis, new polymer-based ME materials were produced, characterized, optimized and their potential for applications was evaluated. Particulate ME composites were produced from materials with strong piezoelectricity (P(VDF)) and magnetostrictive (CFO) responses in the form of film, membranes, fiberes, and spheres. The composites were evaluated and characterized at different levels: morphological, structural, thermal, dielectric, piezoelectric, magnetic and ME properties. The innovations rely on different levels, as new polymer composites and novel polymer preparation techniques were used and, therefore, highly performant ME materials were obtained with improved coupling and flexibility.

Thus, the main objectives of this work:

- To obtain, in the form of films, membranes, fibers and spheres, new and highly responsive and reliable ME composites based in electroactive polymers.
- To get a deeper knowledge of the origin of the ME effect, together with the structural, dielectric, magnetic, thermal and electromechanical properties of the composites and their relationship.
- To relate the processing conditions with the microscopic and macroscopic response of the materials.

- To determine and optimize the range of applicability of these materials both from the point of view of the physical and chemical parameters and also the areas of applications.

1.6. Structure of the thesis

The present thesis is divided in five chapters where three of them are based on published/submitted scientific papers. Beginning with an introduction of the basic concepts of the ME materials, the techniques used to obtain the different morphologies of the materials used. The piezoelectric and the magnetostrictive materials used, P(VDF) and CFO, respectively, were selected due their high quality characteristics, as well as, the high piezoelectricity and magnetostriction. After the introduction of the main concepts, a state of art for each polymer-based ME morphology (film/membrane/fiber/sphere) reported in the literature was presented.

Each chapter between two and four are dedicated to each of the morphologies of the ME composites previously indicated. In the case of film morphology, a study of the fillers dispersion, size, nucleation and anisotropy was evaluated in order to obtain knowledge on the origin of the ME effect. After this understanding, other morphologies were studied, such as membranes, fibers and spheres morphologies. Subsequently, a brief summary of each chapter is made.

Chapter 1 covers the main ME concepts, presenting the main structures of ME materials. The importance and advantages of polymer-based ME novel morphologies is presented with a state of art for each one of them. A deeper study of the state of the art is included in each of the corresponding subchapters. The piezoelectric and magnetostrictive materials selection is also discussed. A short subchapter with the main novel application areas and finally the objectives and the structure of the thesis are reported.

Chapter 2 presents some studies on magnetostrictive filler/piezoelectric polymer-based ME composite films: the effect of dispersion, size, nucleation and filler anisotropy are reported. Each one of these studies leads to a full understanding of the ME mechanism.

Chapter 3 is dedicated to CFO/P(VDF-TrFE) ME membranes. Their ME response, magnetic properties and morphology were evaluated and shows high interest, due to their permeability and high porosity, allowing biomedical applications.

Chapter 4 reports two different morphologies: fibers and spheres. Their production is based on electrospinning and electrospray techniques, for nanofibers and microspheres respectively. Similar parameters were used for each morphology. The ME effect was proved in such morphologies.

Finally, Chapter 5 presents the main conclusions of the thesis, as well as, the suggestions for future works.

1.7. References

1. Spaldin, N.A., *Magnetic Materials: Fundamentals and Applications*. 2 ed. 2010, Cambridge: Cambridge University Press.
2. Martins, P. and S. Lanceros-Méndez, *Polymer-Based Magnetoelectric Materials.* Advanced Functional Materials, 2013. **23**(27): p. 3371-3385.
3. Maceiras, A., et al., *High-temperature polymer based magnetoelectric nanocomposites.* European Polymer Journal, 2015. **64**: p. 224-228.
4. Eerenstein, W., N.D. Mathur, and J.F. Scott, *Multiferroic and magnetoelectric materials.* Nature, 2006. **442**(7104): p. 759-765.
5. Nan, C.-W., et al., *Multiferroic magnetoelectric composites: Historical perspective, status, and future directions.* Journal of Applied Physics, 2008. **103**(3): p. 031101.
6. Fiebig, M., *Revival of the magnetoelectric effect.* J. Phys. D, 2005. **38**: p. R123-R152.
7. Martin, L.W., et al., *Multiferroics and magnetoelectrics: thin films and nanostructures.* Journal of Physics: Condensed Matter, 2008. **20**(43): p. 434220.
8. Gupta, P. and P. Poddar, *Using Raman and dielectric spectroscopy to elucidate the spin phonon and magnetoelectric coupling in DyCrO3 nanoplatelets.* RSC Advances, 2015. **5**(14): p. 10094-10101.
9. Baji, A., et al., *Electrospun barium titanate/cobalt ferrite composite fibers with improved magnetoelectric performance.* RSC Advances, 2014. **4**(98): p. 55217-55223.
10. Chand Verma, K., S.K. Tripathi, and R.K. Kotnala, *Magneto-electric/dielectric and fluorescence effects in multiferroic xBaTiO3-(1 - x)ZnFe2O4 nanostructures.* RSC Advances, 2014. **4**(104): p. 60234-60242.
11. Behrens, S. and I. Appel, *Magnetic nanocomposites.* Current Opinion in Biotechnology, 2016. **39**: p. 89-96.
12. Lawes, G. and G. Srinivasan, *Introduction to magnetoelectric coupling and multiferroic films.* Journal of Physics D: Applied Physics, 2011. **44**(24): p. 243001.

13. Zhu, Y. and J.W. Zu, *A Magnetoelectric Generator for Energy Harvesting From the Vibration of Magnetic Levitation.* IEEE Transactions on Magnetics, 2012. **48**(11): p. 3344-3347.
14. Ma, J., et al., *Recent Progress in Multiferroic Magnetoelectric Composites: from Bulk to Thin Films.* Advanced Materials, 2011. **23**(9): p. 1062-1087.
15. Davino, D., A. Giustiniani, and C. Visone, *The piezo-magnetic parameters of Terfenol-D: An experimental viewpoint.* Physica B: Condensed Matter, 2012. **407**(9): p. 1427-1432.
16. Gao, J., et al., *Enhanced sensitivity to direct current magnetic field changes in Metglas/Pb(Mg1/3Nb2/3)O3–PbTiO3 laminates.* Journal of Applied Physics, 2011. **109**(7): p. 074507.
17. Giap, V., R. Groessinger, and R.S. Tuertelli. *Magnetoelectric Properties of CoFe2O4-BaTiO3 Core-Shell Structure Composites*. in *INTERMAG 2006 - IEEE International Magnetics Conference*. 2006.
18. Curecheriu, L.P., et al., *Functional properties of BaTiO3–Ni0.5Zn0.5Fe2O4 magnetoelectric ceramics prepared from powders with core-shell structure.* Journal of Applied Physics, 2010. **107**(10): p. 104106.
19. Kepler, R.G. and R.A. Anderson, *Piezoelectricity and pyroelectricity in polyvinylidene fluoride.* Journal of Applied Physics, 1978. **49**(8): p. 4490-4494.
20. Ashjari, M., et al., *Efficient Dispersion of Magnetite Nanoparticles in the Polyurethane Matrix Through Solution Mixing and Investigation of the Nanocomposite Properties.* Journal of Inorganic and Organometallic Polymers and Materials, 2010. **20**(2): p. 213-219.
21. Belouadah, R., et al., *Phase switching phenomenon in magnetoelectric laminate polymer composites: Experiments and modeling.* Physica B: Condensed Matter, 2011. **406**(14): p. 2821-2826.
22. Martins, P., et al., *Interface characterization and thermal degradation of ferrite/poly(vinylidene fluoride) multiferroic nanocomposites.* Journal of Materials Science, 2013. **48**(6): p. 2681-2689.
23. Martins, P., et al., *Correlation between Crystallization Kinetics and Electroactive Polymer Phase Nucleation in Ferrite/Poly(vinylidene fluoride) Magnetoelectric Nanocomposites.* The Journal of Physical Chemistry B, 2011. **116**(2): p. 794-801.

24. Martins, P., C. Costa, and S. Lanceros-Mendez, *Nucleation of electroactive β-phase poly(vinilidene fluoride) with CoFe2O4and NiFe2O4 nanofillers: a new method for the preparation of multiferroic nanocomposites.* Applied Physics A: Materials Science & Processing, 2011. **103**(1): p. 233-237.
25. Martins, P., et al., *Role of Nanoparticle Surface Charge on the Nucleation of the Electroactive β-Poly(vinylidene fluoride) Nanocomposites for Sensor and Actuator Applications.* The Journal of Physical Chemistry C, 2012. **116**(29): p. 15790-15794.
26. Wang, Y., et al., *Multiferroic magnetoelectric composite nanostructures.* NPG Asia Mater, 2010. **2**: p. 61-68.
27. Rabe, K.M., C.H. Ahn, and J.-M. Triscone. *Physics of ferroelectrics a modern perspective*. 2007; Available from: http://dx.doi.org/10.1007/978-3-540-34591-6.
28. Kumar, A., et al., *Magnetoelectric Characterization of Multiferroic Nanostructure Materials.* Ferroelectrics, 2014. **473**(1): p. 137-153.
29. Ortega, N., et al., *Multifunctional magnetoelectric materials for device applications.* Journal of Physics: Condensed Matter, 2015. **27**(50): p. 504002.
30. Xie, S., et al., *Multiferroic CoFe2O4-Pb(Zr0.52Ti0.48)O3 core-shell nanofibers and their magnetoelectric coupling.* Nanoscale, 2011. **3**(8): p. 3152-3158.
31. Chen, D., X. Gao, and J.-M. Liu, *Domain structures and magnetoelectric effects in multiferroic nanostructures.* MRS Communications, 2016: p. 1-11.
32. van de Witte, P., et al., *Phase separation processes in polymer solutions in relation to membrane formation.* Journal of Membrane Science, 1996. **117**(1): p. 1-31.
33. Kim, J.F., et al., *Thermally induced phase separation and electrospinning methods for emerging membrane applications: A review.* AIChE Journal, 2016. **62**(2): p. 461-490.
34. Crespy, D., K. Friedemann, and A.-M. Popa, *Colloid-Electrospinning: Fabrication of Multicompartment Nanofibers by the Electrospinning of Organic or/and Inorganic Dispersions and Emulsions.* Macromolecular Rapid Communications, 2012. **33**(23): p. 1978-1995.

35. Reneker, D.H. and A.L. Yarin, *Electrospinning jets and polymer nanofibers.* Polymer, 2008. **49**(10): p. 2387-2425.

36. Anu Bhushani, J. and C. Anandharamakrishnan, *Electrospinning and electrospraying techniques: Potential food based applications.* Trends in Food Science & Technology, 2014. **38**(1): p. 21-33.

37. Quickel, T.E., et al., *Mesoporous bismuth ferrite with amplified magnetoelectric coupling and electric field-induced ferrimagnetism.* Nat Commun, 2015. **6**.

38. Petrov, V.M., et al., *Magnetoelectric effects in porous ferromagnetic-piezoelectric bulk composites: Experiment and theory.* Physical Review B, 2007. **75**(17): p. 174422.

39. Xu, T., C.-A. Wang, and C. Wang, *Synthesis and magnetoelectric effect of composites with CoFe2O4-epoxy embedded in 3–1 type porous PZT ceramics.* Ceramics International, 2015. **41**(9, Part A): p. 11080-11085.

40. Zhang, J.W. and R. Belouadah, *Analysis on Magnetoelectric Responses of Porous Polypropylene and Polyvinyl Chloride after High-Voltage Corona Discharge.* Advanced Materials Research, 2014. **1042**: p. 70-74.

41. Xie, S.-H., Y.-Y. Liu, and J.-Y. Li, *Synthesis, microstructures, and magnetoelectric couplings of electrospun multiferroic nanofibers.* Frontiers of Physics, 2011. **7**(4): p. 399-407.

42. Zhao, Y., et al., *Ferroelectric, piezoelectric properties and magnetoelectric coupling behavior in aurivillius Bi5Ti3FeO15 multiferroic nanofibers by electrospinning.* Journal of Alloys and Compounds, 2016. **675**: p. 441-447.

43. Kumar, A.S., et al., *Multiferroic and magnetoelectric properties of Ba0.85Ca0.15Zr0.1Ti0.9O3–CoFe2O4 core–shell nanocomposite.* Journal of Magnetism and Magnetic Materials, 2016. **418**: p. 294-299.

44. Srinivasan, G., et al., *Magnetic field directed assembly of superstructures of ferrite-ferroelectric core-shell nanoparticles and studies on magneto-electric interactions.* Journal of Applied Physics, 2015. **117**(17): p. 17B904.

45. Chaudhuri, A. and K. Mandal, *Large magnetoelectric properties in CoFe2O4:BaTiO3 core–shell nanocomposites.* Journal of Magnetism and Magnetic Materials, 2015. **377**: p. 441-445.

46. Martins, P., A.C. Lopes, and S. Lanceros-Mendez, *Electroactive phases of poly(vinylidene fluoride): Determination, processing and applications.* Progress in Polymer Science, 2014. **39**(4): p. 683-706.

47. Jain, A., et al., *Dielectric and piezoelectric properties of PVDF/PZT composites: A review.* Polymer Engineering & Science, 2015. **55**(7): p. 1589-1616.

48. Im, J.Y., et al., *Effect of Elongational Deformation on the B-Phase Formation of Poly(vinylidene Fluoride)/Multiwalled Carbon Nanotube Composites and Their Piezoelectric Properties.* Macromolecular Symposia, 2014. **346**(1): p. 7-13.

49. Sanpo, N., *Solution Precursor Plasma Spray System*. SpringerBriefs in Materials, ed. SpringerLink. 2014, Cham: Springer International Publishing :.

50. Maaz, K., et al., *Synthesis and magnetic properties of cobalt ferrite (CoFe2O4) nanoparticles prepared by wet chemical route.* Journal of Magnetism and Magnetic Materials, 2007. **308**(2): p. 289-295.

51. Khaja Mohaideen, K. and P.A. Joy, *Influence of initial particle size on the magnetostriction of sintered cobalt ferrite derived from nanocrystalline powders.* Journal of Magnetism and Magnetic Materials, 2013. **346**: p. 96-102.

52. Wang, J., et al., *CoFe2O4@MnFe2O4/polypyrrole nanocomposites for in vitro photothermal/magnetothermal combined therapy.* RSC Advances, 2015. **5**(10): p. 7349-7355.

53. Jin, J., et al., *Multiferroic Polymer Composites with Greatly Enhanced Magnetoelectric Effect under a Low Magnetic Bias.* Advanced Materials, 2011. **23**(33): p. 3853-3858.

54. Armin, K., C. Gabriel, and M. Leszek, *Biomedical Applications of Multiferroic Nanoparticles*. 2012: INTECH Open Access Publisher.

55. Ribeiro, C., et al., *Proving the suitability of magnetoelectric stimuli for tissue engineering applications.* Colloids and Surfaces B: Biointerfaces, 2016. **140**: p. 430-436.

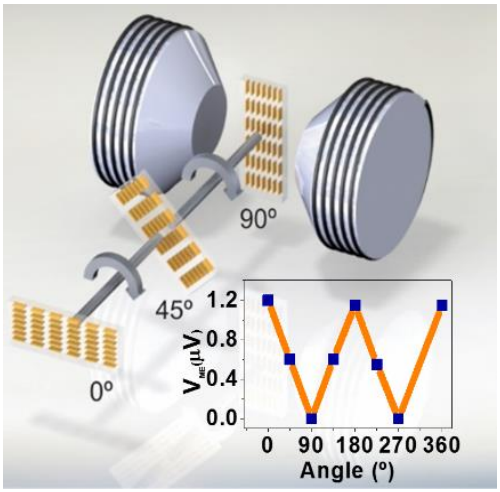

Chapter 2

Development of magnetoelectric films

Studies on magnetostrictive filler/piezoelectric polymer ME composite films are presented and discussed as a function of filler dispersion, size, and anisotropy.

This chapter is based on the following articles:

- P. Martins, R. Gonçalves, S. Lanceros-Mendez, A. Lasheras, J. Gutiérrez, J.M. Barandiarán, *Effect of filler dispersion and dispersion method on the piezoelectric and magnetoelectric response of $CoFe_2O_4$/P(VDF-TrFE) nanocomposites*. Applied Surface Science, 2014. 313: p. 215-219.
- R. Gonçalves, A. Larrea, M. S. Sebastian, V. Sebastian, P. Martins and S. Lanceros-Mendez, *Synthesis and size dependent magnetostrictive response of ferrite nanoparticles and their application on magnetoelectric polymer-based multiferroic sensors*, accepted at Journal of Materials Chemistry C, 2016.
- M. S. Sebastian, A. Larrea, R. Gonçalves, T. Alejo, J. L. Vilas, V. Sebastian, P. Martins and S. Lanceros-Mendez, *Understanding Nucleation Of The Electroactive β-Phase Of poly(vinylidene fluoride) by nanostructures*, submitted, 2016.
- P. Martins, A. Larrea, R. Gonçalves, G. Botelho, E. V. Ramana, S. K.Mendiratta, V. Sebastian and S. Lanceros-Mendez, *Novel Anisotropic Magnetoelectric Effect on δ-FeO(OH)/P(VDF-TrFE) Multiferroic Composites*. ACS Applied Materials & Interfaces, 2015. 7(21): p. 11224-11229.
- R. Gonçalves, A. Larrea, T. Zheng, M. J. Higgins, V. Sebastian, S. Lanceros-Mendez, P. Martins, *Synthesis of highly magnetostrictive nanostructures and their application in a polymer-based magnetoelectric sensing device.* European Polymer Journal, 2016. 84: p. 685-692.

2.1. Introduction

Magnetoelectric (ME) materials have attracted large interest due to the cross-correlation between the magnetic and electrical orders of matter [1, 2], allowing the development of technological applications such as multifunctional devices, transducers, actuators and sensors, among others [3, 4]. Thus, one of the major challenges in the ME research area is to obtain composites with a feasible production method, a flexible structure and without large leakage currents. A possible way to correspond to this quest is to use particulate piezoelectric polymer/magnetostrictive nanoparticle nanocomposites [5, 6].

As one of the most relevant piezoelectric polymer, P(VDF-TrFE) in the poled ferroelectric phase exhibits one of the highest piezoelectric responses among polymer materials over a wide range of temperatures depending on its composition [7]. Polymeric composites may be formed directly from a melt or cast solution, the piezoelectric properties are also strongly dependent on the poling process [6].

Ferrites are an important class of magnetic materials that have gained increasing attention of the scientific community due to their wide range of applications in sensors, communication, electronics, magnetic recording, microwave absorption-based devices, electrical and automobile industries as well as their increasing use in biotechnology and biomedical applications [8-11]. Particularly, nanosized ferrites have attracted large consideration due to their interesting surface reactivity, electrical and magnetic properties, which are largely influenced by the nanostructured phase [8, 12, 13]. Additionally, ferrites are used as magnetostrictive phase in ME composites since they show the largest magnetostrictive coefficients together with high Curie temperatures among different magnetic oxide materials [14-16].

It is theoretically predicted and experimentally proven that high ME response appears in the 0–3 particulate composites with high magnetic phase concentration [3, 17]. However, the percolation of the randomly dispersed ferrite phase with low resistivity makes the electric poling of the composites difficult and the ME properties are reduced because of leakage. In this way, the dispersion of the low-resistance ferrite

nanoparticles in the piezoelectric matrix has to be optimized in order to obtain a significant ME effect [18].

For polymer-based ME materials, the polymer has to be in the electroactive phase, which for P(VDF) is the β-phase. The β-phase of P(VDF) can be produced by conventional polymer processing technologies. Although the nucleation mechanism is not unambiguously stablished, most authors point to the fact that the essential factor for the nucleation of the β-phase on P(VDF) nanocomposites is the static electric interaction between the fillers with a negative surface potential and the CH_2 groups having a positive charge density [19-24]. The main evidence of such mechanism comes from of the inclusion of ferrite nanoparticles, that when were modified with positively charged molecules, lose the ability to induce the formation of the polar phase of P(VDF) [19]. Nevertheless, and surprisingly, the induced formation of dominating β-phase in P(VDF) is sometimes attributed to the interaction between the positively charged surfaces of fillers and the CF_2 dipoles in P(VDF) chains [21, 25, 26].

As rare earth elements are expensive, cytotoxic, show nonlinear response at high fields (2 kOe), and are hysteretic at lower fields, the applications of large magnetostrictive materials such as TD has been restricted [27-29]. Thus there is an urgent need for suitable magnetostrictive nanomaterials which are efficient in their performance, cheaper, non-cytotoxic and with anhysteretic magnetic response, having Fe_3O_4 emerged as one of the most suitable choice [27, 30]. Allied to their biocompatibility, Fe_3O_4 nanoparticles are characterized by excellent electrical, optical and magnetic properties, are easy to prepare, showing a very active surface for adsorptions or immobilization of metals and ligands, which can be separated by magnetic decantation after the reaction [31-33]. On the other hand, the magnetostrictive response of Fe_3O_4 needs to be optimized for values of the same order of magnitude as $CoFe_2O_4$ in order to be competitive for application in magnetostrictive and ME devices [3, 30, 34]. It is noteworthy that despite the unique properties of Fe_3O_4 nanomaterials, and knowing that in nanoscale regime, the particles are usually single domain and their magnetostrictive properties are mainly governed by particle size, size distribution, shape and surface effects [27, 32]. There are no studies reporting on the effect of particle size on the magnetostrictive properties of Fe_3O_4 nanoparticles. This

fact is intimately related to the difficulty of measuring the magnetostrictive properties of Fe_3O_4 nanoparticles on the nanoscale and in their dispersed state [35].

ME coefficients, ranging from 1 to 400 000 $mV.cm^{-1}.Oe^{-1}$, obtained on polymer-based ME nanocomposites allow the fabrication of magnetic sensors with enormous potential for other byproducts related to them: electric current sensors, speed sensors, angular sensors, electronic steering, throttle control, battery management, vehicle transmission, digital compasses and GPS devices [3, 7]. Additionally, it has been reported that the ME magnetic sensors exhibit larger application prospects in geomagnetic field measurements when compared to traditional magnetic sensors such as magnetoresistant sensors or fluxgate sensors [36-38]. In general, high ME anisotropy is critically necessary for ME single-axis sensors, which are capable of probing the magnitude as well as the direction of the magnetic field vector [37].

This new concept of anisotropic ME magnetic sensors, despite having high interest in applications such as navigation, motion tracking, sports and healthcare, remains vaguely explored, [37, 39-41], with it being not possible to find in literature reports on anisotropic magnetic sensors built on ME polymer-based materials.

In order to enhance the magnetostrictive/ME performance, current research is focused on obtaining a nanostructured material, which exhibits higher magnetostrictive strains [42]. Such enhancement on the nanostructure's magnetostriction can further open new application directions such as in ME stimuli for tissue engineering applications [43, 44].

ME film morphology is the most studied morphology due to its easy processability and fabrication. Beyond that, in film morphology it is easier to measure and characterize the composite when compared with other morphologies such as fibers and spheres. In that order, macro- and microeffects of the filler should be studied in such morphology. To understand the effects of the magnetostrictive CFO filler in the ME P(VDF) based composite, the effect of filler dispersion, size and anisotropy was evaluated. First of all, the dispersion method used to prepare the ME composites was investigated. In this study, the ultrasound and the surfactation methods were compared in order to study the more efficient dispersion method. With the intention of understand

how filler size influences the ME effect, three different Fe_3O_4 nanoparticles (9, 30 and 50 nm) were synthetized and used to prepare P(VDF-TrFE) based composites. In this study, P(VDF-TrFE) was used instead the P(VDF) due to necessity of guarantee the total β-phase nucleation and just to focus on the influence of the nanoparticle size. Beyond that, the nucleation effect of the filler on the piezoelectric polymer phase of P(VDF) was also studied. The same three nanoparticles and a Fe_3O_4 nanorods (NRs) were used for the preparation of P(VDF) composites. In this study not only the size but also the filler morphology (spherical and rod) were studied. Last but not least, the effect of the anisotropy of the filler in the ME response was evaluated. The study consisted in measuring the ME response of P(VDF-TrFE) composites with FeO(OH) and CoFeO(OH) nanosheets. According to this, the chapter will be divided with a subchapter in which materials and methods are indicated, followed by subchapters in which dispersion, size and nucleation and anisotropy studies are described.

2.2. Materials and methods

In this subchapter each materials and experimental methods will be presented according to the corresponding study: dispersion, size and nucleation and anisotropy.

2.2.1. Materials

Evaluation of the filler dispersion on the piezoelectric and magnetoelectric response

All the chemicals and nanoparticles were used as received from the suppliers: $CoFe_2O_4$ nanoparticles were purchased from Nanoamor with dimensions between 35-55 nm. N,N-dimethylformamide (DMF, pure grade) was supplied by Fluka, P(VDF-TrFE) was supplied by Solvay Solexis and citric acid was supplied by Sigma-Aldrich. All the chemicals were used as received without further purification.

Evaluation of the filler size on the magnetostriction, polymer phase nucleation and magnetoelectric response of polymer composites

Potassium nitrate (KNO_3, ≥ 99 %) were purchased from Fluka and ethanol absolute from Panreac. Iron (III) acetylacetonate ([Fe(acac)3], ≥ 97 %), ferrous sulfate heptahydrate ($FeSO_4.7H_2O$, ≥ 99 %), iron(III) chloride hexahydrate ($FeCl_3$ $6H_2O$ 99 %),

sodium citrate tribasic dihydrate (99 %), triethylene glycol (TREG, 99 %), sodium hydroxide (NaOH, ≥ 98%), L-lysine crystallized (≥ 98 %), hydrogen peroxide (H_2O_2, 30 %), oleylamine (70 %) branched polyethyleneimine (PEI, Mw 25,000), sulfuric acid (H_2SO_4, 95-98 %), hexane (99.5 %), toluene (99.5 %), N,N-dimethylformamide (DMF, 99.8 %) and ethyl Acetate (HPLC grade) were purchased from Sigma-Aldrich. P(VDF-TrFE) and P(VDF) powder was purchased from Solvay. All the chemicals were used as received without further purification.

Development of anisotropic magnetoelectric polymer composites

P(VDF-TrFE) was obtained from Solvay and sulfuric acid (H_2SO_4 with purity ranging 95-98 %), potassium nitrate (KNO_3 with purity higher than 99 %), cobalt (II) chloride hexahydrate ($CoCl_2.6H_2O$), ferrous sulfate heptahydrated ($FeSO_4.7H_2O$ with purity higher than 99 %), sodium hydroxide (NaOH with purity higher than 98 %) and L-lysine crystallized ($C_6H_{14}N_2O_2$ with purity higher than 98 %) were obtained from Sigma Aldrich Corporation. N,N-Dimethylformamide (DMF, with pure grade) was supplied by Fluka. All chemicals were used as received without any extra treatments.

2.2.2. Methods

The methods used for each study were divided in processing and characterization methods. Each method was divided in the corresponding study.

2.2.2.1. Processing methods

Evaluation of the filler dispersion on the piezoelectric and magnetoelectric response

Composites were prepared by two alternative routes leading to very different dispersion levels of the ferrite nanoparticles in the polymer matrix:

a) The first method consists of using nanoparticles surfactated with citric acid and later added to DMF [45].

b) The second method consists of adding the desired amount of nanoparticles to the DMF solvent and then place the solution in an ultrasound bath during 8 hours.

Further, the obtained mixtures were placed in a Teflon mechanical stirrer with ultrasound bath for complete dissolution of the polymer during 2h. This method is an improvement of the one reported in [46] since the ultrasound absence during the mechanical agitation meant that non surfactated ferrite nanoparticles lead to agglomerates of ≈30 μm [46].

Flexible films were obtained by spreading the solution on a clean glass substrate. Solvent evaporation was first performed inside an oven at a controlled temperature of 210 °C for 10 min. Crystallization was achieved by cooling down the samples to room temperature. The ferrite nanoparticle content varied from 3 to 80 in wt.%, 0.01 to 0.59 in volume fraction, and the thickness of samples was controlled to be approximately 50 μm.

Evaluation of the filler size on the magnetostriction, polymer phase nucleation and magnetoelectric response of polymer composites

a) Synthesis of 9 nm Fe_3O_4 magnetic nanoparticles.

Water-soluble superparamagnetic iron oxide nanoparticles were synthesized by a polyol-mediated method scaling up the synthesis procedure previously described [47, 48]. 4.5 g of $[Fe(acac)_3]$ were vigorously mixed with 90 mL of TREG in a three-neck round-bottom flask equipped with a mechanical stirrer and degassed with Ar. The resulting mixture was heated at 15 °C.min^{-1} to 180 °C and held at this temperature for 30 min in order to achieve the decomposition of the $[Fe(acac)_3]$ precursor. After that, the mixture was heated again at 5 °C.min^{-1} to reach 280 °C and kept at this temperature for 30 min under reflux. The resulting dark solution was cooled to room temperature. After the reaction, the nanoparticles were washed 3 times with a mixture of ethyl acetate and ethanol (9:1) and separated using a magnet. The precipitated nanoparticles after washing cycle were redispersed in polar solvents such as water.

b) Synthesis of 30 nm and 50 nm Fe_3O_4 magnetic nanoparticles

Fe_3O_4 magnetic nanoparticles (MNPs) with an average particle size of 30 nm and 50 nm were synthesized by an oxidative hydrolysis method, following a synthesis pathway described in previous works [49]. Briefly, 30 nm Fe_3O_4 MNPs were produced in a two-stage continuous flow polytetrafluoroethylene (PTFE)-microreactor. The reagent

solutions were prepared as follows. In a 500 mL vessel (solution 1), a 444 mL solution of 180 mM KNO_3, 162 mM NaOH and 1.85 mM L-lysine was prepared using deionized water. In other 500 mL vessel (solution 2), a 444 mL solution of 13 mM ferrous sulfate heptahydrate and 3.38 mM sulfuric acid was prepared using deionized water. Argon gas was bubbled in each solution for 15 minutes. After deoxygenation, solution 1 and solution 2 were filled in a 60 mL plastic Becton Dickinson syringes. In the first stage, solutions were pumped at a flow rate of 1.87 $mL.min^{-1}$ with residence time of 1 min and were mixed in a PEEK polymer Y junction located in an ultrasound bath. Sonication was carried out by maintaining the temperature in between 25 and 30 °C, using a cooling bath. In a second stage a H_2 gas stream was introduced in a PEEK Y junction to form a H_2-liquid segmented flow and heated at 100 °C. The synthesized nanoparticles were centrifuged at 10 000 rpm for 10 minutes, then washed twice with distilled water and finally resuspended in distilled water.

50 nm Fe_3O_4 MNPs were produced in a mechanical mixed batch reactor. A 40 mL aqueous solution 0.1 mM KNO_3, 90 mM NaOH and 1 mM of L-Lysine were bubbled with Argon during 15 minutes. Subsequently, 4.4 mL of an aqueous solution containing 65 mM $FeSO_4.7H_2O$ and of 17 mM H_2SO_4 was added dropwise under constant stirring. When the addition was completed, argon was allowed to pass for another 15 minutes and the suspension was heated at 90 °C for 1 hour in an oil bath. The synthesized nanoparticles were centrifuged at 10 000 rpm for 10 minutes, then washed twice with distilled water and finally re-suspended in distilled water.

c) Synthesis of Fe_3O_4 nanorods

Fe_3O_4 nanorods (NRs) were obtained by reduction of as prepared feroxyhyte (β-FeO(OH)) NRs, according to the method reported by Aslam et al. [50] in a typical synthesis, β-FeO(OH) NRs were prepared by mixing 5.6 g of $FeCl_2$ $6H_2O$ and 0.2 ml of PEI in 100 ml of deionized water. The mixture was heated to 80 °C under stirring in a reaction flask during two hours. The resulting NRs were washed by centrifugation at 6000 rpm during 15 min.

β-FeO(OH) NRs were reduced to Fe_3O_4 NRs using oleylamine (9 mmol) mixed with 120 mg of β-FeO(OH) NRs in a three necked round bottom flask under argon

atmosphere. The mixture was heated to 200 °C during 4 hours under vigorous stirring. The product was precipitated by magnetic separation in mixtures hexane:acetone (1:1) to remove the excess of oleylamine.

d) NRs surface modification with PEI

Fe_3O_4 NRs were treated to surface modification with polyethyleneimine (PEI) to make them stable. The ligand exchange was done by heating 100 mg of NRs dispersed in 10 ml of toluene and 2 ml of PEI in 10 ml of DMF. The solution was heated at 80 °C overnight under argon atmosphere. After the reaction solution was cooled to room temperature, NRs were obtained by magnetic separation and washed three times with ethanol to remove the excess of PEI, and finally dispersed in water.

e) Fabrications of Fe_3O_4 nanostructures/P(VDF) (and P(VDF-TrFE)) composites

In order to obtain a good nanostructure dispersion it was used and experimental procedure that ensures a good dispersion of nanofillers [51, 52], briefly a mixture of magnetic nanostructures in DMF was first placed in an ultrasound bath for 8 h. After this period of time, P(VDF) (or P(VDF-TrFE)) powder was added to the solution. Complete dissolution of the polymer was achieved by using a Teflon mechanical stirrer incorporated in the ultrasound bath during 1 h. Flexible nanocomposite films with an average thickness of ≈ 50 μm and with filler content of 1 wt.% were obtained by spreading the solution at room temperature on a clean glass substrate. Such wt.% of magnetic nanofiller was chosen as previous studies showed that such content is capable to effectively nucleate a significant amount of the P(VDF) in the β-phase [7, 19, 53, 54], suitable for the present investigation.

Three different magnetic/P(VDF-TrFE) nanocomposites were obtained with ≈9 nm Fe_3O_4 nanoparticles (NP 9 nm); with ≈30 nm Fe_3O_4 nanoparticles (NP 30 nm) and with ≈50 nm Fe_3O_4 nanoparticles (NP 50 nm). Four distinct magnetic/P(VDF) nanocomposites were obtained: composites with ≈ 9 nm Fe_3O_4 nanoparticles (NP 9 nm); with ≈ 30 nm Fe_3O_4 nanoparticles (NP 30 nm); with ≈ 50 nm Fe_3O_4 nanoparticles (NP 50 nm); and with Fe_3O_4 NR.

Solvent evaporation was carried out, after sample melting, at a controlled temperature of 210 °C inside an oven (SELECTA, 2000).

Development of anisotropic magnetoelectric polymer composites

a) Synthesis of nanostructures

The feroxyhyte (**δ-FeO(OH)) nanosheets** were synthetized using a polytetrafluoroethylene (PTFE) microfluidic reactor by a liquid-gas segmented flow. Inlet flow A, composed of an aqueous solution 180 mM KNO_3, 162 mM NaOH and 1.85 mM L-lysine was mixed with an inlet flow B which consist of an aqueous solution of 13 mM ferrous sulfate heptahydrate (with Fe^{2+} cations) and 3.38 mM sulfuric acid (figure 2.1).

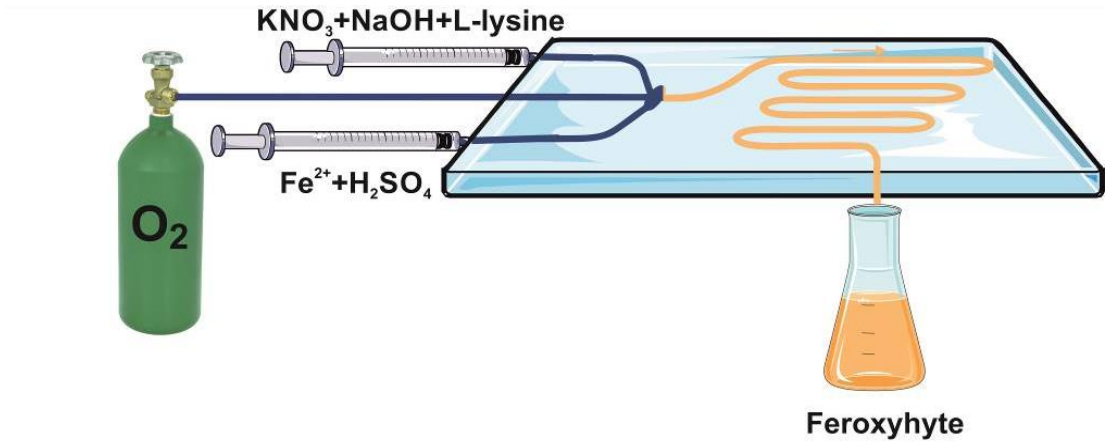

Figure 2.1. Schematic representation of the synthesis process of the feroxhyte nanosheets.

Inlet flows A and B were injected in a Y junction with an O_2 flow at the proper flow rate to achieve a steady segmented flow. The compartmentalized slugs were heated at 90 °C, obtaining at the microreactor outlet an orange solution that was identified with a pure feroxhyte phase. Afterwards, the synthesized nanoparticles were centrifuged at 10 000 rpm for 10 minutes, then washed twice with distilled water and finally resuspended in distilled water for further use.

CoFeO(OH) nanosheets were synthesized by coprecipitation using a modified gas-slugs microfluidic system adapted from [49]. In brief, two distinct solutions, X and Y, were prepared in deionized water and Ar bubbled during 15 minutes to induce deoxygenation (figure 2.2).

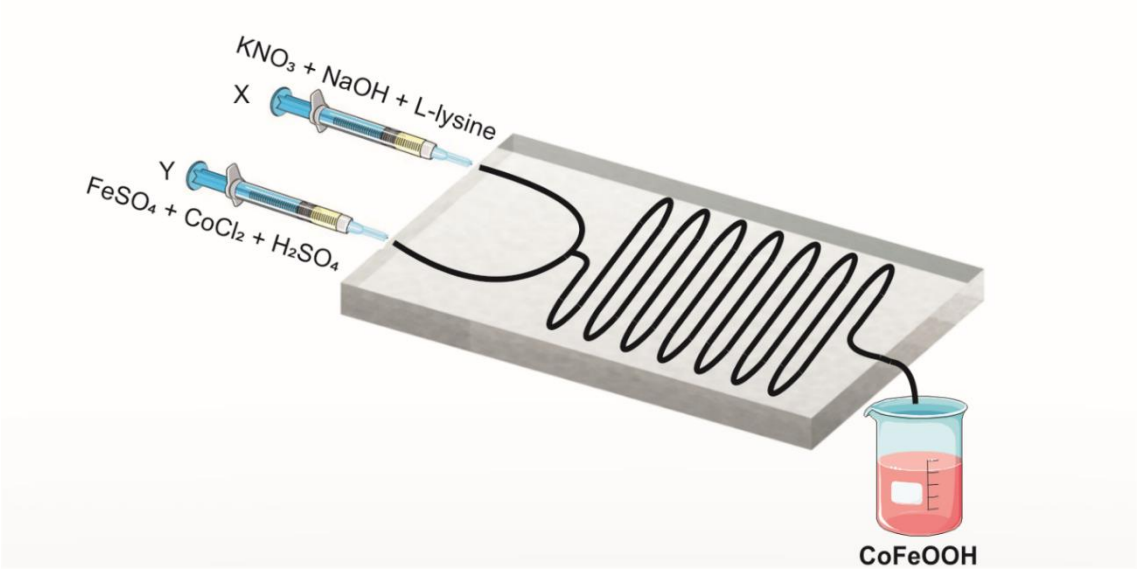

Figure 2.2. Schematic representation of the modified gas-slugs microfluidic system.

The solution X was composed of 180 mM KNO_3, 160 mM NaOH and 1.9 mM L-lysine. In turn, solution Y was constituted of stoichiometric ratio 2:1 of $FeSO_4$ (9 mM) and $CoCl_2$ (4 mM); and sulfuric acid (3.4 mM). After the deoxygenation process, both solutions were placed in plastic Becton Dickinson syringes (60 mL capacity). Solutions X and Y were later injected with an adequate flow rate to obtain a 60 seconds residence time in accordance to the total microfluidic system volume. A constant flow ratio of 1:1 was used to mix Solution X and Y in a PEEK polymer X-junction aiming to ease the synthesis process.

The developed microfluidic system is constituted by a pair of PTFE coils (0.04" ID and 1/16" OD) which are defined as reaction and mixing stages, correspondingly. After, the mixing of X and Y streams was done by sonication in an ultrasound bath, maintaining the bath temperature in the 25-30 °C range. A pure oxygen gas stream was injected after the mixing coil, to achieve stability at the liquid-gas segmented flow in the reaction stage. The reaction stage temperature of 100 °C and the pressure of 1.4 bar were fixed. The resulting synthesized nanostructures were centrifuged for 10 minutes at 10,000 rpm, then double washed with distilled ethanol and water (1:1), and finally resuspended in distilled water.

b) Fabrications of nanostructures/P(VDF-TrFE) composites

The desired amount of the magnetic phase (figure 2.3a) was added to DMF and placed in an ultrasound bath for 8 h in order to ensure a good dispersion of the nanosheets. Flexible ME composite films were prepared (figure 2.3b), with 1, 5, 10 and 20 δ-FeO(OH) filler weigh content (wt.%) and with 1 wt.% (0.01 in volume fraction after solvent evaporation) of CoFeO(OH) filler. Such content was chosen once it allows high ME response and flexible MF samples [3, 15].

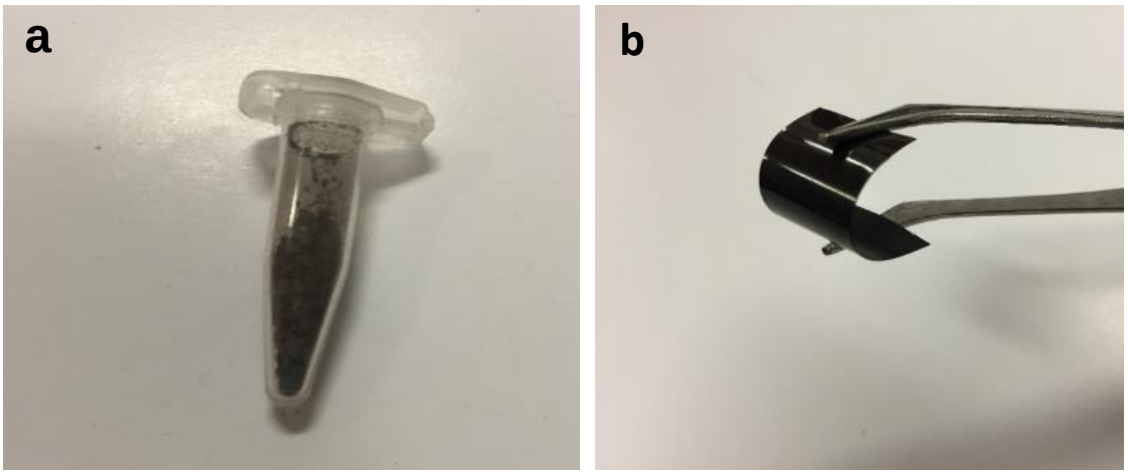

Figure 2.3. a) Obtained feroxhyte nanosheets. b) Flexible MF δ-FeO(OH)/P(VDF-TrFE) composite films.

P(VDF-TrFE) polymer (70/30 molar composition) was then added and mixed during 2 hours with the help of a mechanical Teflon stirrer in an ultrasound bath to avoid the magnetic agglomeration during the mixing process. After that, the solution was spread in a clean glass substrate, and solvent evaporation and samples crystallization took place at 80 °C, while it was placed between the two coils of an electromagnet to ensure the magnetic alignment along the length direction (longitudinal-L samples, figure 2.4a) and along the thickness direction (transversal-T samples, figure 2.4b) of the composite film of the δ-FeO(OH) nanosheets. A sample with random δ-FeO(OH) filler orientation was also prepared (A samples, figure 2.4c).

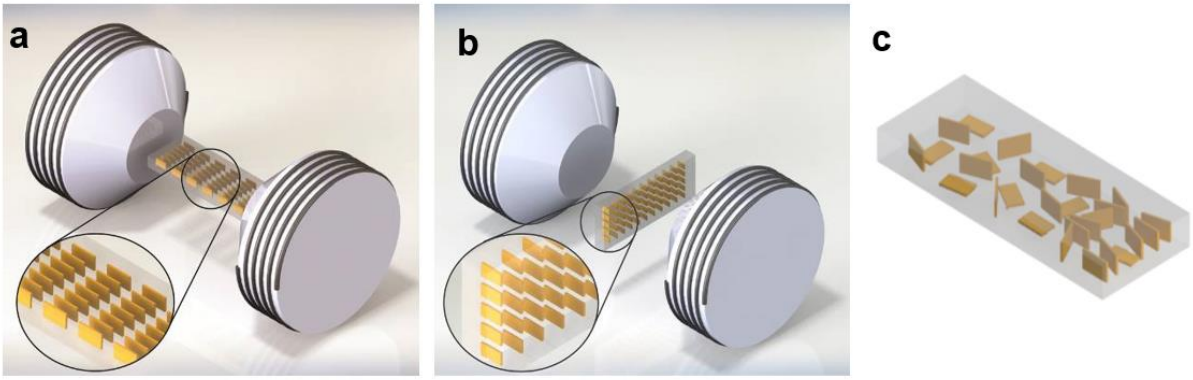

Figure 2.4. Representation of a) magnetic alignment along the length direction; b) magnetic alignment along the thickness direction; c) Randomly oriented samples.

During the alignment process, solvent evaporation occurred at 80 °C in order to obtain flexible films, without pores and with good mechanical properties (figure 2.3b) [55]. Polymer crystallization ended by cooling down films to room temperature. At the end of the process, the flexible film was peeled from the glass substrate and a films with an average thickness of ≈25 µm was obtained for δ-FeO(OH) and ≈30 µm for CoFeO(OH) composites.

2.2.2.2. Characterization methods

Evaluation of the filler dispersion on the piezoelectric and magnetoelectric response

The distribution of the ferrite nanoparticles was investigated by Scanning Electron Microscopy using a NovaTM NanoSEM Scanning Electron Microscope with an acceleration voltage of 15 kV. The nanoparticles average size and their distribution were determined using the Image J software.

The ferroelectric hysteresis loops of the composites were measured at room temperature using Radiant Ferroelectric Premier II LC equipment. After 30 minutes of corona poling at 10 kV and at 120 °C in a home-made chamber, the piezoelectric response (d_{33}) of the poled samples was analyzed with a wide range d_{33}-meter (model 8000, APC Int Ltd).

Magnetic hysteresis loops at room temperature were measured using a vibrating sample magnetometer (Oxford Instruments) up to a maximum field of 1.8 T.

In order to obtain the out-of-plane ME coefficient, a DC and AC magnetic field were applied along the same direction than the electric polarization of the P(VDF-TrFE), i.e., perpendicular to the composite surface. An AC driving magnetic field of 8.1 mOe amplitude at 5 kHz (resonance of the composite) was provided by a pair of Helmholtz coils. The DC field with a maximum value of 1.2 T was applied by an electromagnet. The induced ME voltage was measured with a Standford Research Lock-in amplifier.

Evaluation of the filler size on the magnetostriction, polymer phase nucleation and magnetoelectric response of polymer composites

a) Structural characterization of the nanoparticles

Transmission electron microscopy observations were performed with a T20-FEI microscope with a LaB6 electron source fitted with a "SuperTwin" objective lens allowing a point-to-point resolution of 2.4 Å. The phases of iron oxide nanoparticles were identified by powder X-ray diffraction (XRD). The X-ray patterns were collected between 20° and 80° (2θ) in a D-Max Rigaku diffractometer with Cu K_α radiation.

The particle size distribution was determined by statistical analysis of the dimensions of at least 100 nanoparticles within the transmission electron microscopy (TEM) micrographs.

The magnetic properties of the different nanoparticles were measured as dried powders after solvent evaporation at different temperatures in a superconducting quantum interference device (SQUID MPMS-5S, Quantum Design) from 0 to 40 000 Oe. The samples were measured in a gelatine capsule (a diamagnetic correction for the sample holder was carried out). Magnetic hysteresis loops (plot of the magnetization of the sample as a function of the magnetic field strength) were evaluated at 37 °C.

Zeta potential measurements were performed on a Malvern Zetasizer nano ZS, with an operating range between 0.3 nm to 10 µm, with a laser HeNe 633 nm, Max 4 mW.

b) Structural characterization of the nanocomposites

The vibrational modes of the polymer, used to determine the polymer-phase and phase content, were recorded by Fourier transformed infrared spectroscopy (FTIR) using a Thermo Nicolet Nexus 670 FTIR spectrophotometer from 650 to 4000 cm^{-1} with a resolution of 2 cm^{-1}. 64 scans were performed for each sample. The thermal behavior of the samples was determined by Thermo Gravimetric Analysis (TGA). Samples were transferred to open alumina pans with capacity of 60 µL and analyzed using a TGA METTLER TOLEDO 822e, operating between room temperature and 975 °C. A heating rate of 10 °C.min^{-1} and a nitrogen flow rate of 50 ml.min^{-1} were used.

The d_{33} of the samples was analyzed with a wide range d_{33}-meter (model 8000, APC Int Ltd) after poling the ME composites by corona poling at 10 kV during 120 min at 120 °C in a home-made chamber and cooling down to room temperature under applied field [52].

The capacity and the tan δ, dielectric loss, of the composites were measured with an automatic Quadtech 1929 Precision LCR meter. The applied signal for frequencies in the range of 1 Hz to 1 MHz was 0.5 V. The samples were previously coated by thermal evaporation with circular Au electrodes of 5 mm diameter onto both sides of the sample in order to obtain a parallel condenser geometry. The real part of the dielectric constant, ε', was then obtained taking into account the geometrical characteristics of the samples.

In order to obtain the out-of-plane ME coefficient α_{31}, the first index indicating the collinear ferroelectric poling and electrical measurement directions, and the second indicating the applied magnetic field direction, a DC and AC magnetic fields were applied along the length of the sample. An AC driving magnetic field of 1 Oe amplitude at 7 kHz (resonance of the composite) was provided by a pair of Helmholtz coils and controlled by a signal generator.

In-plane Young's modulus values E_Y were obtained from the initial slope of strain–stress curves measured for nanocomposite samples using a Linkam TST350 tensile stress testing system in tensile mode, with a 2 mm.min^{-1} loading rate.

The magnetostriction of the nanoparticles was determined based on the ME measurements and using the method proposed by Martins-Silva-Lanceros-Mendez [35]. Briefly, the strain derivative, dS/dH, was obtained through equation 2.1:

$$\left(\frac{dS}{dH}\right) = \frac{\alpha}{m_V \times (1 - m_V) \times \left(\frac{d_{33}}{\varepsilon o \times \varepsilon} \times \frac{E_Y \times l \times w}{t}\right)_{piezoelectric}} \quad (2.1)$$

where mV, ε_0, ε, E_Y, l, w and t are the volume fraction of Fe_3O_4 nanoparticles, the vacuum permittivity, the relative permittivity, the Young's modulus, the length, the width and the thickness of the composite, respectively.

Assuming that the magnetostriction (λ) of the nanoparticles increases almost linearly with increasing magnetic field, until saturation is reached, λ can be determined by equation 2.2:

$$\lambda = \left(\frac{dS}{dH}\right) \times B_S \quad (2.2)$$

where B_S is the magnetic field at which magnetostriction saturation is achieved.

Development of anisotropic magnetoelectric polymer composites

The magnetic properties of the nanoparticles were measured as dried powders after solvent evaporation at different temperatures in a superconducting quantum interference device (SQUID MPMS-5S, Quantum Design) from 0 to 40 000 Oe. The samples were measured in a gelatin capsule (a diamagnetic correction for the sample holder was carried out). Magnetic hysteresis loops (magnetization of the sample as a function of the magnetic field strength) were evaluated at 37 °C. Zero-field-cooled field-cooled (ZFC-FC) magnetization analysis was carried out at 50 Oe from 4 to 320 K.

The X-ray patterns of the nanoparticles were identified by powder X-ray diffraction. The X-ray patterns were collected between 20° and 80° (2θ) in a D-Max Rigaku diffractometer with Cu K_α radiation.

The particle morphology and size distribution were determined by transmission electron microscopy (TEM FEI-TECAI T20) operated at 200 kV.

The average size of nanosheets was determined through TEM images and Image J software. Aberration corrected scanning transmission electron microscopy (Cs-corrected STEM) images were obtained through high angle annular dark field detection, using a FEI XFEG TITAN electron microscope with a voltage of 300 kV. Elemental analysis was performed with an energy-dispersive detector - EDS - (EDAX) detector.

The morphology of composites was studied by scanning electron microscopy (SEM) using a Quanta 650 FEI electron microscope with acceleration voltage of 10 kV. Before SEM measurement, the samples were coated with gold by magnetron sputtering. Images were taken in three different locations of the samples and at different magnifications to ensure reproducibility of the observed morphological features.

Composite's d_{33} was evaluated with a wide range d_{33}-meter (8000 model from APC International, Ltd.) Afterwards, the poling of the ME composites was achieved through corona poling for 120 min at 120 °C and 10 kV, and cooling down to room temperature (25 °C) under applied magnetic field, by using a previously optimized poling procedure [15, 56].

In order to obtain the out-of-plane ME coefficient α_{31}, the first index indicating the collinear ferroelectric poling and electrical measurement directions, and the second indicating the applied magnetic field direction, a DC and AC magnetic fields were applied along the length of the sample i.e., in the same direction of the alignment of the nanosheets.

For the δ-FeO(OH), an AC driving magnetic field of 1 Oe amplitude at 7 kHz (resonance of the composite) was provided by a pair of Helmholtz coils and controlled by a signal generator. Such resonance was determined by equation 2.3 [29, 57]:

$$f_n \approx (n/2l)\sqrt{E_Y/\rho} \tag{2.3}$$

where l is the length along the resonant direction, n is the order of the harmonic mode, and ρ and E_Y are density and Young's modulus, respectively.

For the CoFeO(OH) composite, the resonance was verified with 1 Oe amplitude AC magnetic field with frequencies ranging from 1 to 75 kHz was controlled by a signal generator and delivered by two Helmholtz coils.

An electromagnet controlled by a DC source provided the DC magnetic field (H_{DC}) with a 0.15 T (CoFeO(OH)) and 0.5 T (δ-FeO(OH)) maximum magnetic field value. A Standford Research Lock-in amplifier (SR530) was used to measure the produced ME voltage. The magnetic field direction influence on the ME response of the composite was evaluated by sample rotation from 0 to 360° angles (figure 2.5).

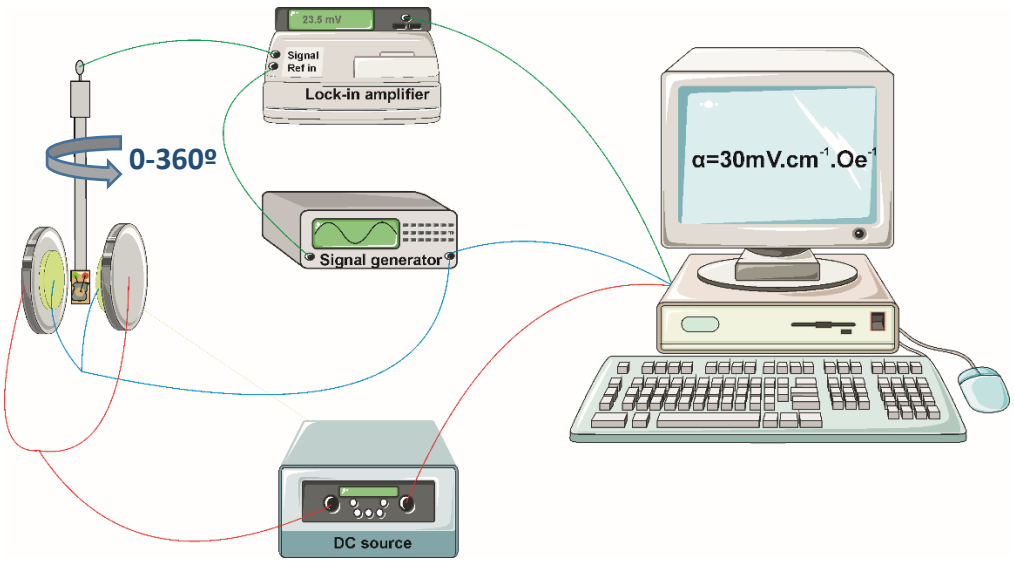

Figure 2.5. Schematic representation of the experimental setup used to study the influence of the magnetic field direction on the ME response of the composites.

Prior to the ME measurements, composites were coated by thermal evaporation with 5 mm diameter circular Au electrodes onto both sides of samples. Three samples for each alignment state (L, T and A) were measured and the error in the obtained ME coefficient was less than 5 %.

The rotation/deformation of the nanosheets was determined based on the ME measurements presented above and the theory proposed by Van den Boomgaard et al. [58], Zubkov et al. [59] and Ryu et al. [60]. In this way, it is possible to determine the strain derivative, dS/dH, through the abovementioned equation 2.1.

Assuming that the deformation generated by the rotation of the nanosheets increases almost linearly with increasing magnetic field, until saturation was reached, λ can be determined by equation 2.2 (abovementioned):

2.3. Evaluation of the filler dispersion on the piezoelectric and magnetoelectric response

It is already well established that the aggregation of the fillers is critical in determining some functional properties of composites such as thermal, electrical and mechanical properties [61-64]. To avoid this problem, one of the most popular strategies is the use of surfactants [46, 65], nevertheless in the case of magnetic nanoparticles polymer, aspects such as the chemical and processing complexity, thermal stability, costs and health issues of such additives have severely constrained the development of upscaled applications of such composites [66, 67]. Bearing this in mind in this work, the influence of the ferrite filler aggregation state in the ME response of the produced polymer composites was studied and determined.

In order to determine the effect of the different dispersion methods in the agglomeration state of the ferrite nanoparticles and their dispersion on the P(VDF-TrFE) matrix, SEM was used. Figure 2.6 shows representative SEM images of the samples prepared with 20 wt.% ferrite content dispersed by ultrasound (figure 2.6a) and with the use of citric acid (figure 2.6b). The results shown for this composite concentration are representative for all samples.

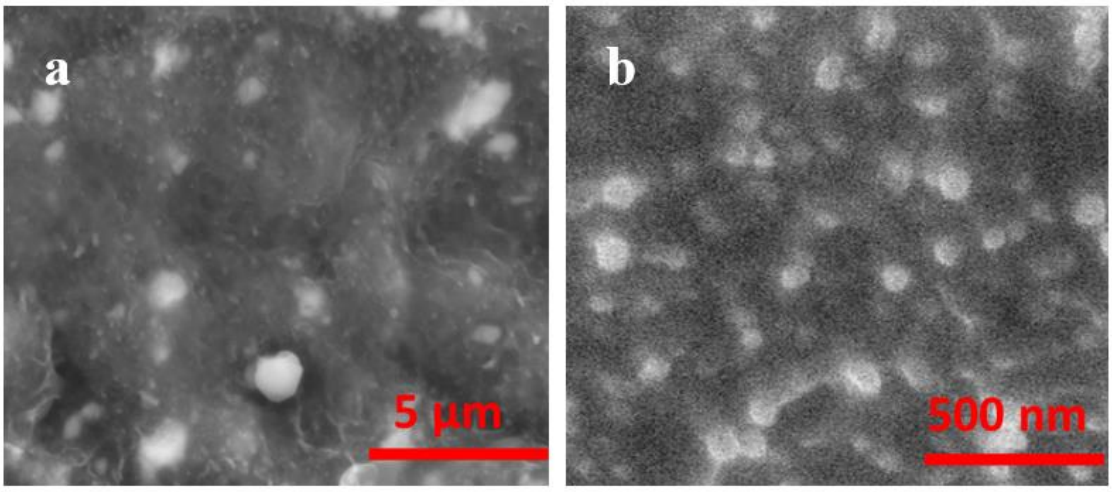

Figure 2.6. Representative cross section SEM images of CFO/P(VDF) composites prepared after dispersion achieved by (a) ultrasound and by (b) surfactation.

The agglomerates observed in figure 2.6a shows a poor dispersion of the ferrite nanoparticles along the polymeric matrix. On the other hand, citric acid surfactation led to a homogeneous distribution of the ferrite nanoparticles by avoiding agglomerates (figure 2.6b) reaching an overall higher nanoparticle surface area interacting with the polymer matrix. Image J software was used to quantify the nanoparticle aggregates in two distinct areas of the samples with 20 wt.% of ferrite content.

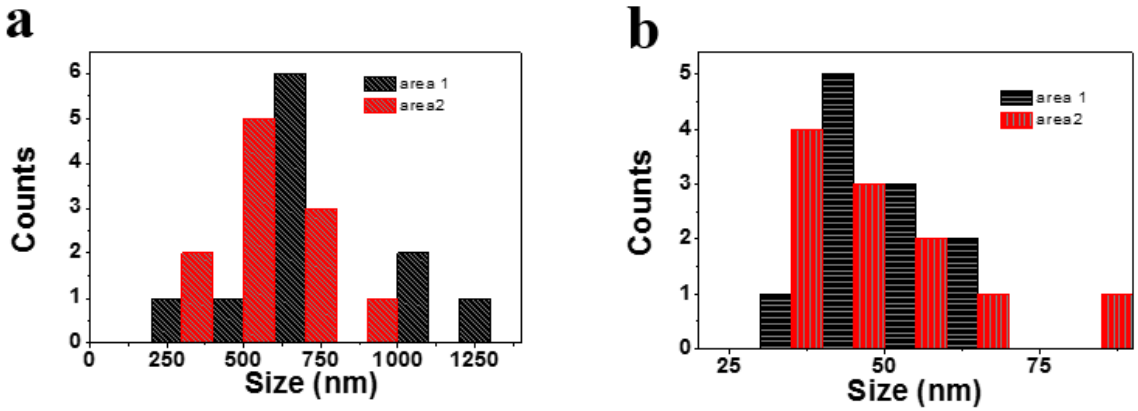

Figure 2.7. a) Cluster distribution for ultrasound dispersed composites. b) Nanoparticle/cluster distribution for composites prepared by nanoparticle surfactation.

It was verified (figure 2.7a) that the cluster average diameter obtained in the non surfactated particles was 668 ± 256 nm and the average diameter of the surfactated ferrite nanoparticle/cluster was 49 ± 12 nm (figure 2.7b), clearly indicating the effectiveness of surfactation in preventing nanoparticle aggregation. The use of ultrasound during the mechanical agitation in the non-surfactated composites led, on the other hand, to lower agglomerates as the ones reported in [46].

The ferroelectric hysteresis loops as well as the piezoelectric response of the composites obtained by both dispersion methods are presented in figures 2.8a and 2.8b, respectively.

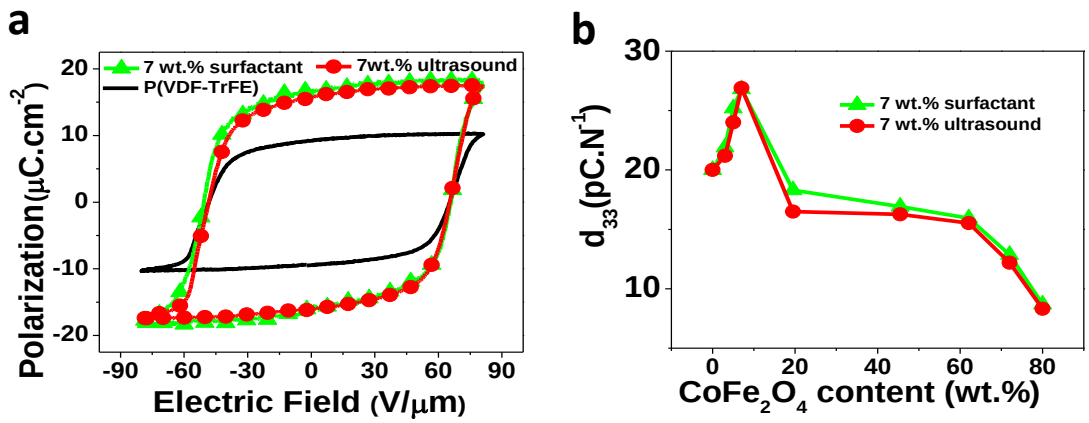

Figure 2.8. a) Ferroelectric hysteresis loops of samples with 7 wt.% of $CoFe_2O_4$ content. b) Ferrite weight fraction-dependent d_{33} for the samples prepared by the two dispersion methods.

Figure 2.8 shows that the dispersion method has no relevant influence in the ferroelectric and piezoelectric responses of the samples. Figure 2.8b illustrates the correlation between the piezoelectric response of the composites and the CFO content. As ferrite concentration increases, the piezoelectric response increases until a maximum value ≈27 $pC.N^{-1}$ at a concentration of 7 wt.% ferrite content. For higher concentrations, the values of both remnant polarization and piezoelectric response decrease, being this decrease stronger for concentrations above 60 wt.% ferrite content. Figure 2.8 makes clear that the dispersion method has no influence in the polarization and piezoelectric responses of the MF films being independent of the large cluster differences. The piezoelectric and ferroelectric responses are fully determined by the polymeric piezoelectric phase, indicating that, independently of the ferrite cluster size, polymer crystallization occurs in a similar way, leading to a well crystallized sample with no defects that would prevent sample poling [68]. It should be noted that samples prepared by the ultrasound method reported in [46] were not possible to be polarized due to the size of the ferrite clusters, leading to sample dielectric breakdown.

Figure 2.9 shows magnetic hysteresis loops measured for the different nanocomposites.

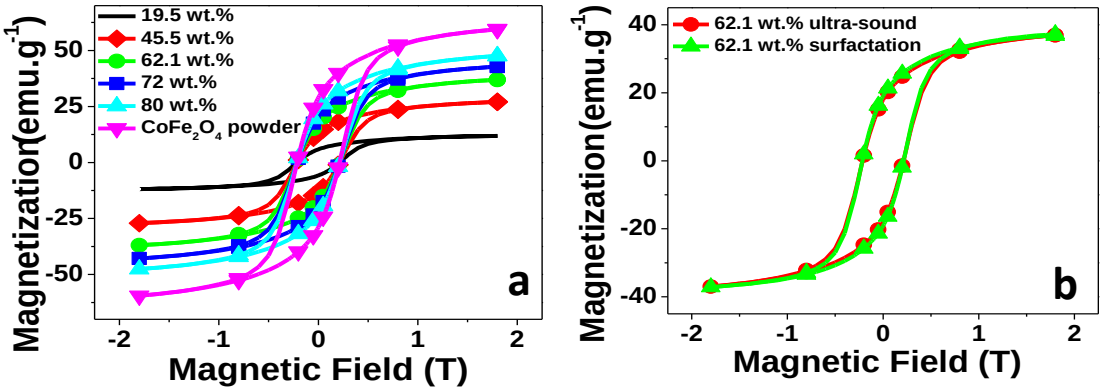

Figure 2.9. a) Room temperature hysteresis loops for the pure ferrite nanoparticle powder and for P(VDF-TrFE)/$CoFe_2O_4$ nanocomposites. b) Room temperature hysteresis loops measured for the composite with 62.1 wt.% of ferrite for the different dispersion methods.

The shape and magnetization maximum values of the measured hysteresis loops demonstrates that magnetic nanoparticles are randomly oriented within the polymer matrix. For all composites a coercive field of 0.21 T was measured, higher than the one measured in similar nanocomposites but prepared by other methods [6] since the coercive field value strongly depends on factors such as the calcinations temperature, size, shape and structure of the formed nanoparticles [69]. It was found that the dispersion method has no influence in the magnetic response of the nanocomposites, demonstrating that the use of surfactants does not change the magnetic properties of the nanoparticles. Additionally, it can be noted that contrary to what was reported for other magnetic nanoparticles [70], the nanoparticle magnetic response is independent of the nanoparticle aggregation state, at least with respect to clusters up to ≈10 nanoparticles.

Finally, figure 2.10 shows the variation of the ME voltage coefficient for samples with different ferrite concentrations and with the DC magnetic field, for films obtained by both dispersion methods.

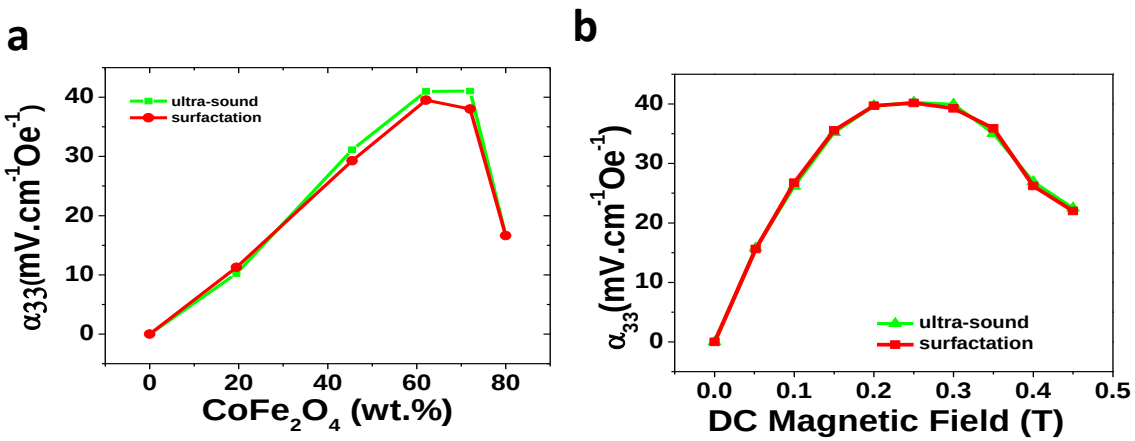

Figure 2.10. a) ME coefficients as a function of CFO filler content for the different dispersion methods. b) In plane and out of plane ME response of 72 wt.% ferrite content samples for samples with different dispersion methods.

Figure 2.10a shows the ME response of the nanocomposites at a bias field of 2.5 kOe for increasing CFO loadings. The initial increase in the ME voltage is explained by the increase of the magnetostrictive elongation arising in the magnetostrictive ferrite phase. This response is optimized at 72 wt.% CFO content (for both dispersion methods). For higher concentrations, nanoparticles lead to the disruption of the ferroelectric copolymer phase [6], having as a result an abrupt decrease in the ME response of the nanocomposite [15].

No differences are detected in the ME response of the samples when comparing both dispersion methods (figure 2.10b), demonstrating that the disruption of the ferroelectric polymer phase occurs for the same filler content, independently of the cluster size in the measured size range. This is in agreement with the developed theories that accurately fit the experimental ME results without consideration of the filler size or surface area [6, 71, 72]. It was reported in a previous work that the ME response of PZT/Ni ferrite composite ceramics was improved with the increase of the nickel ferrite powder surface area [73]. This increased surface area was obtained with a simultaneous increase in the ferrite density that in fact also influences parameters such as Young´s modulus, shear modulus and bulk modulus which also play a relevant parameter in the ME response.

Our results show that the optimization in the ME response in such composites cannot be uniquely attributed to the change in the nanoparticle surface area. Filler content and good distribution turns out to be key parameters independently of filler dispersion method during ME composite fabrication process. Such result is of special interest for industrial large scale processes, in which feasibility for fabrication of smart structures is one of the main tasks.

2.4. Evaluation of the filler size on the magnetostriction, polymer phase nucleation and magnetoelectric response of polymer composites

Having this interesting discussion being centered on the surface charge of the nanostructures, a key factor was left out: the size and shape factor of the nanostructures, at the origin of specific electrical field geometries around the nanoparticle surface and to confinement effects [74, 75]. This issue is also particularly relevant when different nanoparticle shapes are increasingly being used for the development of novel sensors, such as anisotropic ME magnetic field sensors [51]. Considering also this parameter, this work aimed to create a unifying mechanism that could be used to explain the ambiguity and solve the existing controversy in the current literature about the nucleation of the β-phase of P(VDF) with nanostructures as well as to definitively set light on the significance of the key factors prompting the nucleation of the electroactive β-phase of this important electroactive polymer. In this way, this work used two types of magnetic nanostructures, Fe_3O_4 NRs and Fe_3O_4 nanoparticles, with distinct sizes and surface charges, to study, isolate and discuss the effects of the size, ion−dipole interactions and shape on the formation of the β-phase crystalline structure of P(VDF). On the other hand, Fe_3O_4 was synthesized with different sizes in order to improve their magnetostriction and magnetic properties. Additionally, Fe_3O_4/P(VDF-TrFE) composites were produced to study the influence of particle size on the magnetostrictive properties of Fe_3O_4 nanoparticles and validated the use of the Fe_3O_4/P(VDF-TrFE) nanocomposites and ME materials for device applications [3]. In this scope, P(VDF-TrFE) was selected as piezoelectric polymer since it shows the highest piezoelectric responses among the small class of polymers that exhibit piezoelectricity [7], being polymer-based ME materials the most interesting ones from the application point of view [3, 76].

Nanoparticles

Figure 2.11 shows representative TEM micrographs of the obtained magnetic nanomaterials, together with their room-temperature magnetic response.

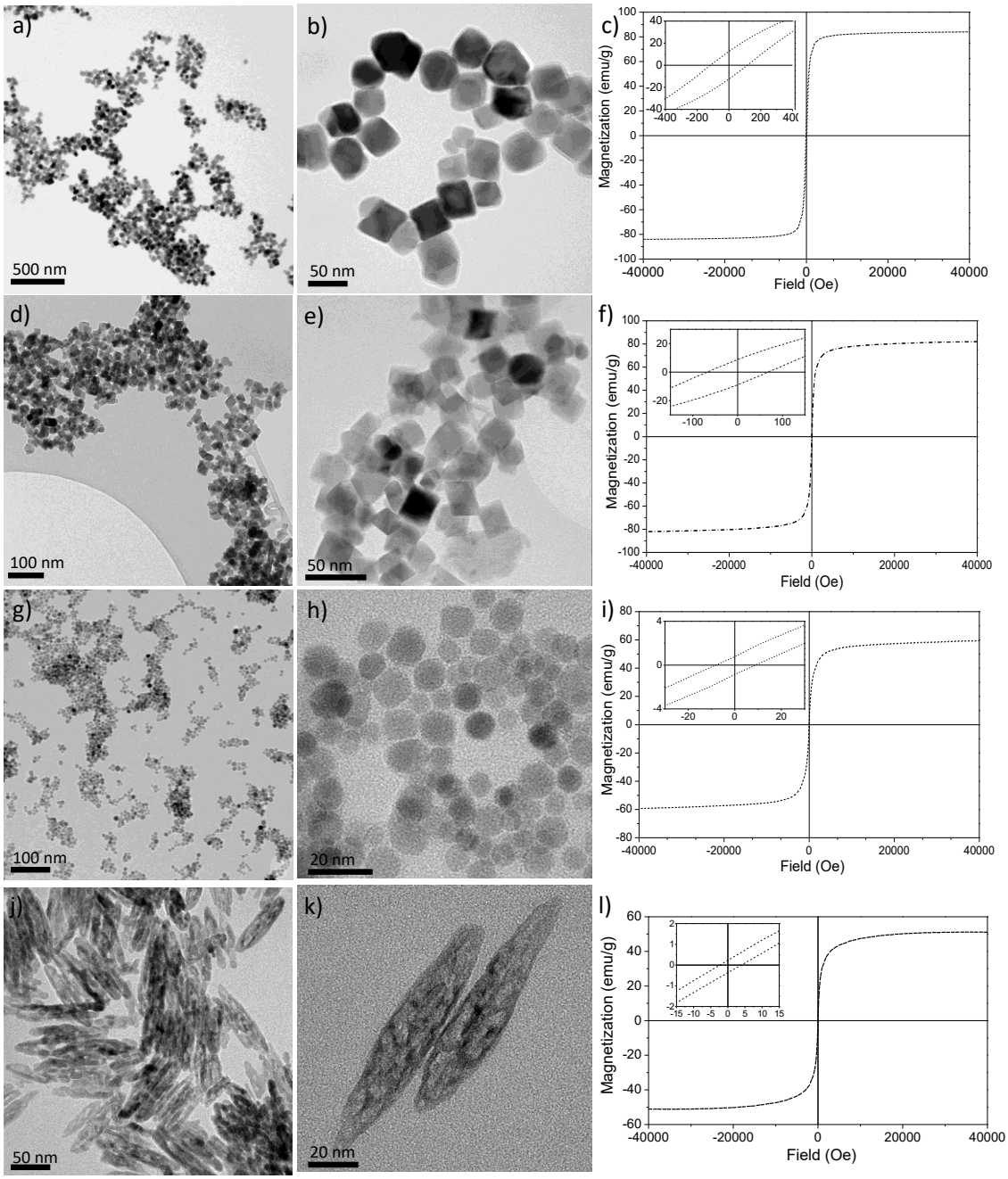

Figure 2.11. Morphology and magnetic characteristic of the obtained magnetic nanomaterials nanoparticles produced by oxidative hydrolysis: a-b) TEM images of nanoparticles D= 50 nm, c) magnetization curve at 300 K. d-e) TEM images of nanoparticles D= 30 nm, f) magnetization curve at 300 K. Nanoparticles produced by the polyol-mediated method. g-h) TEM images of nanoparticles D= 9 nm. i) magnetization curve at 300 K. Anisotropic growth of iron oxide nanostructures. j-k) TEM images of nanoparticles D= 30nm, l) magnetization curve at 300 K.

Figures 2.11a-b and figure 2.11d-e show that the morphology of the nanoparticles produced by an oxidative hydrolysis method was octahedral with a rather uniform size. The particle size distribution was determined by statistical analysis of the dimensions of at least 100 nanoparticles measured on the TEM micrographs. Fitting to a log-normal distribution yielded an average particle size of 47.7 ± 9.6 nm and 29.5 ± 7.2 nm. Figure 2.11g-h shows the nanoparticles produced by the polyol-mediated method, obtaining nanoparticles of roughly spherical morphology, rather uniform in size (average size 9.2 ± 2.3 nm), and well dispersed.

The magnetization curves of the iron oxide nanoparticles, with average size of D=50 nm and D=30 nm show a ferromagnetic behavior with a coercivity (H_c) of 110 and 65 Oe, respectively (figures 2.11c and 2.11f). The M_s at 40 000 Oe is 84 emu.g^{-1} for Fe_3O_4 50 nm and 82 emu.g^{-1} for Fe_3O_4 30 nm. However, the magnetization curve of Fe_3O_4 D=9 nm shows a superparamagnetic behavior with a small H_c of 9 Oe and a Ms of 59.6 emu.g^{-1} at 40 000 Oe. These results are consistent with the literature [77] and the fact that Fe_3O_4 loses its permanent magnetism when its size is smaller than 20 nm, becoming superparamagnetic [78].

The anisotropic growth of magnetic nanomaterials has promising advantages over the spherical shape in areas such as lithium-ion batteries, gas sensors magnetic compasses [79]. The use of nanoparticles with an anisotropic configuration has not been properly demonstrated in the literature because their preparation is a challenging task as surface energy considerations favor the formation of spherical nanoparticles [50]. The production of magnetic NRs was conducted in this work by a novel and simple procedure, leading to FeO(OH) NRs with an aspect ratio higher than 8 and a rod diameter of ~ 13 nm. After a thermal treatment, hematite NRs were obtained, maintaining the morphological structure (figure 2.11j-k). The magnetization curves of Fe_3O_4 NRs (figure 2.11l) show a ferromagnetic behavior with a H_c of 120 Oe and a M_s of 0.8 emu.g^{-1} at 40 000 Oe. The low magnetization values of the NRs are being attributed to the existence of a surface spin disorder layer which decreases with the particle size [50].

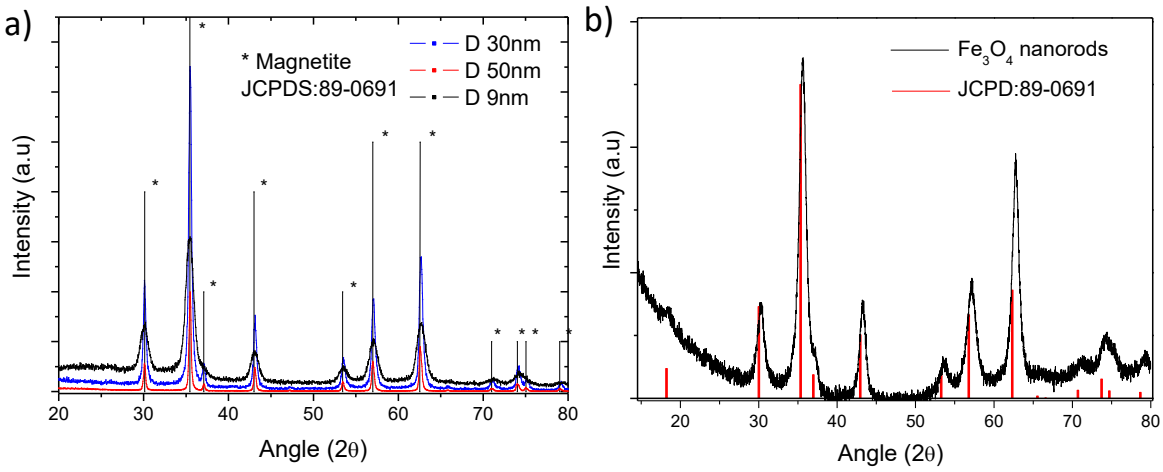

Figure 2.12. XRD patterns of the prepared magnetic nanomaterials (the characteristic patters of Fe_3O_4 are included for comparison).

The typical X-ray diffraction patterns of the 50 nm, 30 nm and 9 nm nanoparticles are shown in figure 2.12a. The XRD patterns of these samples were assigned to the phase of bulk Fe_3O_4 (JCPDS card number 89-0691). The XRD pattern of figure 2.12b confirms the transformation of FeO(OH) to Fe_3O_4.

Nanocomposites P(VDF-TrFE)

With respect to the Fe_3O_4/P(VDF-TrFE) composites, the ME effect required to determine the magnetostriction of the Fe_3O_4 nanoparticles is generated as a product property between magnetostrictive and piezoelectric components and, consequently, the high piezoelectric coefficient of the polymer matrix will induce a higher ME coupling [29]. The variation of the modulus (d_{33} values are negative for P(VDF) and its copolymers) of the piezoelectric $|d_{33}|$ coefficient for the composites with the Fe_3O_4 nanoparticles of different sizes as well as its stability over time are represented in figure 2.13.

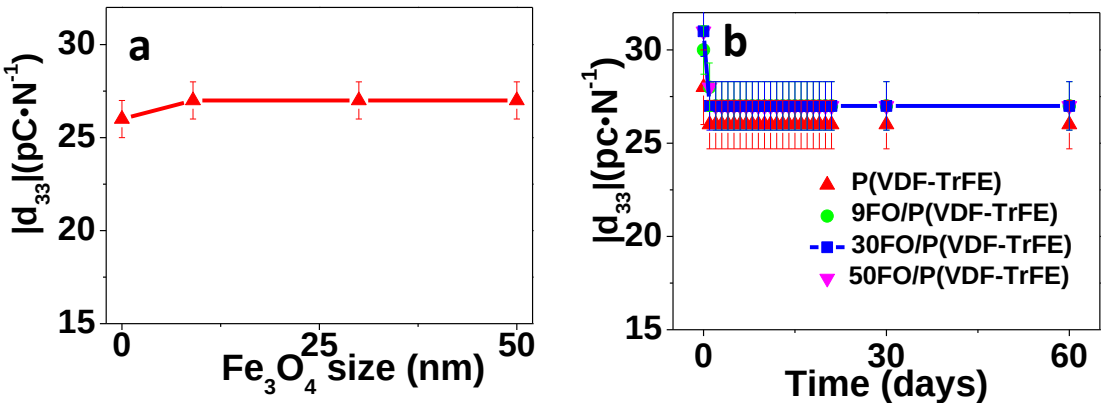

Figure 2.13. a) Variation of the Fe_3O_4/P(VDF-TrFE) $|d_{33}|$ value as a function of Fe_3O_4 size; b) evolution of the Fe_3O_4/P(VDF-TrFE) $|d_{33}|$ coefficient over time.

No significant differences are detected in the piezoelectric response of the composites prepared with Fe_3O_4 nanoparticles with different sizes (figure 2.13a) for a given ferrite content (1 wt.%), which is expected as the piezoelectricity is fully ascribed to the polymer and for the low filler concentrations used in this experiments, no nanoparticle aggregates are observed, that can hinder mechanical and electromechanical responses [52]. Further, the piezoelectric response of the different composites is stable over time as revealed on figure 2.13b, assuring the suitability of the developed materials for applications.

Figure 2.14 shows the variation of the ME voltage coefficient with DC magnetic field and with Fe_3O_4 nanoparticle size, measured under an AC field of 1 Oe at 5 kHz resonance frequency.

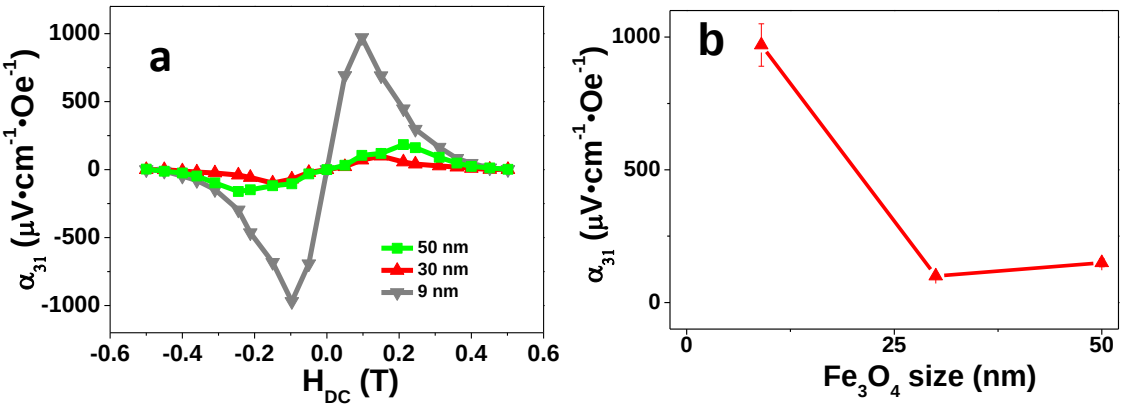

Figure 2.14. a) ME coefficients as a function of the bias field for the different Fe_3O_4/P(VDF-TrFE) composites; b) evolution of the Fe_3O_4/P(VDF-TrFE) α_{31}coefficient with Fe_3O_4 size.

Figure 2.14a reveals a similar ME response for the three nanocomposite films, the ME response increasing with increasing DC magnetic field until a maximum is reached due to the increase of the effective piezomagnetic coefficient, and then decreasing as a response to the saturation of the magnetostriction coefficient [30].

Maximum ME voltage coefficients (α_{31}) of 970, 100 and 150 μV.cm^{-1}.Oe^{-1} at 970, 1500 and 2120 Oe, respectively for the nanocomposites prepared with 9 nm, 30 nm and 50 nm. Thus, a strong increase of the ME response (figure 2.14b) is observed with reducing filler average size, in particular for the nanocomposite with the smaller Fe_3O_4 size (9 nm) as a consequence of its superparamagnetic behavior. By the method presented in the characterization methods and using the data from table 2.1, the magnetostrictive coefficient (λ) was calculated for each nanoparticle from the ME response of the nanocomposites.

Table 2.1. α_{31}(mV.cm^{-1}Oe^{-1}), mV, d_{33} (pC.N^{-1}), ε, EY (GPa), l (mm), w (mm), and t (μm) values used to determine λ (ppm).

NP	α_{31}	m_V	d_{33}	ε	E_Y	W, l, t	λ
9 FO	0.97				1.11		167.0
30 FO	0.10	0.0036	27	12	1.13	6, 12,50	17.2
50 FO	0.15				1.16		25.8

A strong increase of the λ (± 5 ppm) value was found to the 9 nm nanoparticles with respect to those with 30 nm and 50 nm average size.

Fe_3O_4 is a ferrimagnetic iron oxide with a cubic inverse spinel structure with oxygen anions forming a face centred cubic (FCC) closed packed structure and cations (iron) located at the interstitial tetrahedral sites and octahedral sites. The electron can balance between Fe^{2+} and Fe^{3+} ions in the octahedral sites at room temperature imparting half metallic property to Fe_3O_4 [80]. As the particle size decreases, there is a relative decrease in oxygen content of the sample, which consequently, leads to lowering the valance state of the cations [80]. The increase in unit cell volume with the reduction in particle size of the Fe_3O_4 particles, implies an increase in Fe^{2+} content in the sample, as the ionic radius of Fe^{2+} (0.74 Å) is larger than that of Fe^{3+} (0.64 Å). Since the resultant magnetic moment in Fe_3O_4 is regarded to be due to the divalent ions (Fe^{2+}), which explains the increase in magnetostriction for the 9 nm nanoparticles [80].

The decrease in the oxygen content is also responsible for the superparamagnetic behavior of the 9 nm nanoparticles that results from the requirement of charge balance in the crystal structure related with the oxygen-free lattice sites that become occupied by doubly charged donors [81]. Furthermore and resulting from the high magnetostriction of the Fe_3O_4 nanoparticles with 9 nm size, their ME response of the corresponding nanocomposites is one order of magnitude higher than for the nanocomposites with 30 nm and 50 nm nanoparticles. Interestingly, the value of the ME response is in the same order of magnitude that for CFO/P(VDF-TrFE) nanocomposites that exhibits the highest ME response for polymer-based ME nanocomposites, validating their use for ME devices such as sensors and actuators [3, 52].

Nanocomposites P(VDF)

FTIR has proved to give quantitative information about P(VDF) structure allowing to distinguish and quantify the different crystalline forms. In particular, specific bands such as those at 766 and 840 cm^{-1} , were identified to correspond to the α and β-phase of P(VDF), respectively [7]. These specific bands have been used for identification and quantification of P(VDF) phases in the present study.

By assuming that the infrared absorption follows the Lambert–Beer law, for a system containing both α- and β-phases, the relative β-phase content, F(β), can be determined using equation 2.4 [82]:

$$F(\beta) = \frac{A_\beta}{(K_\beta / K_\alpha) \times A_\alpha + A_\beta} \tag{2.4}$$

where F(β), represents the β-phase content; A_α and A_β the absorbance at 766 and 840 cm^{-1}; K_α and K_β the absorption coefficients at the respective wavenumber (6.1×10^4 and 7.7×10^4 $cm^2.mol^{-1}$), respectively.

Typical spectra and the variation of the relative fraction of the β-phase for the nanocomposites prepared with each different of filler are presented in figure 2.15.

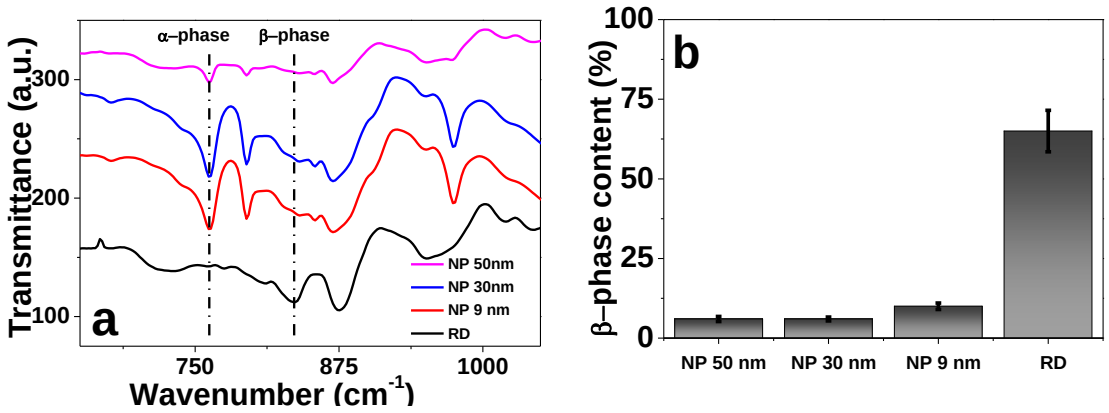

Figure 2.15. a) Infrared spectra of the Fe_3O_4/P(VDF) nanocomposites; b) electroactive β-phase content of the Fe_3O_4/P(VDF) nanocomposites samples calculated from the infrared spectra by equation 2.4.

Figure 2.15 shows that just Fe_3O_4 NRs successfully nucleate the β-phase of the polymer as indicated by the appearance of the β-phase peak at 840 cm^{-1} and the vanishing of the α-phase peak at 766 cm^{-1} (figure 2.15a).

Figure 2.15b shows that both nanocomposites with Fe_3O_4 nanoparticles of 50 nm and 30 nm (NP 50 nm and NP 30 nm) have the lowest percentage of β-phase (6 %), and the nanocomposite with Fe_3O_4 nanoparticles with 9 nm reveals 10 % of β-phase, being the remainder in the α-phase. FTIR results raise the possibility that can exist a shape factor in the mechanism of the β-phase formation, once nanocomposites with Fe_3O_4 NRs reveal a much larger nucleation effect (F(β)≈70 %) than nanocomposites with Fe_3O_4

nanoparticles (NP 50 nm, NP 30 nm and NP 9 nm), independently of the size of the nanoparticle.

Trying to investigate whether the amount of polymer that is electrostatically interacting the surface of the nanostructure (interface) has some influence on the β-phase nucleation ability, the percentage of polymer located at such interface was determined by TGA (figure 2.16).

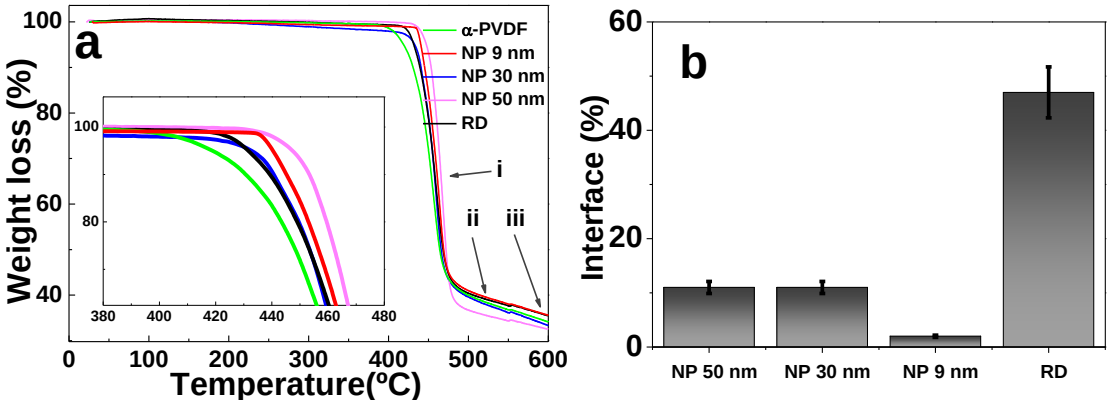

Figure 2.16. a) TG thermograms of Fe_3O_4/P(VDF) nanocomposites; b) interface wt.% for each of the Fe_3O_4/P(VDF) nanocomposites.

The mass fraction of the polymer located at the interface, m_I, was determined following the procedure presented in [83], by using equation 2.5:

$$m_I = \frac{m(x)_{I0} - m_{I0}}{m_{I0}} \tag{2.5}$$

where m_{I0} is the mass of the pristine polymer at the temperature at which the mass loss rate is maximum and $m(x)_{I0}$ is the mass of the composite that has not degraded at the temperature at which the mass loss rate of the pristine polymer is maximum. The difference between m_{I0} and $m(x)_{I0}$ values is related with the enhancement of the thermal stability of the polymer chains located at the interface. For all Fe_3O_4/P(VDF) nanocomposites is observed the characteristic two step (i and ii) thermal degradation mechanism typical of P(VDF) [84]. The first degradation step occurs between 400 and 500 °C, being the P(VDF) maximum degradation temperature dependent on the presence of the nanostructures within the polymer. In this first step, the degradation mechanism is chain-stripping where carbon-hydrogen and carbon fluorine scission

occurs and the presence of both hydrogen and fluorine radicals leads to the formation of hydrogen fluoride [19], leading to the weight loss observed in the first degradation step. In turn, the second degradation step occurs between 500 and 600 °C, and the detected differences in the plots when compared to the pure P(VDF) are attributed to the presence of the nanostructures, as the thermal degradation is independent of the polymer phase. This second step is a complex degradation procedure resulting in poly(aromatization). The polymeric sequence, previously formed on the first degradation step is unstable and, therefore, the formed macromolecules undergo further reactions leading to scission followed by the formation of aromatic molecules [84]. The residual weight that remains at high temperatures corresponds mainly to the nanostructures together with the residual char from the previous degradation steps [83]. An extra degradation step (iii) at temperatures around 600 °C, when compared to the pure polymer was also identified in the nanocomposite samples. The emergence such new step of degradation in comparison to pure P(VDF) is related to the increase of an interphase in the interface volume between nanoparticles and polymer. The onset temperature for the degradation of neat P(VDF) (452 °C) is lowest than those of Fe_3O_4/P(VDF) nanocomposites (456, 457, 460 and 465 °C for the NP 30 nm, RD, NP 9 nm and NP 50 nm respectively), indicating that the thermal stability of the matrix is improved with the addition of Fe_3O_4 nanostructures. By using data from figure 2.16a and equation 2.5, it is possible to determine that NP 9 nm shows the lower interface value (2 %) and the other NP samples exhibited similar interface values (≈ 11%). The low interface value of the NP 9 nm sample can be related with the formation of clusters and aggregation of Fe_3O_4 nanoparticles. The RD composite sample revealed ≈50 % of interface value, indicating the anisotropic structure of Fe_3O_4 rods potentiates the existence of more amount of polymer in the nanostructure/polymer interface. Such interface is related with the amount of polymer that is electrostatically interacting the surface of the nanostructure. By comparing figures 2.15b and 2.16b, and contrary to other studies [83], there is no obvious relation between β-phase content and interface values.

Finally, Zeta potential analysis (figure 2.17a) was used to evaluate the electrostatic charge on the surface of the nanostructures, in order to determine its

influence on the β-phase nucleation mechanism, since previous studies indicated this as the main factor responsible for the β-phase nucleation (figure 2.17b) [21, 25, 26, 85].

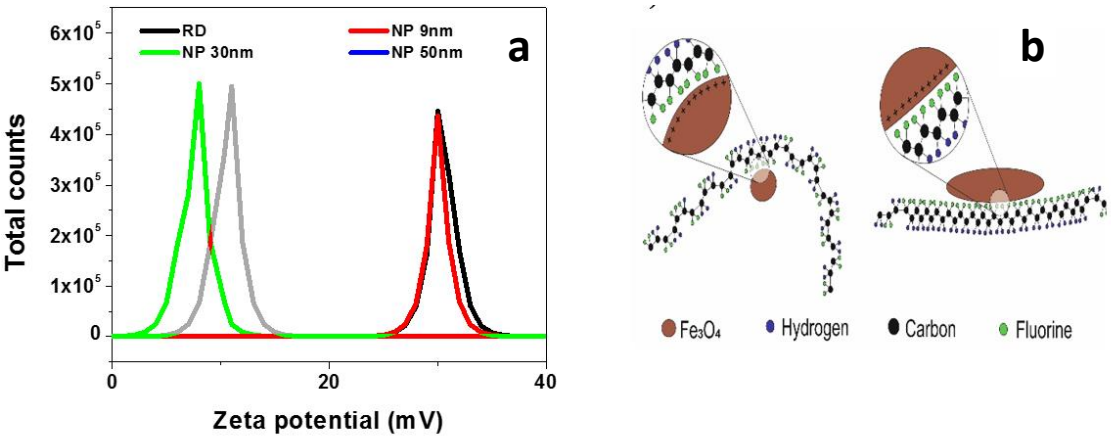

Figure 2.17. a) Zeta potential of the different Fe_3O_4 nanostructures; b) schematic representation of the β-phase nucleation mechanism through positive Ion−CF_2 dipole interactions.

All nanostructures revealed positive surface charges, being 8 and 11 mV the values for NP 30 nm and NP 50 nm, respectively. Interestingly both NP 9 nm and RD nanocomposite revealed the same value of surface charge: 30 mV.

Previous works [53, 54] showed that negative surfaces charges (-22 mV) on magnetic nanoparticles promoted F(β)≈20 % on P(VDF) composites with the same nanoparticles content (1 wt.%). The low value of F(β) (≤ 10 %) found for the present NP composites is thus related to the positive values of zeta-potential, once the electrostatic interaction between the positively charged magnetic spherical nanoparticles and the polymer is less intense. The low β-phase nucleation observed for NP nanocomposites confirms once again the previous experimental evidences detected CFO@cetrimonium bromide and CFO@citric acid magnetic P(VDF) nanocomposites: magnetic spherical nanoparticles with positive surface charge are not suitable for the nucleation of the β-phase of the polymer [19, 54]. Further, this fact is independent of the size of the spherical NP. On the other hand, the positively surface charged Fe_3O_4 rods (30 mV) reveals a F(β) of ≈70 %. This interesting fact indicates an underlying factor other than the electrostatic interaction between nanofillers and polymer for the β-phase formation on P(VDF) nanocomposites. The advantageous β-phase formation by Fe_3O_4 NRs with

respect to their spherical counterparts indicates directly at the relevance of the shape on the β-phase formation mechanism. Thus, it is possible to highlight that the crystallization of P(VDF) in its β-phase through positive Ion−CF_2 dipole interactions is assisted via nanostructures (in the form of substrates or templates) endowed with 1D (rod/tube) or 2D (planar) geometry through the organization of bonding sites, once β-phase conformation can extend beyond local ordering [74] (figure 2.17b). Through arranged bonding sites, β-phase conformation can be induced and extended. In this way, can now be understood that radial intermolecular interaction surrounding positively charged Fe_3O_4 nanoparticles may not be able to retain the polar conformation in long range order with competing entropy [74]. However, the Fe_3O_4 rod shape is capable to induce such β-phase conformation beyond the local ordering, thus leading to the formation of the polar β-phase along most of the polymer crystalline phase. Additionally, confinement effects on the crystallization of the P(VDF) with NRs fillers may allow a long range arrangement that optimizes the interaction between fillers and polymer chains, leading to the P(VDF)'s β-phase [74, 75].

In this way it is possible to conclude that: a) negatively charged nanofillers promote the β-phase of P(VDF) nucleation thought negative Ion−CH_2 dipole Interactions; b) nanoparticles with positive surface charge fail to nucleate the β-phase of P(VDF) and; c) rod or planar nanofillers with positive surface charge assist the nucleation of β-P(VDF) thought positive Ion−CF_2 dipole interactions, favored by confinement effects.

Such conclusion is supported by the data of the present work and by other reported cases in the literature: a) negatively charged ferrite nanoparticles nucleate the β-phase of the polymer and positively charged ferrite nanoparticles failed to induce the polar β-P(VDF) [19, 20, 53, 54]; b) nearly spherical Ag and $BaTiO_3$ cannot improve the β-phase formation [86, 87]; c) multi-walled carbon nanotubes promote the β-phase growth even before post-processing [88]; d) graphene induces polar phase formation [89]; e) optimized β-phase formation by m-SiO_2 NRs when compared to their spherical counterparts [74] and f) flat surface of organoclays facilitates the β-phase formation on P(VDF) composites [26]. Hence, both anisotropic shape and negatively charged surfaces benefit the β-phase conformation in P(VDF) nanocomposites.

2.5. Development of anisotropic magnetoelectric polymer composites

In this study, the anisotropy of the ME response [90] was obtained by the introduction of magnetic nanosheets of δ-FeO(OH) and CoFeO(OH) in a P(VDF-TrFE) piezoelectric matrix.

The ME effect on the δ-FeO(OH)/P(VDF-TrFE) composites will not arise in the traditional way, by the coupling between the magnetostriction and piezoelectricity, but instead by the alignment of the δ-FeO(OH)nanosheets, as a response to the applied magnetic field, on the P(VDF-TrFE) matrix.

On the other hand, novel high magnetostrictive anisotropic nanofillers are developed by doping FeO(OH) nanosheets with the largest room-temperature magnetostrictive pure element, Cobalt [91], thus allowing the fabrication of Co(II)Fe(III)-O(OH)/P(VDF-TrFE) composites with high ME anisotropic response. Thus, the CoFeO(OH)/P(VDF-TrFE) composite with anisotropic and optimized ME response will allow its implementation into anisotropic sensor/actuator applications especially on innovative magnetic compasses [3, 92, 93].

Nanoparticles

X-ray diffraction was used for nanosheet characterization [94].

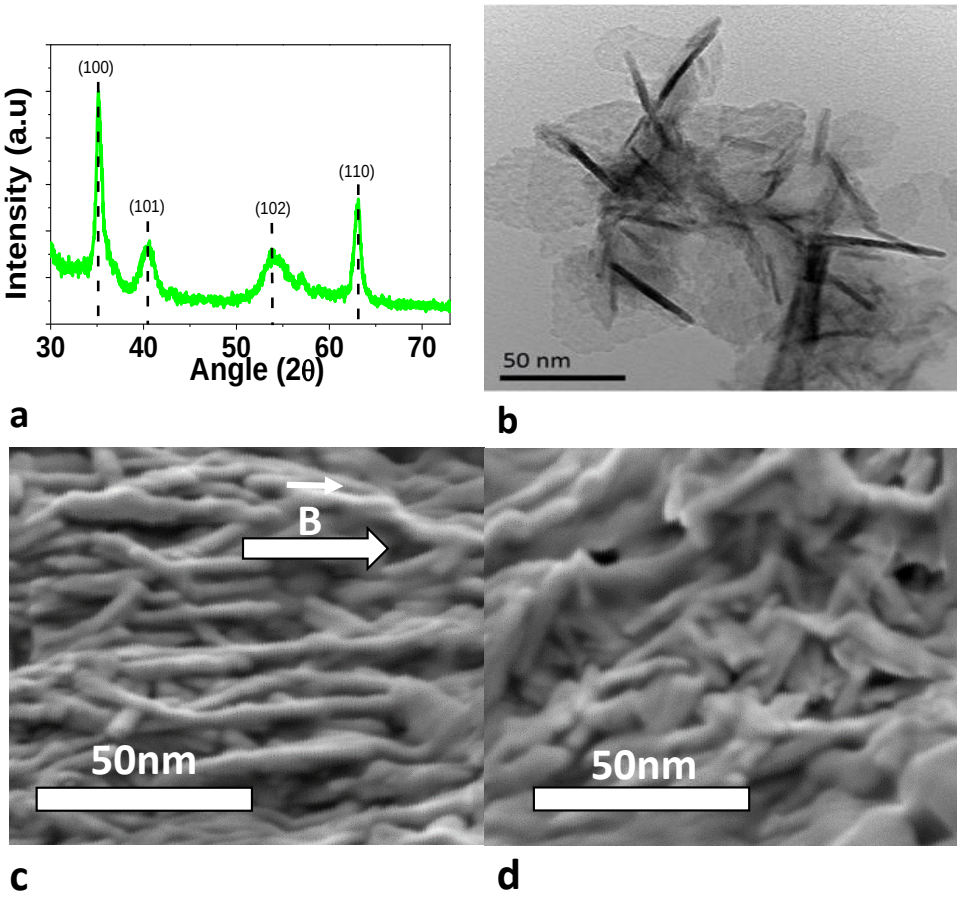

Figure 2.18. a) X-ray powder diffraction patterns of δ-FeO(OH) nanosheets; b) Representative TEM images of the nanosheets; c) L-alignment of the δ-FeO(OH) nanosheets within the P(VDF-TrFE) matrix; d) Randomly distributed δ-FeO(OH) nanosheets within the P(VDF-TrFE) matrix.

Figure 2.18a displays the X-ray patterns of the synthesized nanopowders, showing the typical characteristic structural parameters of the δ-FeO(OH) phase, with reflections corresponding to planes (100), (101), (102) and (110) [95]. The morphology of the δ-FeO(OH) nanosheets was monitored by TEM, whose images (figure 2.18b) revealed an anisotropic sheet structure with dimensions of the order of ≈ 50 nm x 70 nm x 5 nm. Such anisotropy will allow the magnetic alignment of the nanosheets [96, 97]. SEM images (figure 2.18c-d) reveal the alignment of δ-FeO(OH) within the polymer matrix when the δ-FeO(OH)/ P(VDF-TrFE) composites were prepared under a DC magnetic field (figure 2.18c) during the material processing. Further, a random

nanoparticle distribution is observed in the δ-FeO(OH)/P(VDF-TrFE) composites not submitted to the DC magnetic field during processing, as shown by the random microstructural features of figure 2.18d, when compared to the oriented ones on figure 2.18c. At lower magnifications the nanoparticles are not observed (and, therefore, the information about nanoparticle orientation) and the same typical morphology of P(VDF-TrFE) processed by solvent evaporation at 80 °C is obtained for all samples [55].

The synthesized CoFeO(OH) nanosheets were characterized by TEM (figures 2.19a-b), XRD (figures 2.19c-d), magnetization measurements at room temperature (figure 2.19e) and ZFC-FC magnetization measurements (figure 2.19f).

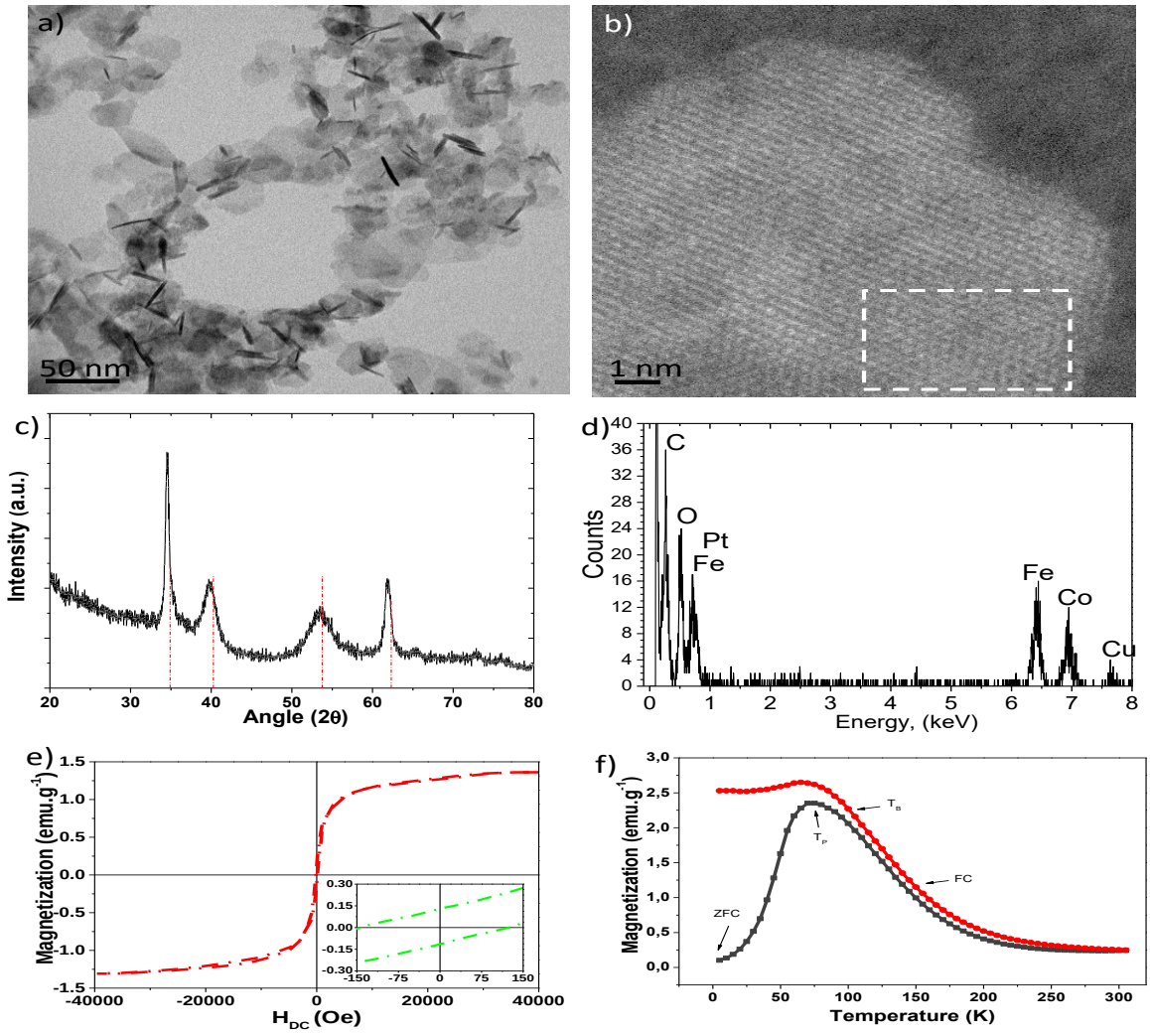

Figure 2.19. CoFeO(OH) nanosheets characterization: a) Representative TEM image; b) Cs-corrected HR-STEM-HAADF image; c) X-ray powder diffraction patterns of as-made nanosheets and standard JCPDS No. 14-00558; d) EDS analysis of the selected area in figure 2.19b; e) Hysteresis loops at room temperature for the CoFeO(OH) nanosheets powder and f) ZFC-FC magnetization.

The production of CoFeO(OH) nanosheets was achieved using a novel synthesis strategy based on a slug-flow microfluidic system [49, 98]. This approach allows a precise control of the reaction conditions (reaction time, temperature, reactants concentration, and stoichiometry), and its high surface-area-to-volume ratio and mixing characteristic help to mitigate temperature and concentration in homogeneities. This versatile reactor enables the flow segmentation using air slugs which have a double role: 1) Promote mixing by the recirculating flows inside the fluid segments [99]; 2) Provide the oxidative environment to promote the anisotropic growth of nanostructures [49, 100].

Considering previous results to produce feroxyhyte, a new study of synthesis parameters was performed, achieving the most stable and homogenous FeCo based nanomaterials at a residence time of 1 min and 100 °C. TEM characterization reveals that the air-segmented flow microfluidic reactor enables the fast and controlled production of sheet shaped nanostructures with dimensions of the order of ≈ 40 nm x 60 nm x 5 nm (100 measurements) (figure 2.19a).

HR-STEM images obtained with a High Angle Annular Dark Field (HAADF) detector show that the nanostructures present a high crystalline structure, but there is not HAADF z-contrast related with a segregation of Fe and Co atoms on the surface of the nanosheets (figure 2.19b). This implies that Fe and Co atoms are homogenously distributed. The chemical composition was studied by EDS analysis, proving the presence of both elements (figure 2.19d). Further, XRD pattern of produced nanosheets correspond to crystalline structure of cobalt iron oxide-hydroxide Co(II)Fe(III)-O(OH) (CoFeO(OH)) (JCPDS No. 14-00558); Figure 2.19c. Since the magnetic properties of the magnetostrictive phase are critical aspects in the development of ME composites [15, 30], CoFeO(OH) magnetization was measured at room temperature (figure 2.19e) and as a function of temperature (figure 2.19f).

The room temperature hysteresis loops of the CoFeO(OH) powders reveal almost absence of hysteresis, remanence and coercivity (≈100 Oe), evidencing a superparamagnetic behavior. In this way, since room temperature is above the blocking temperature, magnetic moments of the nanosheets are free to rotate in response to the applied magnetic field, allowing their magnetic alignment in the P(VDF-TrFE) matrix.

The magnetization processes irreversibility degree is high, as evidenced by the separation of FC and ZFC lines at 100 K. Such irreversibility in nanostructures ascends from the struggle between the energy needed for a structure reorientation and the magnetoelasticity, shape and crystalline anisotropy energies [54]. The bifurcation between the two curves happens at a temperature TB (100 K) that corresponds to the blocking temperature of the biggest magnetic structures in the assembly. Below T_B, on the ZFC curve at a temperature TP (70 K) can be found a maximum that delimits the blocking of all structures (independently of the size). This sharp peak pronounces a narrow CoFeO(OH) sheets size distribution, confirming also the good synthesis control achieved in the microfluidic reactor. The value of T_B also specifies a lower temperature frontier for the superparamagnetic behavior. Therefore, CoFeO(OH) has a clear superparamagnetic behavior at room temperature (≈300 K) as already shown in the room temperature magnetic hysteresis loops.

The magnetic behavior of the obtained δ-FeO(OH)/P(VDF-TrFE) composites is represented in figure 2.20.

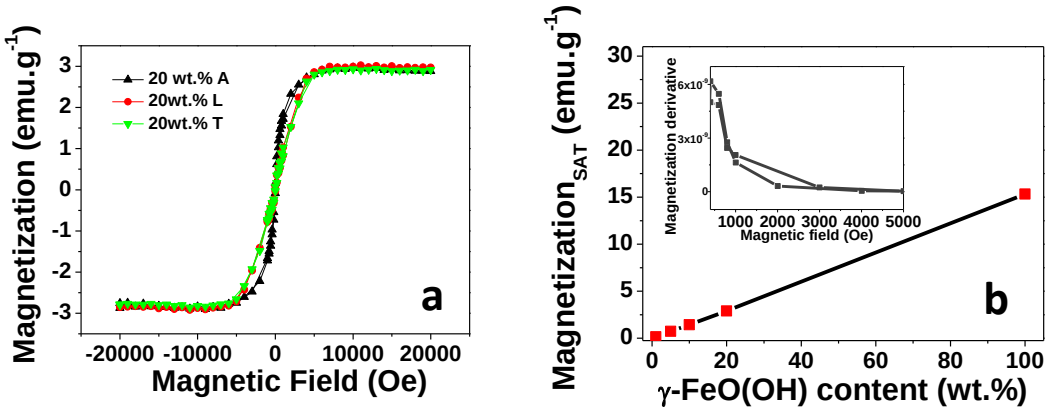

Figure 2.20. a) Room temperature hysteresis loops for the composites with 20 wt.% of δ-FeO(OH) with A, L and T alignments; b) δ-FeO(OH) wt.% dependent M_S. The inset shows the derivative of the magnetization curves of the aligned samples.

The shape and magnetization maximum value (3 emu.g^{-1}), which corresponds to ≈ 20 % of the maximum magnetization of the pure δ-FeO(OH) nanosheets of the hysteresis loops measured in the sample with randomly oriented nanosheets (A samples) demonstrate that the magnetic response is directly proportional to filler

content (figure 2.20a). A very small difference is detected between the randomly oriented sample and the oriented samples (L and T) which can be attributed to the magnetization through easy and hard magnetization directions, respectively [39, 40]. As expected, for all compositions, the magnetization saturation of the composite increases with increasing δ-FeO(OH) content (figure 2.20b). The nanocomposites showing negligible magnetic coercivity and remanence and a magnetization saturating at 8000 Oe.

Because piezoelectricity is a fundamental requirement on ME composites, the piezoelectric response as a function of the δ-FeO(OH) nanosheets content and over time for the δ-FeO(OH)/P(VDF-TrFE) composites are shown in figure 2.21.

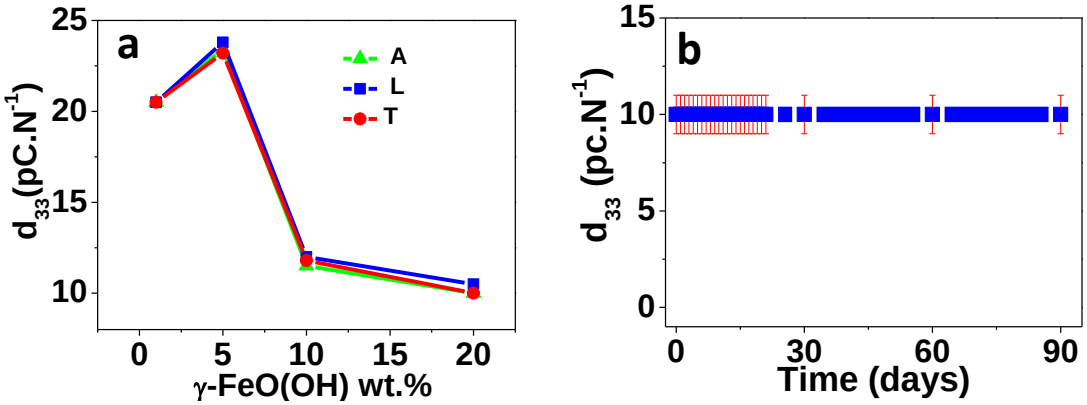

Figure 2.21. a) δ-FeO(OH) wt.% dependent modulus of d_{33} for the samples with nanosheets with A, L and T orientations; b) modulus of the piezoelectric response over time measured for all the δ-FeO(OH)/P(VDF-TrFE) composites with 20 wt.% nanosheets content. It should be noted that the d_{33} value is negative and it is given as the modulus in the figures.

Figure 2.21a reveals first an increase in the piezoelectric response with increasing nanosheets content, as a result of the increased dipolar orientation of the polymer matrix near the interface [29], due to the strong electrostatic interactions, reaching a maximum value of ≈24 pC.N^{-1} (in modulus) in the sample with 5 wt.% of δ-FeO(OH). This effect is related to nanoscale polarization contributions that have been proven to increase the piezoelectric response [101-104]. With increasing filler concentration, the piezoelectric response decreases due to an increasingly defective and stiffer polymer matrix [29, 105]. Additionally, the piezoelectric response of the polymer matrix is fully

dependent on the content of δ-FeO(OH) filler and independent of the filler orientation. Such piezoelectric response is stable over time, until at least 90 days (figure 2.21b).

The ME response of the composite with 20 wt.% of δ-FeO(OH) nanosheets is represented as a function of the intensity of the applied DC magnetic field and the magnetic field direction (figure 2.22).

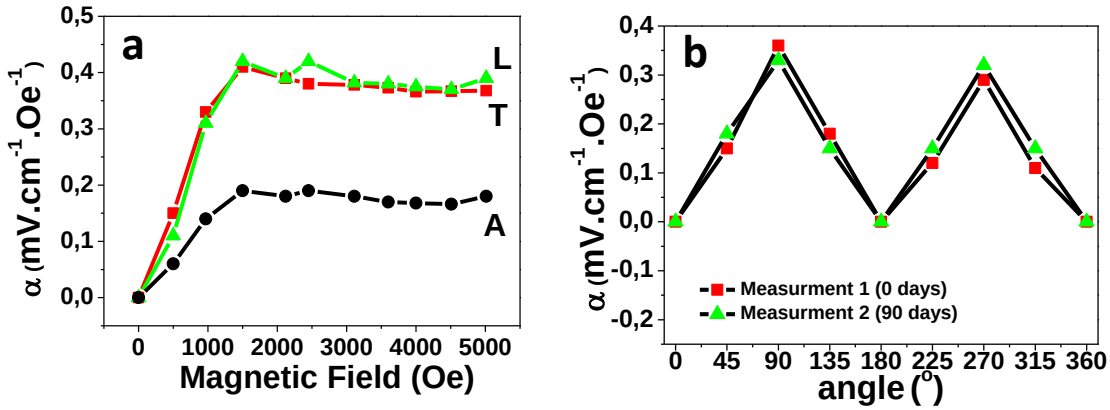

Figure 2.22. a) ME response α as a function of the applied magnetic field (parallel to the nanosheet length direction) for the T, L and A aligned composites, with 20 wt.% of nanosheets. b) ME response α, for the composite T aligned, with 20 wt.% of nanosheets, as a function of the angle between the length direction of the δ-FeO(OH) nanosheets and the DC magnetic field direction.

Figure 2.22a shows that the α value increases with the applied DC magnetic field until reaching its maximum value (0.4 $mV.cm^{-1}.Oe^{-1}$) at ≈1800 Oe, with the α value remaining approximately constant with magnetic field increase.

The samples with 1, 5 and 10 wt.% δ-FeO(OH) content (with A, L and T alignments) show no ME response, i.e. the response is too small to be observed in the used experimental setup. On composites with 20 wt.% δ-FeO(OH), samples with L-alignment exhibit similar ME response to the samples with T-alignment; on the other hand, samples with no alignment (A samples) show ≈50 % lower ME response (figure 2.22a).

The highest ME responses were observed when the DC magnetic field was applied perpendicularly to the δ-FeO(OH) length direction alignment (90° and 270°); no ME response was observed when the magnetic field was applied parallel to the alignment (0°, 180° and 360°) and an intermediate ME response was observed when the

magnetic field was applied at angles of 45°, 135°, 225° and 315° relative to the δ-FeO(OH) alignment (figure 2.22b). Those observations are maintained for L aligned samples. The ME response of the samples has been measured to be stable, as the piezoelectric response, up to 90 days, with no relevant variation or aging over time. The ME response angle sensitivity, such as the one represented on figure 2.22b, recently proved its applicability on innovative anisotropic magnetic sensors [37]. For practical applications and in order to distinguish, for example, the 45° angle from the 135° one, both with the same ME response, two ME materials, X and Y, should be integrated within the same magnetic sensor with a well-known angle between them, the comparison of the materials response allowing the unambiguous determination of the magnetic field direction.

Such behavior can be related with the impossibility/difficulty of the magnetic moments reorientation and with the anisotropy of the magnetization resulting from the crystallographic restrictions for specific directions [106]. Additionally, it is observed that the ME response saturates at ≈1800 Oe, at the same magnetic field value where the magnetization derivative reaches its minimum (inset of figure 2.20b). For higher fields, and contrary to what happens with the usual ME composites (constituted by piezoelectric and magnetostrictive materials) [3, 15], the ME response does not decrease, maintaining its maximum value. In this way, increasing the magnetic field from ≈1800 Oe will cause no additional substantial magnetization on δ-FeO(OH) nanosheets [107], no rotation/movement is promoted, no significant stress is induced on P(VDF-TrFE) and as a consequence no additional ME response is detected. It should be noted that this represents a novel ME response with respect to the previously reported in the literature.

After preparation of the aligned CoFeO(OH)/polymer composites through the mechanism proposed on [98], the magnetic and ME response of the sensor was evaluated (figure 2.23).

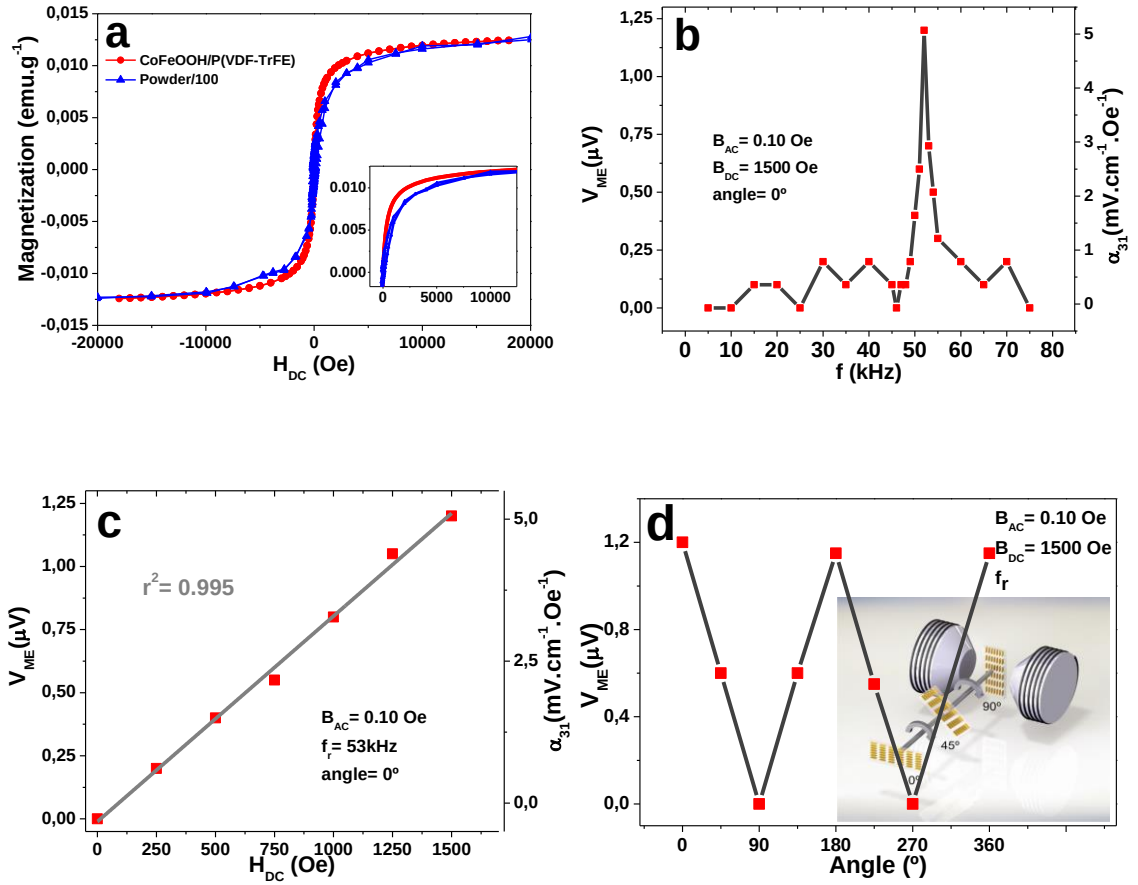

Figure 2.23. a) Room temperature hysteresis loops for the composite in comparison with the pure powder form; b) ME voltage (V_{ME}) and ME coefficient (α_{31}) as a function of the frequency; c) Room temperature ME voltage (V_{ME}) and ME coefficient (α_{31}) as a function of the H_{DC}; d) Room temperature ME response as a function of the angle between HDC and the composite length.

Figure 2.23a shows the magnetization of the pure powder divided by 100, in order to allow comparison of the magnetic response of the same quantity of CoFeO(OH) nanosheets inside the polymeric composites and in the pure powder form. On the CoFeO(OH)/P(VDF-TrFE) sample, measured in parallel with the DC magnetic field, the magnetization process is slightly faster with the applied field while in the powder sample magnetization process is slightly slower due to the magnetization through easy/hard directions [39, 40]. Additionally the maximum magnetization value (1.26×10^{-2} emu.g^{-1}) on the composite samples corresponds effectively to 1 % of the maximum magnetization value (1.26 emu.g^{-1}) of pure CoFeO(OH) powder, indicating that the P(VDF-TrFE) matrix has no influence on the magnetic response of the nanosheets. ME measurements not

only will validate the use of the CoFeO(OH)/P(VDF-TrFE) composite as an innovative magnetic sensing material but also allows to quantify the magnetostriction of the CoFeO(OH) nanostructures. Such ME measurements as a function of the frequency (figure 2.23b) reveal that the electromechanical resonance of the composite is ≈53 kHz as a result of the length along the resonant direction (7 mm), composite density (1800 $kg.m^{-3}$) and Young's modulus (0.5 GPa) values [29]. Once the ME response was optimized at the resonance frequency of the composite, its response as a function of the H_{DC} magnetic field was evaluated on figure 2.23c. Such measurements were performed in the H_{DC} range from 0 to 1500 Oe, once between those magnetic field values the magnetic (and as a consequence the ME) response shows a linear behavior, which is of interest for the development of polymer-based ME sensors [108]. The high r^2 value (0.995) demonstrates the good linearity of the developed ME sensor, being among the best values reported in the literature [109]. It was found that the ME response increases with increasing magnetic field due to increasing effective piezomagnetic coefficient up, until the optimal H_{DC} is achieved [98].

Higher contents of CoFeO(OH) nanosheets would lead to an increase of the produced ME voltage, on the other hand, for the 1wt.% content sample, the voltage is already high enough to be detected and eventually amplified by interface electronics, and consequently there is no need for using higher concentrations of CoFeO(OH) once this would increase the cost and decrease the flexibility of the magnetic sensor [52].

In order to validate the use of the CoFeO(OH)/P(VDF-TrFE) composites as magnetic compasses and sensors, the ME response was studied at the 53 kHz resonance frequency as a function of the H_{DC} direction, in the experimental setup schematically represented in the inset of figure 2.23d. Such setup allows the rotation of the sample and therefore the orientation of the fillers with respect to the applied magnetic field. Figure 2.23d shows that for the CoFeO(OH)/P(VDF-TrFE) sample the maximum V_{ME} of 1.20 μV is obtained for 0, 180 and 360° (where the magnetic fields has the same direction of the nanosheet length) and a minimum V_{ME} of 0 mV is obtained for 90 and 270 degrees (where the magnetic fields and the nanosheet length are perpendicular).

Since for the CoFeO(OH)/P(VDF-TrFE) composite sample the magnetostrictive response is optimized along the length direction of the composite (resulting from the

magnetic alignment of the nanosheets), when the H_{DC} is applied along the perpendicular direction of the fillers, no ME response is observed.

On the basis of equations 2.1 and 2.2, is possible to determine the strain produced by the rotation of the δ-FeO(OH) nanosheets inside the polymer matrix (table 2.2).

Table 2.2. α, mV, d_{33}, ε, E_Y, l, w, and t values used to determine λ and dS/dH.

Alignment	α ($mV.cm^{-1}.Oe^{-1}$)	mv	$\|d_{33}\|$ $pC.N^{-1}$	ε	E_Y GPa	w × l × t (mm×mm×μm)	ds/dH $\times10^{-12}$	λ ppm
L	0.42	0.08	11	12	1.14	6.5 × 12.5 × 50	4.27	0.51
T	0.41						4.17	
A	0.19						1.93	0.23

The results from table 2.2 reveal small strains caused by the rotation of the δ-FeO(OH) nanosheets on P(VDF-TrFE) (≈0.2-0.5 ppm) when compared to the typical strains that are transmitted to the piezoelectric polymers by magnetostrictive nanoparticles. Nevertheless, this new ME concept allows the development of polymer-based anisotropic sensors that meet all the most challenging and innovative requirements of the actual magnetic field sensors industry [3, 36-38].

The obtained ME response of CoFeO(OH)/P(VDF-TrFE) is fully ascribed to the anisotropic behaviors of both q and λ in the CoFeO(OH) fillers that strongly depend on the angle of the applied H_{DC} [5, 110, 111].

Finally, equations 2.1 and 2.2, and the performed measurements allow determination of the effective magnetostrictive coefficient (λ_E) of the CoFeO(OH) nanosheets following the procedure introduced in [30].

Table 2.3. α, mV, d_{33}, ε, E_Y, l, w, and t values used to determine λ_E and dS/dH and a comparison with the magnetostrictive properties of CFO nanoparticles and δ-FeO(OH) nanosheets.

NP	Matrix	α $mV.cm^{-1}Oe^{-1}$	m_v	Ref.	d_{33} $pC.N^{-1}$	ε	E_Y GPa	w×l×t mm×mm×μm	ds/dH ($\times10^{-9}$)	λ_E ppm
CFO	P(VDF-TrFE)	3.25	0.02	[15]	23	11	0.80	6.5 × 12.5 × 50	1.09	217
CoFeO(OH)-R		2.50	0.01	This work	30	10		5×7× 25	2.08	249
CoFeO(OH)		5.10							4.25	507
δ-FeO(OH)-R		0.19	0.08	[98]	11	12	1.14	6.5×12.5×50	0.002	0.23
δ-FeO(OH)-L		0.42							0.004	0.51

Table 2.3 shows that the CoFeO(OH) nanosheets present a λ_E of the same order of magnitude of the high magnetostrictive CFO nanoparticles. Further, a CoFeO(OH)-R/P(VDF-TrFE) composite with CoFeO(OH) nanosheets randomly oriented on the polymer matrix (data not shown) has been added to comparison, allowing to verify that the effective magnetostriction is strongly optimized with the magnetic alignment of the CoFeO(OH) nanosheets.

Comparing the ME performance of both magnetostrictive fillers, CoFeO(OH) and CFO, in the same piezoelectric matrix (P(VDF-TrFE)), and with the same filler content (1 wt.%), the higher ME response on CoFeO(OH)/P(VDF-TrFE) composites (5.1 $mV.cm^{-1}.Oe^{-1}$), relatively to the CFO/P(VDF-TrFE) composites (≈0.7 $mV.cm^{-1}.Oe^{-1}$), is noticed.

Additionally, the previously reported anisotropic ME response of δ-FeO(OH)/P(VDF-TrFE) composites is three orders smaller than the one found in the present study. This can be explained by the small λ_E of δ-FeO(OH) (0.5 ppm) emerging from the magnetic rotation of δ-FeO(OH) nanosheets within the piezoelectric P(VDF-TrFE) polymer matrix.

2.6. Conclusions

ME film nanocomposites were successfully produced using P(VDF-TrFE) as piezoelectric phase and CFO nanoparticles as magnetostrictive phase by two different solvent casting methods including ultrasound bath and surfactation. It was demonstrated that no differences were observed in the piezoelectric, magnetic and ME response of the nanocomposites when the two distinct dispersion methods were compared, being these responses independent of the filler size for filler sizes up to 500 nm. Key parameters in the ME composite preparation were found to be filler content and distribution, this fact being of special interest for industrial large scale processes, in which feasibility for fabrication of smart structures is one of the main tasks.

Fe_3O_4 nanoparticles were successfully synthesized with 9, 30 and 50 nm of average size and 167, 17 and 26 ppm magnetostriction, respectively. Fe_3O_4/P(VDF-TrFE) ME nanocomposites were produced with the different nanoparticles, leading to nanocomposites with ME voltage coefficients (α_{31}) of 920 (9 nm), 100 (30 nm) and 150 (50 nm) $\mu V.cm^{-1}.Oe^{-1}$.

Thus, a strong increase of the magnetostriction and the ME response is obtained for the nanocomposite with 9 nm nanoparticles, which is related to the increase in unit cell volume with the reduction in particle size of the Fe_3O_4 particles that implies an increase in Fe^{2+} content in the sample. In this way, it is shown that it is possible to tailor and optimize the magnetostriction and ME response at the nanoscale, with large potential applications in the areas of biomedicine and sensors and actuators.

Beyond that, Fe_3O_4 NRs were also synthetized. These NRs a simple and efficient method to synthesize β-P(VDF) films was developed. The effects of surface charge and filler structure on the crystallization behavior of P(VDF) were systematically studied by using two types of nanostructures, Fe_3O_4 NRs and spherical nanoparticles of different sizes, with distinct surface charges, in order to study, isolate and discuss the effects of the different ion−dipole interactions, size and shape on the nucleation of the β-phase of P(VDF).

Having almost the same interface values (≈10 %), different Fe_3O_4/P(VDF) composites exhibited distinct β-phase values. Fe_3O_4 nanoparticles with different sizes and distinct zeta potential values; 9 nm (30 mV), 30 nm (8 mV) and 50 nm (11 mV) failed to induce high fraction values of β-phase within the composites. In contrast, Fe_3O_4 rods (30 mV) nucleated ≈70 % of β-P(VDF) within the nanocomposites. When compared to their spherical nanoparticle counterparts, the use of Fe_3O_4 NRs has the advantages of anisotropic shape and organized crystallization that direct polar molecular conformation towards oriented growth of β-P(VDF). Besides optimizing intermolecular interaction, NRs promote a confinement effect essential to induce oriented ordering of molecular conformation towards long range order. The proposed β-phase nucleation mechanism could be used to unambiguously explain the existing controversy in current literature reports for the β-phase nucleation on P(VDF) nanocomposites and can be taken to advantage for the crystallization of β-P(VDF) form with a variety of intermolecular interactions, which largely benefits and dynamizes current development in P(VDF) based materials for electroactive devices applications.

δ-FeO(OH)/P(VDF-TrFE) and CoFeO(OH)/P(VDF-TrFE) ME composites have been produced by a simple low-temperature processing method. The nanosheets fillers have been introduced in different filler contents and alignment states (random, transversal

and longitudinal). The piezoelectric response (10-24 $pC.N^{-1}$), the shape and magnetization maximum value (3 $emu.g^{-1}$) depend on δ-FeO(OH) content. The obtained ME voltage coefficient, with a maximum of ≈0.4 $mV.cm^{-1}.Oe^{-1}$, depends on filler content and alignment state as well as on both incident magnetic field direction and intensity. Further, a new ME effect is proposed based on the magnetic rotation of the δ-FeO(OH) nanosheets inside the piezoelectric P(VDF-TrFE) polymer matrix. As a conclusion, polymer composites suitable to be used as magnetic field sensor for advanced applications, were developed.

As shown, new CoFeO(OH) highly magnetostrictive (λ=507 ppm) and anisotropic nanostructures were synthesized by a coprecipitation method using a modified gas-slugs microfluidic system. The microfluidic approach enables to grow anisotropic FeCo based nanostructures in a reproducible and continuous way under a time scale of 1 min. Further, flexible CoFeO(OH)/P(VDF-TrFE) composites reveal an interfacial ME coupling strongly dependent on the angle between H_{DC} and CoFeO(OH) length direction, with a maximum α_{31} of 5.10 $mV.cm^{-1}.Oe^{-1}$. The high magnetostriction, anisotropic ME magnetic sensing capability and good linearity (r^2 value =0.995) allows the use of CoFeO(OH)/P(VDF-TrFE) composites in polymer-based magnetic sensor devices, actuators and in the biomedical field.

2.7. References

1. Nan, C.-W., et al., *Multiferroic magnetoelectric composites: Historical perspective, status, and future directions.* Journal of Applied Physics, 2008. 103(3): p. 031101.
2. Zhou, Z., et al., *Low-temperature spin spray deposited ferrite/piezoelectric thin film magnetoelectric heterostructures with strong magnetoelectric coupling.* Journal of Materials Science: Materials in Electronics, 2014. 25(3): p. 1188-1192.
3. Martins, P. and S. Lanceros-Méndez, *Polymer-Based Magnetoelectric Materials.* Advanced Functional Materials, 2013. 23(27): p. 3371-3385.
4. Lam, K.H., C.Y. Lo, and H.L.W. Chan, *Post-curing effect on magnetoelectric performance of single PZT rod/continuous Terfenol-D fiber/epoxy 1-1-3 composites.* Journal of Materials Science, 2012. 47(6): p. 2910-2914.
5. Dong, X.W., et al., *Ultra-sensitive detection of magnetic field and its direction using bilayer PVDF/Metglas laminate.* Sensors and Actuators A: Physical, 2009. 153(1): p. 64-68.
6. Zhang, J.X., et al., *The effect of magnetic nanoparticles on the morphology, ferroelectric, and magnetoelectric behaviors of CFO/P(VDF-TrFE) 0–3 nanocomposites.* Journal of Applied Physics, 2009. 105(5): p. 054102.
7. Martins, P., A.C. Lopes, and S. Lanceros-Mendez, *Electroactive phases of poly(vinylidene fluoride): Determination, processing and applications.* Progress in Polymer Science, 2014. 39(4): p. 683-706.
8. Hazra, S. and N.N. Ghosh, *Preparation of Nanoferrites and Their Applications.* Journal of Nanoscience and Nanotechnology, 2014. 14(2): p. 1983-2000.
9. Jia, Z. and R.D.K. Misra, *Micromagnetic modelling of new generation of FePt and FeRh nanostructures for heat assisted magnetic recording.* Materials Technology, 2011. 26(4): p. 200-205.
10. Rana, S., et al., *On the suitability of nanocrystalline ferrites as a magnetic carrier for drug delivery: Functionalization, conjugation and drug release kinetics.* Acta Biomaterialia, 2007. 3(2): p. 233-242.
11. Jia, Z. and R.D.K. Misra, *Magnetic sensors for data storage: perspective and future outlook.* Materials Technology, 2011. 26(4): p. 191-199.

12. Gubbala, S. and R.D.K. Misra, *Magnetic behaviour of nanocrystalline nickel ferrite: Part 2 – Effect of dilution.* Materials Science and Technology, 2006. 22(7): p. 845-851.

13. Jia, Z., N. Seetala, and R.D.K. Misra, *Magnetic behavior of chemically synthesized FePt–FeRh nanostructures.* Physica B: Condensed Matter, 2010. 405(9): p. 2189-2193.

14. Wang, J., et al., *Enhanced magnetoelectric coupling in Pb(Zr0.52Ti0.48)O3 film-on-CoFe2O4 bulk ceramic composite with LaNiO3 bottom electrode.* Journal of Materials Science, 2013. 48(3): p. 1021-1026.

15. Martins, P., et al., *Optimizing piezoelectric and magnetoelectric responses on CoFe 2 O 4 /P(VDF-TrFE) nanocomposites.* Journal of Physics D: Applied Physics, 2011. 44(49): p. 495303.

16. Shi, M., et al., *Magnetoelectric properties of CoFe2O4–Pb(Zr0.52Ti0.48)O3 multilayered composite film via sol–gel method.* Journal of Materials Science, 2011. 46(13): p. 4710-4714.

17. Nan, C.-W., *Magnetoelectric effect in composites of piezoelectric and piezomagnetic phases.* Physical Review B, 1994. 50(9): p. 6082-6088.

18. Devan, R.S., S.B. Deshpande, and B.K. Chougule, *Ferroelectric and ferromagnetic properties of (x)BaTiO 3 + (1 − x)Ni 0.94 Co 0.01 Cu 0.05 Fe 2 O 4 composite.* Journal of Physics D: Applied Physics, 2007. 40(7): p. 1864.

19. Martins, P., et al., *On the origin of the electroactive poly(vinylidene fluoride) [small beta]-phase nucleation by ferrite nanoparticles via surface electrostatic interactions.* CrystEngComm, 2012. 14(8): p. 2807-2811.

20. Roy, S., et al., *Enhanced electroactive [small beta]-phase nucleation and dielectric properties of PVdF-HFP thin films influenced by montmorillonite and Ni(OH)2 nanoparticle modified montmorillonite.* RSC Advances, 2016. 6(26): p. 21881-21894.

21. Yu, L. and P. Cebe, *Crystal polymorphism in electrospun composite nanofibers of poly(vinylidene fluoride) with nanoclay.* Polymer, 2009. 50(9): p. 2133-2141.

22. Li, Y., et al., *Role of Ion–Dipole Interactions in Nucleation of Gamma Poly(vinylidene fluoride) in the Presence of Graphene Oxide during Melt*

Crystallization. The Journal of Physical Chemistry B, 2012. 116(51): p. 14951-14960.

23. Xing, C., et al., *Impact of Ionic Liquid-Modified Multiwalled Carbon Nanotubes on the Crystallization Behavior of Poly(vinylidene fluoride).* The Journal of Physical Chemistry B, 2012. 116(28): p. 8312-8320.
24. Wu, Y., et al., *The Role of Surface Charge of Nucleation Agents on the Crystallization Behavior of Poly(vinylidene fluoride).* The Journal of Physical Chemistry B, 2012. 116(24): p. 7379-7388.
25. Liang, C.-L., et al., *Induced Formation of Dominating Polar Phases of Poly(vinylidene fluoride): Positive Ion–CF2 Dipole or Negative Ion–CH2 Dipole Interaction.* The Journal of Physical Chemistry B, 2014. 118(30): p. 9104-9111.
26. Wang, J., Q. Fu, and Q. Zhang, *Inducing of dominant polar forms in poly(vinylidene fluoride) with super toughness by adding alkyl ammonium salt.* Polymer, 2012. 53(24): p. 5455-5458.
27. Balaji, G., et al., *Giant magnetostriction in magnetite nanoparticles.* Materials Science and Engineering: B, 2012. 177(1): p. 14-18.
28. Tomitaka, A., et al., *Evaluation of magnetic and thermal properties of ferrite nanoparticles for biomedical applications.* Journal of Magnetics, 2011. 16(2): p. 164-168.
29. Martins, P., et al., *Linear anhysteretic direct magnetoelectric effect in Ni 0.5 Zn 0.5 Fe 2 O 4 /poly(vinylidene fluoride-trifluoroethylene) 0-3 nanocomposites.* Journal of Physics D: Applied Physics, 2011. 44(48): p. 482001.
30. Martins, P., et al., *Tailored Magnetic and Magnetoelectric Responses of Polymer-Based Composites.* ACS Applied Materials & Interfaces, 2015. 7(27): p. 15017-15022.
31. Liu, X., et al., *Review on the Synthesis and Applications of Nanomaterials.* Journal of Nanomaterials, 2013. 2013: p. 7.
32. Gawande, M.B., P.S. Branco, and R.S. Varma, *Nano-magnetite (Fe3O4) as a support for recyclable catalysts in the development of sustainable methodologies.* Chemical Society Reviews, 2013. 42(8): p. 3371-3393.

33. Cheng, F.-Y., et al., *Characterization of aqueous dispersions of Fe3O4 nanoparticles and their biomedical applications.* Biomaterials, 2005. 26(7): p. 729-738.

34. Jayakumar, O.D., et al., *Inorganic-organic multiferroic hybrid films of Fe3O4 and PVDF with significant magneto-dielectric coupling.* Journal of Materials Chemistry C, 2013. 1(23): p. 3710-3715.

35. Martins, P., M. Silva, and S. Lanceros-Mendez, *Determination of the magnetostrictive response of nanoparticles via magnetoelectric measurements.* Nanoscale, 2015. 7(21): p. 9457-9461.

36. Gun Lee, D., et al., *Ultra-sensitive magnetoelectric microcantilever at a low frequency.* Applied Physics Letters, 2012. 101(18): p. 182902.

37. Chen, S., et al., *Fabrication and characterization of shape anisotropy AlN/FeCoSiB magnetoelectric composite films.* Ceramics International, 2014. 40(2): p. 3419-3423.

38. Liu, M., et al., *Electric field modulation of magnetoresistance in multiferroic heterostructures for ultralow power electronics.* Applied Physics Letters, 2011. 98(22): p. 222509.

39. Lin, W., et al., *Two-Dimensional Magnetic Field Vector Sensor Based on Tilted Fiber Bragg Grating and <newline/>Magnetic Fluid.* Journal of Lightwave Technology, 2013. 31(15): p. 2599-2605.

40. Oh, Y.S., et al., *Quantitative determination of anisotropic magnetoelectric coupling in BiFeO3–CoFe2O4 nanostructures.* Applied Physics Letters, 2010. 97(5): p. 052902.

41. Ettelt, D., et al., *3D Magnetic Field Sensor Concept for Use in Inertial Measurement Units (IMUs).* Journal of Microelectromechanical Systems, 2014. 23(2): p. 324-333.

42. Chandra Sekhar, B., et al., *Magnetic and magnetostrictive properties of Cu substituted Co-ferrites.* Journal of Magnetism and Magnetic Materials, 2016. 398: p. 59-63.

43. Ribeiro, C., et al., *Proving the suitability of magnetoelectric stimuli for tissue engineering applications.* Colloids and Surfaces B: Biointerfaces, 2016. 140: p. 430-436.

44. Nappini, S., et al., *Magnetically Triggered Release From Giant Unilamellar Vesicles: Visualization By Means Of Confocal Microscopy.* The Journal of Physical Chemistry Letters, 2011. 2(7): p. 713-718.

45. Campelj, S., D. Makovec, and M. Drofenik, *Preparation and properties of water-based magnetic fluids.* Journal of Physics: Condensed Matter, 2008. 20(20): p. 204101.

46. Martins, P., et al., *Nanoparticle Dispersion and Electroactive Phase Content in Polyvinylidene Fluoride/Ni0.5Zn0.5Fe2O4 Nanocomposites for Magnetoelectric Applications.* Journal of Nanoscience and Nanotechnology, 2012. 12(8): p. 6845-6849.

47. Cai, W. and J. Wan, *Facile synthesis of superparamagnetic magnetite nanoparticles in liquid polyols.* Journal of Colloid and Interface Science, 2007. 305(2): p. 366-370.

48. Miguel-Sancho, N., et al., *Development of Stable, Water-Dispersible, and Biofunctionalizable Superparamagnetic Iron Oxide Nanoparticles.* Chemistry of Materials, 2011. 23(11): p. 2795-2802.

49. Larrea, A., et al., *Gas Slug Microfluidics: A Unique Tool for Ultrafast, Highly Controlled Growth of Iron Oxide Nanostructures.* Chemistry of Materials, 2015. 27(12): p. 4254-4260.

50. Mohapatra, J., et al., *Iron oxide nanorods as high-performance magnetic resonance imaging contrast agents.* Nanoscale, 2015. 7(20): p. 9174-9184.

51. Martins, P., et al., *Novel Anisotropic Magnetoelectric Effect on δ-FeO(OH)/P(VDF-TrFE) Multiferroic Composites.* ACS Applied Materials & Interfaces, 2015. 7(21): p. 11224-11229.

52. Martins, P., et al., *Effect of filler dispersion and dispersion method on the piezoelectric and magnetoelectric response of CoFe2O4/P(VDF-TrFE) nanocomposites.* Applied Surface Science, 2014. 313: p. 215-219.

53. Martins, P., C. Costa, and S. Lanceros-Mendez, *Nucleation of electroactive β-phase poly(vinilidene fluoride) with CoFe2O4and NiFe2O4 nanofillers: a new method for the preparation of multiferroic nanocomposites.* Applied Physics A: Materials Science & Processing, 2011. 103(1): p. 233-237.

54. Martins, P., et al., *Role of Nanoparticle Surface Charge on the Nucleation of the Electroactive β-Poly(vinylidene fluoride) Nanocomposites for Sensor and Actuator Applications.* The Journal of Physical Chemistry C, 2012. 116(29): p. 15790-15794.

55. California, A., et al., *Tailoring porous structure of ferroelectric poly(vinylidene fluoride-trifluoroethylene) by controlling solvent/polymer ratio and solvent evaporation rate.* European Polymer Journal, 2011. 47(12): p. 2442-2450.

56. Sencadas, V., et al. *Influence of the processing conditions and corona poling on the morphology of β-PVDF*. in *2005 12th International Symposium on Electrets*. 2005.

57. Israel, C., et al., *Magnetically tuned mechanical resonances in magnetoelectric multilayer capacitors.* Applied Physics Letters, 2009. 95(7): p. 072505.

58. Van Den Boomgaard, J., A.M.J.G. Van Run, and J.V. Suchtelen, *Magnetoelectricity in piezoelectric-magnetostrictive composites.* Ferroelectrics, 1976. 10(1): p. 295-298.

59. Zubkov, A.S., *Impulsive piezoceramic generators with magnetostrictive drive.* Electrical Technology, 1978(2): p. 59-78.

60. Ryu, J., et al., *Magnetoelectric Effect in Composites of Magnetostrictive and Piezoelectric Materials.* Journal of Electroceramics, 2002. 8(2): p. 107-119.

61. Ramesan, M.T., *Fabrication, characterization, and properties of poly(ethylene-co-vinyl acetate)/magnetite nanocomposites.* Journal of Applied Polymer Science, 2014. 131(7): p. n/a-n/a.

62. Righetti, M.C., et al., *Thermal and mechanical properties of PES/PTFE composites and nanocomposites.* Journal of Applied Polymer Science, 2013. 130(5): p. 3624-3633.

63. de Guzman, R.C., et al., *A silicon nanoparticle/reduced graphene oxide composite anode with excellent nanoparticle dispersion to improve lithium ion battery performance.* Journal of Materials Science, 2013. 48(14): p. 4823-4833.

64. Park, D.H., et al., *Effect of multi-walled carbon nanotube dispersion on the electrical and rheological properties of poly(propylene carbonate)/poly(lactic acid)/multi-walled carbon nanotube composites.* Journal of Materials Science, 2013. 48(1): p. 481-488.

65. Li, R., et al., *Application of polymerizable surfactant in the preparation of polystyrene/nano-Fe3O4 composite.* Journal of Wuhan University of Technology-Mater. Sci. Ed., 2010. 25(2): p. 184-187.

66. Luechinger, N.A., et al., *Surfactant-Free, Melt-Processable Metal–Polymer Hybrid Materials: Use of Graphene as a Dispersing Agent.* Advanced Materials, 2008. 20(16): p. 3044-3049.

67. Krishnadas, K.R., P.R. Sajanlal, and T. Pradeep, *Pristine and Hybrid Nickel Nanowires: Template-, Magnetic Field-, and Surfactant-Free Wet Chemical Synthesis and Raman Studies.* The Journal of Physical Chemistry C, 2011. 115(11): p. 4483-4490.

68. Martins, P., et al., *Correlation between Crystallization Kinetics and Electroactive Polymer Phase Nucleation in Ferrite/Poly(vinylidene fluoride) Magnetoelectric Nanocomposites.* The Journal of Physical Chemistry B, 2012. 116(2): p. 794-801.

69. Falqui, A., et al., *A Transmission Electron Microscopy Study of CoFe2O4 Ferrite Nanoparticles in Silica Aerogel Matrix Using HREM and STEM Imaging and EDX Spectroscopy and EELS.* Microscopy and Microanalysis, 2010. 16(2): p. 200-209.

70. Huang, J., et al., *Improving the magnetic resonance imaging contrast and detection methods with engineered magnetic nanoparticles.* Theranostics, 2012. 2(1): p. 86-102.

71. Zhou, Y. and F.G. Shin, *Magnetoelectric effect of mildly conducting magnetostrictive/piezoelectric particulate composites.* Journal of Applied Physics, 2006. 100(4): p. 043910.

72. Priya, S., et al., *Recent advancements in magnetoelectric particulate and laminate composites.* Journal of Electroceramics, 2007. 19(1): p. 149-166.

73. Laletin, V.M. and V.V. Pan'kov, *Influence of powder surface area on the magnetoelectric effect in barium lead zirconate titanate/nickel ferrite composite ceramics.* Inorganic Materials, 2012. 48(1): p. 87-92.

74. Yuan, D., et al., *[small beta] phase PVDF-hfp induced by mesoporous SiO2 nanorods: synthesis and formation mechanism.* Journal of Materials Chemistry C, 2015. 3(15): p. 3708-3713.

75. Garcia-Gutierrez, M.-C., et al., *Understanding crystallization features of P(VDF-TrFE) copolymers under confinement to optimize ferroelectricity in nanostructures.* Nanoscale, 2013. 5(13): p. 6006-6012.

76. Sun, F.-C., et al., *Temperature dependent structural, elastic, and polar properties of ferroelectric polyvinylidene fluoride (PVDF) and trifluoroethylene (TrFE) copolymers.* Journal of Materials Chemistry C, 2015. 3(32): p. 8389-8396.

77. Larrea , A., et al., *Microfluidic Continuous Approaches to Produce Magnetic Nanoparticles with Homogeneous Size Distribution.* International Journal of Chemical, Molecular, Nuclear, Materials and Metallurgical Engineering, 2015. 9: p. 791-798.

78. Hao, R., et al., *Synthesis, Functionalization, and Biomedical Applications of Multifunctional Magnetic Nanoparticles.* Advanced Materials, 2010. 22(25): p. 2729-2742.

79. Wu, C., et al., *Synthesis of Hematite (α-Fe2O3) Nanorods: Diameter-Size and Shape Effects on Their Applications in Magnetism, Lithium Ion Battery, and Gas Sensors.* The Journal of Physical Chemistry B, 2006. 110(36): p. 17806-17812.

80. Thapa, D., et al., *Properties of magnetite nanoparticles synthesized through a novel chemical route.* Materials Letters, 2004. 58(21): p. 2692-2694.

81. Koroleva, L.I., et al., *Effect of oxygen deficiency on the magnetic, electrical, magnetoelectric, and magnetoelastic properties of La1 − x Sr x MnO3 − δ manganites.* Physics of the Solid State, 2008. 50(12): p. 2298-2302.

82. Gregorio, J.R. and M. Cestari, *Effect of crystallization temperature on the crystalline phase content and morphology of poly(vinylidene fluoride).* Journal of Polymer Science Part B: Polymer Physics, 1994. 32(5): p. 859-870.

83. Martins, P., et al., *Interface characterization and thermal degradation of ferrite/poly(vinylidene fluoride) multiferroic nanocomposites.* Journal of Materials Science, 2013. 48(6): p. 2681-2689.

84. Botelho, G., et al., *Relationship between processing conditions, defects and thermal degradation of poly(vinylidene fluoride) in the β-phase.* Journal of Non-Crystalline Solids, 2008. 354(1): p. 72-78.

85. Quickel, T.E., et al., *Mesoporous bismuth ferrite with amplified magnetoelectric coupling and electric field-induced ferrimagnetism.* Nat Commun, 2015. 6.

86. Gao, L., et al., *Large Enhancement in Polarization Response and Energy Storage Properties of Poly(vinylidene fluoride) by Improving the Interface Effect in Nanocomposites.* The Journal of Physical Chemistry C, 2014. 118(2): p. 831-838.

87. Chae, D.W. and S.M. Hong, *Dynamic crystallization behavior, morphology, and physical properties of highly concentrated poly(vinylidene fluoride)/silver nanocomposites.* Journal of Polymer Science Part B: Polymer Physics, 2010. 48(22): p. 2379-2385.

88. Ahn, Y., et al., *Enhanced Piezoelectric Properties of Electrospun Poly(vinylidene fluoride)/Multiwalled Carbon Nanotube Composites Due to High β-Phase Formation in Poly(vinylidene fluoride).* The Journal of Physical Chemistry C, 2013. 117(22): p. 11791-11799.

89. Zhang, L., et al., *Formation of Superhydrophobic Microspheres of Poly(vinylidene fluoride– hexafluoropropylene)/Graphene Composite via Gelation.* Langmuir, 2011. 27(14): p. 8943-8949.

90. Liu, R., et al., *Structure and magnetic properties of low-temperature phase Mn-Bi nanosheets with ultra-high coercivity and significant anisotropy.* Journal of Applied Physics, 2014. 115(17): p. 17A742.

91. Richter, F. and U. Lotter, *On the Volume Magnetostriction of Nickel, Iron, and Cobalt.* physica status solidi (b), 1969. 34(2): p. K149-K152.

92. Wang, Y., J. Li, and D. Viehland, *Magnetoelectrics for magnetic sensor applications: status, challenges and perspectives.* Materials Today, 2014. 17(6): p. 269-275.

93. Basterretxea-Iribar, I., I. Sotés, and J.I. Uriarte, *Towards an Improvement of Magnetic Compass Accuracy and Adjustment.* Journal of Navigation, 2016: p. 1-16.

94. Tan, Y., et al., *Crystallization mechanism analysis of noncrystalline Ni-P nanoparticles through XRD, HRTEM and XAFS.* CrystEngComm, 2014. 16(41): p. 9657-9668.

95. Chagas, P., et al., *δ-FeOOH: a superparamagnetic material for controlled heat release under AC magnetic field.* Journal of Nanoparticle Research, 2013. 15(4): p. 1-7.

96. Ten, E., L. Jiang, and M.P. Wolcott, *Strategies for Preparation of Oriented Cellulose Nanowhiskers Composites*, in *Functional Materials from Renewable Sources*. 2012, American Chemical Society. p. 17-36.

97. Gu, Y. and K.G. Kornev, *Alignment of Magnetic Nanorods in Solidifying Films.* Particle & Particle Systems Characterization, 2013. 30(11): p. 958-963.

98. Gonçalves, R., et al., *Magnetoelectric CoFe2O4/polyvinylidene fluoride electrospun nanofibres.* Nanoscale, 2015. 7(17): p. 8058-8061.

99. Sebastian Cabeza, V., et al., *Size-Controlled Flow Synthesis of Gold Nanoparticles Using a Segmented Flow Microfluidic Platform.* Langmuir, 2012. 28(17): p. 7007-7013.

100. Sebastian, V., S. Basak, and K.F. Jensen, *Continuous synthesis of palladium nanorods in oxidative segmented flow.* AIChE Journal, 2016. 62(2): p. 373-380.

101. Chu, B., et al., *Large enhancement in polarization response and energy density of poly(vinylidene fluoride-trifluoroethylene-chlorofluoroethylene) by interface effect in nanocomposites.* Applied Physics Letters, 2007. 91(12): p. 122909.

102. Guo, D., F. Zeng, and B. Dkhil, *Ferroelectric polymer nanostructures: fabrication, structural characteristics and performance under confinement.* J Nanosci Nanotechnol, 2014. 14(2): p. 2086-100.

103. Guo, D. and N. Setter, *Impact of Confinement-Induced Cooperative Molecular Orientation Change on the Ferroelectric Size Effect in Ultrathin P(VDF-TrFE) Films.* Macromolecules, 2013. 46(5): p. 1883-1889.

104. Guo, D., I. Stolichnov, and N. Setter, *Thermally Induced Cooperative Molecular Reorientation and Nanoscale Polarization Switching Behaviors of Ultrathin Poly(vinylidene fluoride-trifluoroethylene) Films.* The Journal of Physical Chemistry B, 2011. 115(46): p. 13455-13466.

105. Li, J., et al., *Nanocomposites of Ferroelectric Polymers with TiO2 Nanoparticles Exhibiting Significantly Enhanced Electrical Energy Density.* Advanced Materials, 2009. 21(2): p. 217-221.

106. Aida, T., et al., *Relationship Between Magnetostriction and Magnetic Domain Structure in Fe-Based Alloy Single-Crystal Films With bcc(001) Orientation.* IEEE Transactions on Magnetics, 2014. 50(11): p. 1-4.

107. Yuan, J., et al., *Alignment of Tellurium Nanorods via a Magnetization–Alignment–Demagnetization ("MAD") Process Assisted by an External Magnetic Field.* ACS Nano, 2009. 3(6): p. 1441-1450.

108. Shi, Z., et al., *Magnetoelectric sensor with miniature universal tunable bias magnetic circuit.* Applied Physics Letters, 2013. 103(3): p. 032903.

109. Reis, S., et al., *Optimized anisotropic magnetoelectric response of $Fe_{61.6}Co_{16.4}Si_{10.8}B_{11.2}$/PVDF/$Fe_{61.6}Co_{16.4}Si_{10.8}B_{11.2}$ laminates for AC/DC magnetic field sensing.* Smart Materials and Structures, 2016. 25(5): p. 055050.

110. Jones, J.L., J.D. Starr, and J.S. Andrew, *Anisotropy in magnetoelectric composites.* Applied Physics Letters, 2014. 104(24): p. 242901.

111. Uusimaki, T., et al., *Three dimensional quantitative characterization of magnetite nanoparticles embedded in mesoporous silicon: local curvature, demagnetizing factors and magnetic Monte Carlo simulations.* Nanoscale, 2013. 5(23): p. 11944-11953.

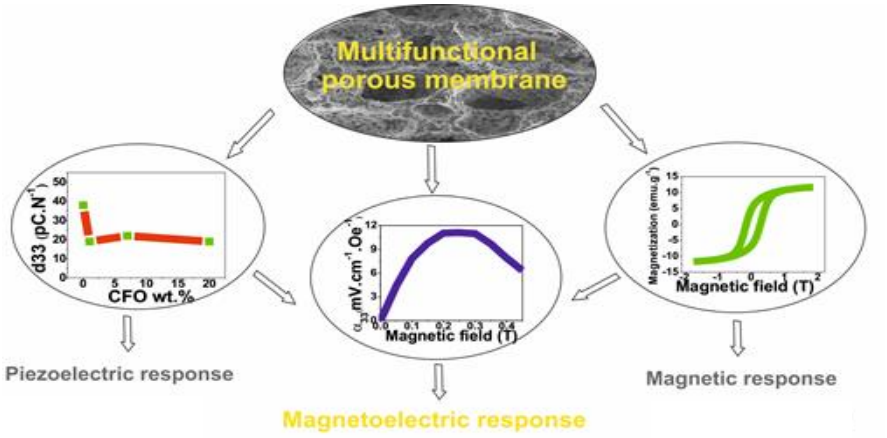

Chapter 3

Development of magnetoelectric polymer-based membranes

CFO/P(VDF-TrFE) magnetoelectric (ME) membranes were processed and their ME response, magnetic properties and morphology evaluated. It is shown that the membranes have large interest, due to their piezoelectric, magnetic and ME response, and high porosity.

This chapter is based on the following articles:

- P. Martins, R. Gonçalves, A. C. Lopes, E. Venkata Ramana, S.K.Mendiratta and S. Lanceros-Mendez, *Novel hybrid multifunctional magnetoelectric porous composite films*, Journal of Magnetism and Magnetic Materials, 2015. 396: p. 237-241.

3.1. Introduction

Porous films and membranes are playing an increasingly important role in various fields, such as energy, environment, chemical and medical industries, being regarded as one of the most promising functional materials [1-3]. They are attracting increasing attentions both at a research and application levels and experiencing strong development in novel theories, technologies and applications [1, 4, 5].

Porous films can be prepared from (organic) polymers, inorganic materials, liquids (immobilized liquid composite membranes) and from self-assembled smaller molecules (in analogy to biological membranes). Polymer membranes dominate a very broad range of industrial applications due to the large variety of polymeric materials commercially available that can be prepared by versatile and industrially scalable methods with tailored microstructure and properties. Further, polymer-based membranes can be produced in large areas and with various membrane shapes (flat sheet, tubular, hollow-fiber, capillary, capsule) and formats including modules with high packing densities [1].

Among polymeric porous films, the ones based on P(VDF) and its copolymers are emerging as one of the most promising membranes due to their good mechanical and thermal properties and chemical stability [6, 7]. Compared to its P(VDF) homo-polymer, P(VDF-TrFE) displays further advantages such as high dipole moment, high dielectric constant, and possibility of controlling porosity at room temperature [7]. Furthermore, P(VDF-TrFE), for TrFE contents between 50 and 80%, crystallizes in the piezoelectric phase independently of the processing method, allowing the preparation of piezoelectric porous films with improved flux and fouling in the case of filtration and separation membranes [8, 9], improved sensing properties for biomedical monitoring [10] and with the possibility of environmental energy storage and harvesting [11].

The incorporation of magnetic nanoparticles in porous structures is still very recent [12] and the use of such nanoparticles in multifunctional porous films is essentially unexplored. Nevertheless, the addition of magnetic nanoparticles can take a step forward these materials concerning the development of multifunctional porous films able to separate components with distinct magnetic properties (e.g. oxygen is

paramagnetic while nitrogen is diamagnetic) [13], generate heat [14], large and controlled deflections [15] or in-situ pore size switching [16]. If the magnetic particles are also magnetostrictive, other innovative applications such as magnetostrictive ultrasonic thrombolysis membranes [17] or magnetic sensor membranes [18] can be also developed. Additionally, the inclusion of magnetostrictive nanoparticles in a piezoelectric porous structure can allow the preparation of ME membranes [19].

The ME effect within porous structures will allow novel applications in areas – figure 3.1- such as sensors, actuators, transformers and microwave devices [19, 20], in technological applications such as separation membranes, water treatment, drug release, cell culture or medical devices [16, 21, 22]. In this way, ME porous structures represent an innovative concept to be added to the increasingly large variety of applications of porous structures [6, 23, 24].

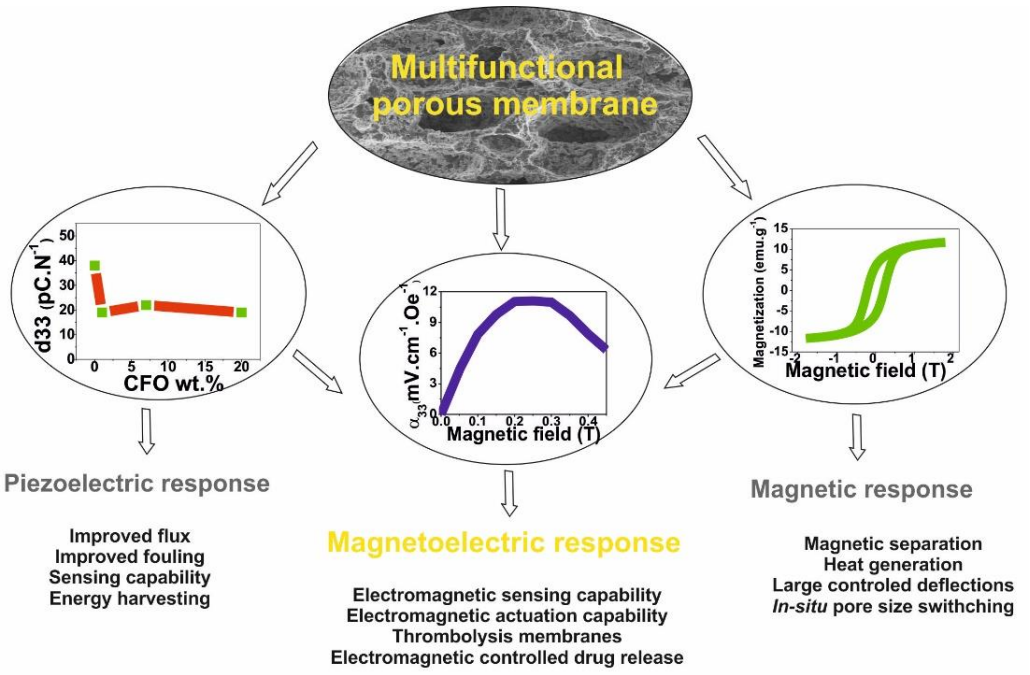

Figure 3.1. Porous ME composite structure, its main responses and possible applications.

Despite this promising and interesting potential, just few reports have vaguely addressed the concept of ME porous structures [25, 26].

3.2. Materials and methods

CFO/P(VDF-TrFE) porous piezoelectric, magnetic, magnetostrictive and ME films were developed. P(VDF-TrFE) was chosen as piezoelectric material since it exhibits one of the highest piezoelectric responses among polymer materials over a wide range of temperature depending on its composition [28] and CFO nanoparticles were chosen as the magnetic/magnetostrictive phase due to the large magnetostrictive coefficients and high Curie temperatures [29].

3.2.1. Materials

CFO nanoparticles were purchased from Nanoamor, with dimensions between 35 and 55 nm. N,N-Dimethylformamide (DMF, pure grade) was supplied by Fluka and P(VDF-TrFE) was supplied by Solvay Solexis.

3.2.2. Methods

The methods used for the study were divided in processing and characterization.

3.2.2.1. Processing methods

Composite porous films of CFO/P(VDF-TrFE) with 1, 7 and 20 nanoparticles wt.% were prepared by solvent casting and crystallization at room temperature, with thickness of ranging from 200 to 400 μm. Higher contents of ferrite nanoparticles were not used to avoid damaging the porous structure and the agglomeration of ferrite nanoparticles in the porous surface as demonstrated with other nanoparticles [27]. Previously, the CFO nanoparticles were added to 8 mL of DMF and placed in an ultrasound bath during 8 hours to ensure a good dispersion of the nanoparticles in the solution and also to avoid loose aggregates. After that, 2 g of P(VDF-TrFE) were added to this suspension, achieving a polymer/solvent ratio of 20:80, and mixed with a Teflon mechanical stirrer until complete dissolution of polymer. Finally, the material was placed on a dried glass substrate at room temperature to ensure the complete evaporation of the solvent.

3.2.2.2. Characterization methods

The structure of the ME porous films was investigated using a Quanta 650 FEG (FEI) Environmental Scanning Electron Microscope with an acceleration voltage of 5 kV. Poling of the films was achieved, after an optimization procedure, by corona poling at 10 kV during 120 min at 120 °C in a home-made chamber and cooling down to room temperature under applied field. The d_{33} of the samples was analyzed with a wide range d_{33}-meter (model 8000, APC Int Ltd).

Magnetic hysteresis loops at room temperature were measured using an ADE 3473-70 Technologies vibrating sample magnetometer.

In order to obtain the out-of-plane ME coefficient α_{33}, the first index indicating the collinear ferroelectric poling and electrical measurement directions, and the second indicating the applied magnetic field direction, a DC and AC magnetic field were applied along the direction of the electric polarization of the P(VDF-TrFE), i.e., perpendicular to the composite membrane surface.

An AC driving magnetic field of 1 Oe amplitude at 7 kHz (resonance of the composite) was provided by a pair of Helmholtz coils. A DC field with a maximum value of 0.5 T was applied by an electromagnet. The induced ME voltage was measured with a Standford Research Lock-in amplifier (SR530).

3.3. Development of magnetoelectric membranes

The typical microstructure of pure copolymer film samples and composites is presented in figure 3.2.

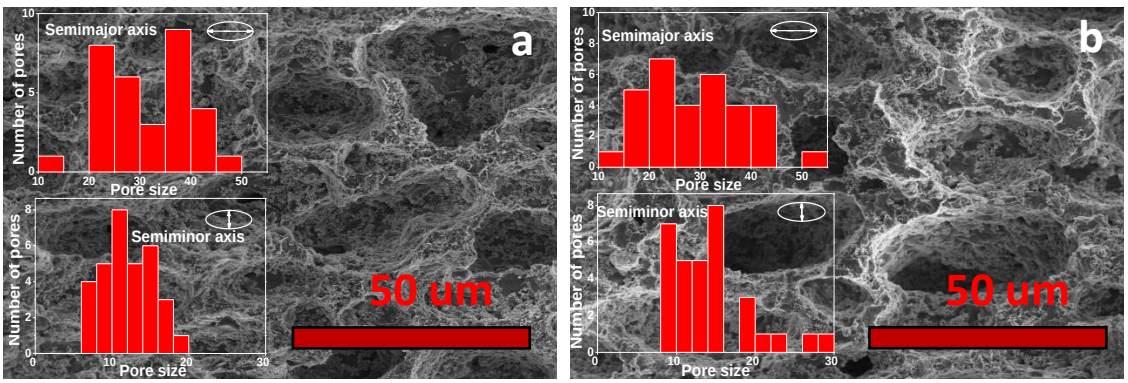

Figure 3.2. Morphology of CFO/P(VDF-TrFE) nanocomposite membranes with 20 wt.% of ferrite content, a) before and b) after poling.

It can be observed that the porous structure characteristic of neat P(VDF-TrFE) polymer is maintained, however the typical spherical shape [6, 7] of these pores is replaced by an ellipse shaped structure. The origin of this change can be explained by the high weight of CFO nanoparticles during the slow polymer crystallization by solvent casting method. Further, it is observed that some of the nanoparticles are inside the polymer matrix and others are coating the pores surface. The corona poling process, involving high temperature and electric field, does not significantly alter the microstructure of the films and the average size of the ellipse shaped pores, both with respect to the semimajor and semiminor axes, is maintained before and after the poling process.

Piezoelectric and magnetic properties of the composite membrane prove the multifunctionality of the polarized porous membrane (PPM) and will determine its ME response [30] (figure 3.3).

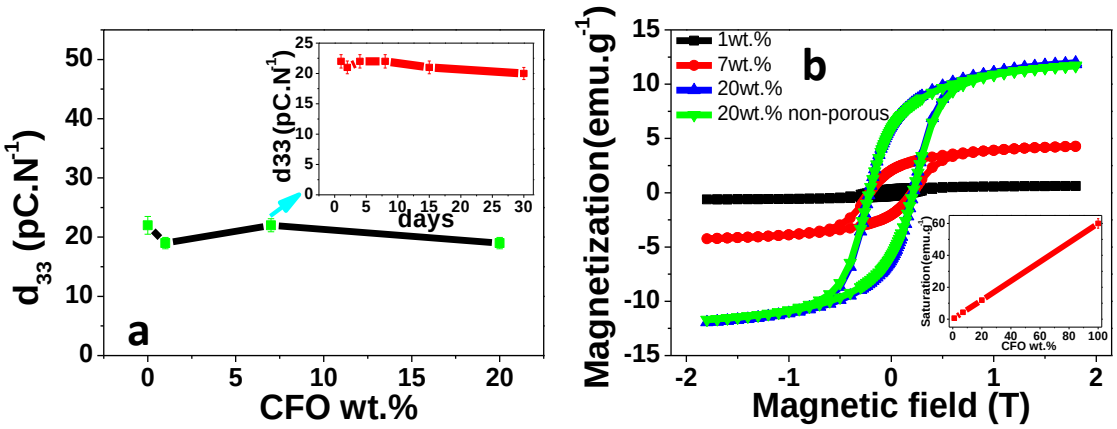

Figure 3.3. a) Ferrite wt.% dependent d_{33} for the ME PPM. b) Room temperature hysteresis loops for the ME PPM.

Figure 3.3a shows that the existence of pores decreases to almost one half the piezoelectric response of the porous film with respect to the pristine polymer P(VDF-TrFE) films [28] (from 37 to 22 pC.N^{-1}). On the other hand, this value is still among the largest among polymers and comparable to those obtained for CFO/P(VDF-TrFE) MF composites films with similar compositions [31]. Porous films without CFO nanoparticles

exhibit piezoelectric response similar to those with CFO nanoparticles, indicating that the addition of nanoparticles not affect the piezoelectric response of the resulting membrane. Such piezoelectric response is stable over temperature (samples were heated until 120 °C in the poling process) and time, with no signal degradation for over 30 days (inset of figure 3.3a).

The room-temperature magnetization loops of the ME porous membranes (figure 3.3b) show that nanocomposite magnetization increases with increasing CFO content (inset of figure 3.3b). The maximum magnetization value of 12 emu.g^{-1} was obtained in the PPM with 20 wt.% of ferrite content. The nanocomposites show 0.2 T coercivity, remanence and the magnetization saturates at the applied magnetic field of 1.8 T, consistent with the ferromagnetic behavior of the nanoparticles [31].

The ME response in the porous films was measured as a function of the applied DC magnetic field and the CFO content (figure 3.4).

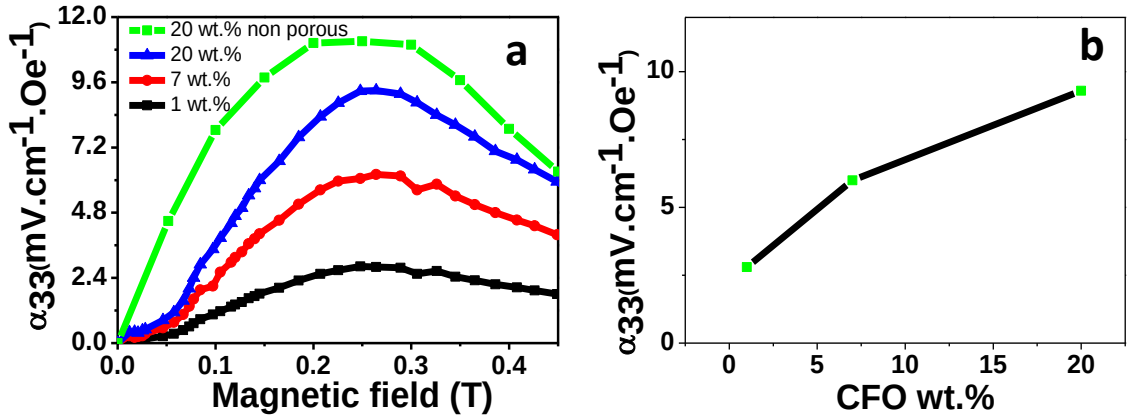

Figure 3.4. a) ME response α_{33} as a function of the applied magnetic field for the different ME porous membranes; b) ME coefficients as a function of CFO filler content for the different ME PPM at 0.3 T magnetic DC field.

For the porous ME film, the α_{33} value increases with applied DC magnetic field until the magnetostriction saturation at ≈0.3 T; increasing the magnetic field further leads to a decrease in the α_{33}. A small decrease (≈ 20 %) in the ME response of the porous structure with respect to the values obtained for the corresponding MF composite films [31] is observed. This decrease is attributed to the lower mechanical coupling between

the CFO nanoparticles and the polymer matrix due to the existence of pores [32]. Moreover, the poor elastic coupling resulting from the soft structure of the film leads to a poor transition of the mechanical stress between magnetostrictive and piezoelectric phases and thus contributing towards lower ME response [33]. Additionally, as seen on figure 3.2, some of the ferrite nanoparticles are located in the surface of the pore, being only a part of its surface in contact with the polymer matrix.

Figure 3.4b shows an increase in the ME response with increasing CFO content, which is naturally explained by the increased magnetostriction of the sample due to the substantial increase of the magnetostrictive phase, being observed the maximum ME response (9 $mV.cm^{-1}.Oe^{-1}$) in the sample with highest content CFO nanoparticles (20 wt.%). Porous films with higher content of magnetostrictive nanoparticles were not produced in order to avoid collapsing the pore structure [27].

3.4. Conclusions

The porous films developed in the present work show a piezoelectric response with an effective d_{33} coefficient of -22 $pC.N^{-1}$, a maximum magnetization of 12 $emu.g^{-1}$ and a maximum ME coefficient of 9 $mV.cm^{-1}.Oe^{-1}$. Such features make this membrane suitable for innovative applications ranging from biomedical or drug delivery systems to water treatment [16, 21, 22].

3.5. References

1. Yuan, W., et al., *Porous metal materials for polymer electrolyte membrane fuel cells – A review.* Applied Energy, 2012. **94**: p. 309-329.
2. Chang, S., et al., *In situ Growth of Silver Nanoparticles in Porous Membranes for Surface-Enhanced Raman Scattering.* ACS Applied Materials & Interfaces, 2010. **2**(11): p. 3333-3339.
3. Tao, Y., et al., *Tunable Hydrogen Separation in Porous Graphene Membrane: First-Principle and Molecular Dynamic Simulation.* ACS Applied Materials & Interfaces, 2014. **6**(11): p. 8048-8058.
4. Hasani-Sadrabadi, M.M., et al., *Magnetically Aligned Nanodomains: Application in High-Performance Ion Conductive Membranes.* ACS Applied Materials & Interfaces, 2014. **6**(10): p. 7099-7107.
5. Zhang, P., et al., *Electrospun Doping of Carbon Nanotubes and Platinum Nanoparticles into the β-Phase Polyvinylidene Difluoride Nanofibrous Membrane for Biosensor and Catalysis Applications.* ACS Applied Materials & Interfaces, 2014. **6**(10): p. 7563-7571.
6. Nunes-Pereira, J., et al., *Porous Membranes of Montmorillonite/Poly(vinylidene fluoride-trifluorethylene) for Li-Ion Battery Separators.* Electroanalysis, 2012. **24**(11): p. 2147-2156.
7. Costa, C.M., et al., *Poly(vinylidene fluoride)-based, co-polymer separator electrolyte membranes for lithium-ion battery systems.* Journal of Power Sources, 2014. **245**: p. 779-786.
8. Darestani, M.T., et al., *Piezoelectric membranes for separation processes: Fabrication and piezoelectric properties.* Journal of Membrane Science, 2013. **434**: p. 184-192.
9. Li, C., et al., *Poly(vinylidene fluoride) membrane with piezoelectric β-form prepared by immersion precipitation from mixed solvents containing an ionic liquid.* Journal of Applied Polymer Science, 2014. **131**(15): p. n/a-n/a.
10. Ono, Y., et al. *5H-2 A Piezoelectric Membrane Sensor for Biomedical Monitoring*. in *2006 IEEE Ultrasonics Symposium*. 2006.
11. Liu, Y., et al., *Study on performance of PVDF piezoelectric film for the separator in Li-ion rechargeable cell.* Science China Technological Sciences, 2013. **56**(11): p. 2646-2648.

12. Uehara, T.M., et al., *A Detailed Investigation on the Interactions between Magnetic Nanoparticles and Cell Membrane Models.* ACS Applied Materials & Interfaces, 2013. **5**(24): p. 13063-13068.
13. Borys, P. and Z.J. Grzywna, *Effect of the magnetic membrane magnetization on the oxygen solubility.* Journal of Membrane Science, 2013. **445**: p. 107-111.
14. Amarjargal, A., et al., *Controlled assembly of superparamagnetic iron oxide nanoparticles on electrospun PU nanofibrous membrane: A novel heat-generating substrate for magnetic hyperthermia application.* European Polymer Journal, 2013. **49**(12): p. 3796-3805.
15. Fatemeh, P., C. Luna, and C. Mu, *A magnetic poly(dimethylesiloxane) composite membrane incorporated with uniformly dispersed, coated iron oxide nanoparticles.* Journal of Micromechanics and Microengineering, 2010. **20**(1): p. 015032.
16. Gajda, A.M. and M. Ulbricht, *Magnetic Fe3O4 nanoparticle heaters in smart porous membrane valves.* Journal of Materials Chemistry B, 2014. **2**(10): p. 1317-1326.
17. Cho, S.H., H.J. Kim, and Y.Y. Kim. *Feasibility study of a membrane-type magnetostrictive acoustic transducer for ultrasonic thrombolysis*. in *2009 IEEE International Ultrasonics Symposium*. 2009.
18. Gerngross, M.-D., et al., *Porous InP as Piezoelectric Component in Magneto-Electric Composite Sensors.* ECS Transactions, 2011. **35**(8): p. 67-72.
19. Martins, P. and S. Lanceros-Méndez, *Polymer-Based Magnetoelectric Materials.* Advanced Functional Materials, 2013. **23**(27): p. 3371-3385.
20. Silva, M., et al., *Optimization of the Magnetoelectric Response of Poly(vinylidene fluoride)/Epoxy/Vitrovac Laminates.* ACS Applied Materials & Interfaces, 2013. **5**(21): p. 10912-10919.
21. Drašler, B., et al., *Effects of magnetic cobalt ferrite nanoparticles on biological and artificial lipid membranes.* International Journal of Nanomedicine, 2014. **9**: p. 1559-1581.
22. Rybak, A., et al., *Magnetic mixed matrix membranes in air separation.* Chemical Papers, 2014. **68**(10): p. 1332-1340.

23. Zhu, B., J. Li, and D. Xu, *Porous biomimetic membranes: fabrication, properties and future applications.* Physical Chemistry Chemical Physics, 2011. **13**(22): p. 10584-10592.

24. Ferreira, A., et al., *Poly(vinylidene fluoride-trifluoroethylene) (72/28) interconnected porous membranes obtained by crystallization from solution.* MRS Proceedings, 2011. **1312**.

25. Petrov, V.M., et al., *Magnetoelectric effects in porous ferromagnetic-piezoelectric bulk composites: Experiment and theory.* Physical Review B, 2007. **75**(17): p. 174422.

26. Seiji, N., et al., *Ferroelectric and magnetoelectric properties of BiFeO[3] thin films prepared on a membrane structure*. Vol. 51. 2007, Seoul, COREE, REPUBLIQUE DE: Korean Physical Society. 5.

27. Stephens, J.R., et al., *Diffusive Flux and Magnetic Manipulation of Nanoparticles through Porous Membranes.* Analytical Chemistry, 2010. **82**(8): p. 3155-3160.

28. Martins, P., A.C. Lopes, and S. Lanceros-Mendez, *Electroactive phases of poly(vinylidene fluoride): Determination, processing and applications.* Progress in Polymer Science, 2014. **39**(4): p. 683-706.

29. Martins, P., et al., *Effect of filler dispersion and dispersion method on the piezoelectric and magnetoelectric response of CoFe2O4/P(VDF-TrFE) nanocomposites.* Applied Surface Science, 2014. **313**: p. 215-219.

30. Srinivasan, G. and A. DN, *Magnetoelectric Composites Magnetoelectric effect in chromium oxide.* Annual Review of Materials Research, 2010. **40**(1): p. 153-178.

31. Martins, P., et al., *Optimizing piezoelectric and magnetoelectric responses on CoFe 2 O 4 /P(VDF-TrFE) nanocomposites.* Journal of Physics D: Applied Physics, 2011. **44**(49): p. 495303.

32. Ryu, J., et al., *Piezoelectric and Magnetoelectric Properties of Lead Zirconate Titanate/Ni-Ferrite Particulate Composites.* Journal of Electroceramics, 2001. **7**(1): p. 17-24.

33. Adnan Islam, R. and S. Priya, *Progress in Dual (Piezoelectric-Magnetostrictive) Phase Magnetoelectric Sintered Composites.* Advances in Condensed Matter Physics, 2012. **2012**: p. 29.

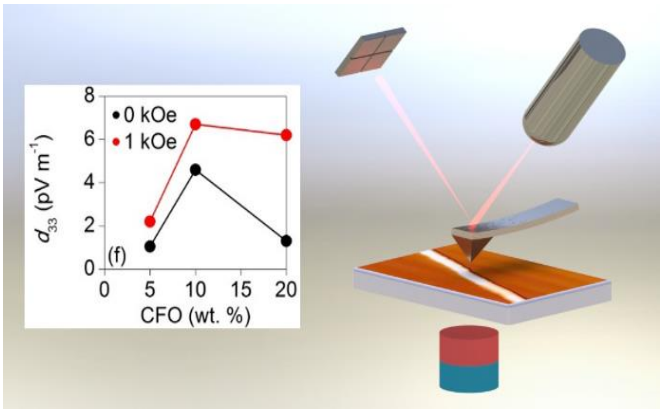

Chapter 4

Development of polymer-based magnetoelectric fibers and spheres

Two different morphologies: fibers and spheres were studied. Their production is based on electrospinning and electrospray techniques, for nanofibers and microspheres, respectively. The magnetoelectric response was proven in both morphologies.

This chapter is based on the following articles:

- R. Gonçalves, P. Martins, X. Moya, M. Ghidini, V. Sencadas, G. Botelho, N. D. Mathur, S. Lanceros-Mendez, *Magnetoelectric $CoFe_2O_4$/polyvinylidene fluoride electrospun nanofibres*. Nanoscale, 2015. 7(17): p. 8058-8061.
- R. Gonçalves, P. Martins, D. M. Correia, V. Sencadas, J. L. Vilas, L. M. Leon, G. Botelho, S. Lanceros-Mendez, *Development of magnetoelectric $CoFe_2O_4$ /poly(vinylidene fluoride) microspheres*. RSC Advances, 2015. 5(45): p. 35852-35857.

4.1. Introduction

ME composites comprising magnetic nanoparticles embedded in a ferroelectric polymer matrix can have several advantages, namely: strain coupling typically does not deteriorate with operation as the magnetic material is in direct contact with, and completely surrounded by, the ferroelectric material, and ME voltage coefficients in composites comprising magnetic nanoparticles and fluorinated-polymer matrices are relatively large both at moderate [1] and high [2, 3] magnetic fields.

Polymer-based ME fibers and spheres composed by magnetostrictive nanoparticles within a piezoelectric polymer matrix, can open new applications areas and solve some drawbacks of the traditional polymer-based structures (nanocomposites, polymer as a binder and laminates) such as agglomeration, irregular distributions and the difficulty to shape in a miniaturized form [4, 5].

Polymer-based nanofibers and spheres undergo an increasing demand and applicability as biomaterials for cell culture, drug delivery systems, electro-optic and luminescent devices, heterogeneous catalysis and polymer powder impregnation of inorganic fibers in composites [6-9].

Particularly, low-scale piezoelectric materials show strong potentials for improved energy harvesters with higher volume efficiency, nanosensors and nanoactuators and nanomats guiding cell distribution [10, 11]. The addition of magnetostrictive materials into the piezoelectric microspheres allows the use of the resulting composite also as magnetic nanosensors and actuators, as well as to take advantage of the induced the ME phenomenon [12].

4.2. Materials and methods

This subchapter is divided in materials and methods.

4.2.1. Materials

Poly(vinylidene fluoride), P(VDF), reference Solef 1010, was acquired from Solvay. Analytical grade tetrahydrofuran (THF) and N,N-dimethyl formamide (DMF) were purchased from Panreac and Merck, respectively. $CoFe_2O_4$, CFO, nanoparticles

with 35–55 nm particle size, was purchased from Nanoamor. Laboratory grade Triton X-100 was purchased from Sigma-Aldrich.

4.2.2. Methods

The methods used for the study was divided in processing and characterization.

4.2.2.1. Processing methods

CFO contents were chosen since they can contribute to obtaining nanofibers and microspheres with good morphology and high ME coupling [2]. The use of lowerCFO contents results in an abrupt decrease in the ME response, higher contents, on the other hand, will cause substantial changes on polymer solution properties such as surface tension, conductivity, and viscosity, thereby hindering the electrospinning/electrospray process and affecting the desired fiber/sphere morphology [13, 14]. ME composite nanofibers and microspheres, with CFO nanoparticle content 5, 10 and 20 wt. % for fibers and 10, 40 70 wt. % for microspheres, were prepared using the following procedure:

(i) CFO nanoparticles were added to the DMF and the solution was placed in an ultrasound bath during 4 h to ensure good dispersion and avoid nanoparticle agglomeration (in case of the microspheres, Triton X-100 was added to);

(ii) P(VDF) powder (and THF in case of microspheres) was added and the resultant solution was mixed using a Teflon mechanical stirrer and an ultrasound bath until the polymer was completely dissolved. The relation between the contents of polymer and solvent were previously optimized in order to obtain nanofibers and microspheres with the desired morphology, crystallinity and crystal phase [15]. For such reason the relations were kept 20/80 (20 % P(VDF) + 80 % DMF by wt.%);

(iii) the composite solution was introduced into the electrospinning/electrospray deposition setup, using a plastic syringe connected to a flux regulator; in order to create a jet, high voltage was applied between the syringe steel needle and an aluminium foil, where the electrospun nanofibers (or electrospray microspheres) were collected, forming a mat; deposition conditions were 20 kV bias (PS/FC30P04 power source), 0.5

mm needle inner diameter, 0.5 ml.h^{-1} flow rate (1 ml.h^{-1} to the microspheres), and 20 cm needle-collector distance.

4.2.2.2. Characterization methods

The morphology of the CFO/P(VDF) nanofibers and microspheres was evaluated by Scanning Electron Microscopy (SEM) (Quanta 650, from FEI) with an accelerating voltage of 5 kV (microspheres) and 10 kV (nanofibers). Average diameter and distribution were calculated over approximately 30 nanofibers and microspheres using SEM images (5000 X magnification) and the Image J software.

Fourier Transform Infrared Spectroscopy (FTIR) technique was carried out at room temperature in a Bruker alpha apparatus in ATR mode from 4000 to 400 cm^{-1} using 24 scans at a resolution of 4 cm^{-1}. Specific bands such as the ones at 766 and 840 cm^{-1} were identified to correspond to the α- and β-phase, respectively, allowing the calculation of the polymer phase content after the procedure described in [16]. The β-phase fraction (F(β)) can thus be determined by applying equation 4.1:

$$F(\beta) = \frac{A_\beta}{\left(\frac{K_\beta}{K_\alpha}\right)A_\alpha + A_\beta} \tag{4.1}$$

where F(β) represents the β-phase content; A_β and A_α the absorbance at 840 and 766 cm^{-1}, respectively and K_β (7.7 x 10^4 cm^2.mol^{-1}) and K_α (6.1 x 10^4 cm^2.mol^{-1}) are the absorption coefficients at the respective wavenumber for both phases [16].

The thermal behavior of the samples was determined by Differential Scanning Calorimetry (DSC), measurements in a Mettler Toledo 822e apparatus with sample robot and STAR software, using a heating rate of 10 °C.min^{-1} under nitrogen purge (50 mL.min^{-1}); and by ThermoGravimetric Analysis (TGA). For the TGA measurements, samples were transferred to open ceramic crucibles with capacity of 60 µL and analyzed using a METTLER TGA/SDTA 851 thermobalance operating between 200 °C and 700 °C. A heating rate of 10 ± 0.2 °C.min^{-1} and nitrogen flow rate of 50 mL.min^{-1} were used.

The crystallinity content (X_c) of the samples was calculated applying equation 4.2 [17]:

$$X_c = \frac{\Delta H}{x\Delta H_\alpha + y\Delta H_\beta} \quad (4.2)$$

where ΔH is the melting enthalpy of the sample; ΔH_α and ΔH_β are the melting enthalpies of a 100 % crystalline sample in the α and β phase and x and y indicate the amount of α and β phase present in the sample, respectively. ΔH_α and ΔH_β were considered as 93.07 and 103.4 $J.g^{-1}$ [18].

Form the TGA results, the filler/polymer interface region of the CFO/P(VDF) microspheres was obtained, applying equation 4.3 [19]:

$$m_I = \frac{m(x)_{IO} - m_{IO}}{m_{IO}} \times 100 \quad (4.3)$$

where m_{I0} is the mass of the pristine polymer at the temperature at which the mass loss rate is maximum and $m(x)_{I0}$ is the mass of the composite containing a given wt.% of nanoparticles that has not degraded at the temperature at which the mass loss rate of the pristine polymer is maximum.

After poling conditions optimization, 30 min of corona poling at 10 kV and 120 °C were applied in a home-made chamber in order to optimize the piezoelectric response of the microspheres. Then, the d_{33} of the samples was analyzed with a wide range d_{33}-meter (model 8000, APC Int Ltd). In case of the fibers piezoelectric coefficients d_{33} were determined using a Digital Instruments Dimension 3100 for piezoresponse force microscopy (PFM), with conductive Cr/Pt-coated tips of stiffness 40 $N.m^{-1}$. d_{33} measurements were performed using a 2 V peak-to-peak AC bias at 13 kHz, with and without a 1 kOe magnetic field that was applied using a permanent magnet. Prior to local measurements of the fibers piezoresponse, the cantilever deflection amplitude was calibrated via force distance measurements [20, 21].

The magnetic properties of the MF nanofibers and microspheres were evaluated by measuring the magnetization loops $M_{(H)}$ up to 10 kOe using an Oxford Instruments vibrating sample magnetometer.

The ME character of the CFO/P(VDF) microspheres was evaluated by the difference in the piezoelectric response obtained with and without the application of a 220 Oe DC magnetic field (Δd_{33}).

4.3. Development of magnetoelectric nanofibers

Here, we extend the range of geometries available for polymer-based ME composites by fabricating nanofibres comprising CFO ferromagnetic particles and P(VDF) matrix. One-dimensional polymer-based ME fibers have not been hitherto reported, and may allow the development of new ME devices that could be exploited for e.g. non-invasive control of cell growth and differentiation, active drug release, tissue stimulation, heterogeneous catalysis and energy harvesting [7, 22-24].

The studied CFO/P(VDF) electrospun nanofibers have an average diameter of 325 nm, and are randomly distributed in the aluminium-foil collector (figure 4.1).

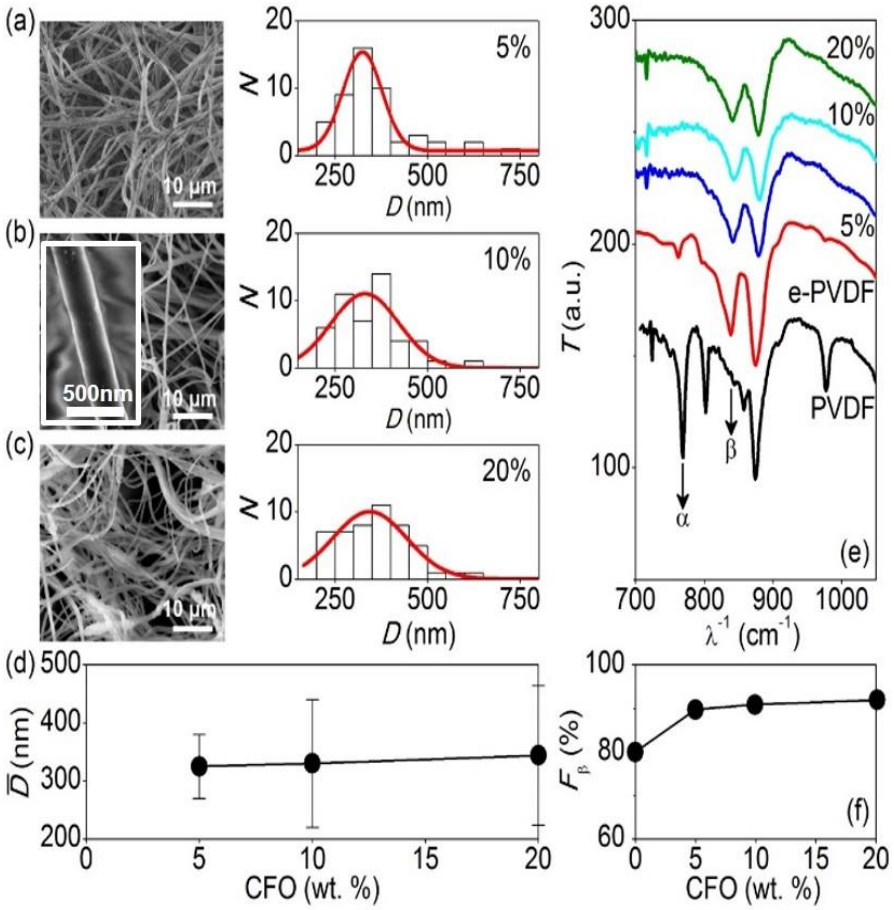

Figure 4.1. SEM image and the corresponding distribution of nanofiber diameter $\bar{D}$ for CFO/P(VDF) nanofibers with a) 5 wt. % CFO, b) 10 wt. % CFO (inset: detail of single composite fiber) and c) 20 wt.% CFO. Red lines are Gaussian fits, which were used to estimate the average diameter. d) Nanofiber average diameter $\bar{D}$ as a function of CFO content. e) FTIR spectra for CFO/P(VDF) nanofibers, and two pure polymer samples in film (P(VDF)) and nanofiber (e-P(VDF)) form. Vertical arrows indicate the traces for the α (766 cm^{-1}) and β (840 cm^{-1}) phases. f) β-phase volume fraction F_β as a function of CFO content.

The CFO nanoparticle content has no significant impact on the nanofiber average diameter [figure 4.1a-d]. The CFO/P(VDF) nanofibers show a strong enhancement in the volume fraction of electroactive β-phase (F_β) [16, 25] when compared to pure P(VDF) electrospun nanofibers (figure 4.1e and 4.1f), as the interaction between the negatively charged surface of the CFO nanoparticles (whose zeta potential is -22 mV) and the positively charged polymer CH_2 groups promotes nucleation of the polar β-phase, as seen in CFO/P(VDF) films [2]. The increase in the β-phase volume fraction is also assisted by the low evaporation temperature of the solvent (≤ 60 °C) and the stretching that occurs during jet formation [15].

The magnetization of the nanofibers increases with increasing CFO content (figure 4.2), as expected [1, 2, 4].

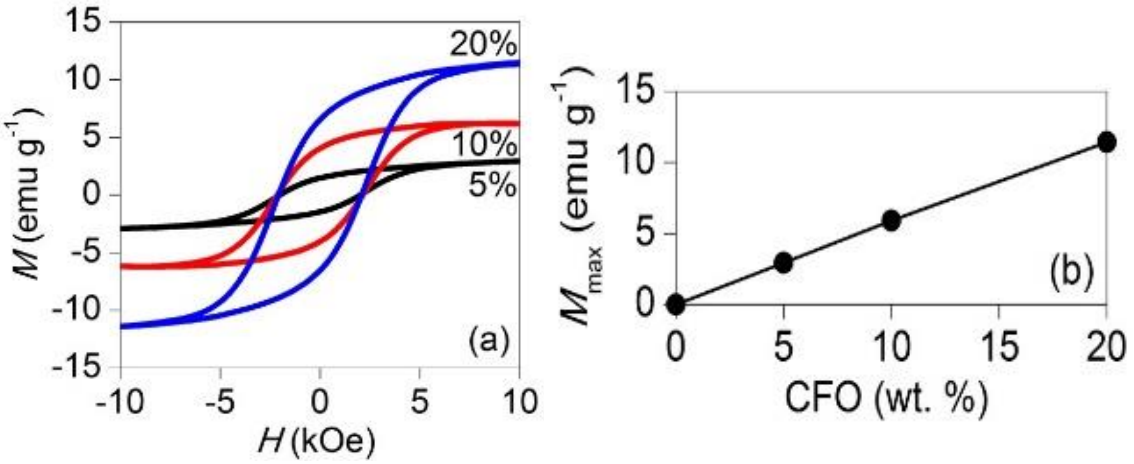

Figure 4.2. a) Room-temperature magnetization $M_{(H)}$ of CFO/P(VDF) nanofiber composites with different CFO concentration. Magnetization was measured along the out-of-plane direction of the nanofiber mats [complementary in-plane $M_{(H)}$ measurements (not shown) evidenced the isotropic magnetic character of the nanofiber composites]. b) Magnetization M_{max} measured at 10 kOe as a function of CFO content.

The shape of the magnetization loops is determined by the mixture of single domain and multidomain nanoparticles, [26] and the magnetization does not saturate at the maximum applied magnetic field of 10 kOe, due to the strong magnetic anisotropy (> 30 kOe) of the CFO nanoparticles [27].

To establish the ME character of the nanofiber composites, we performed PFM experiments in single fibers, with and without an applied magnetic field (figure 4.3).

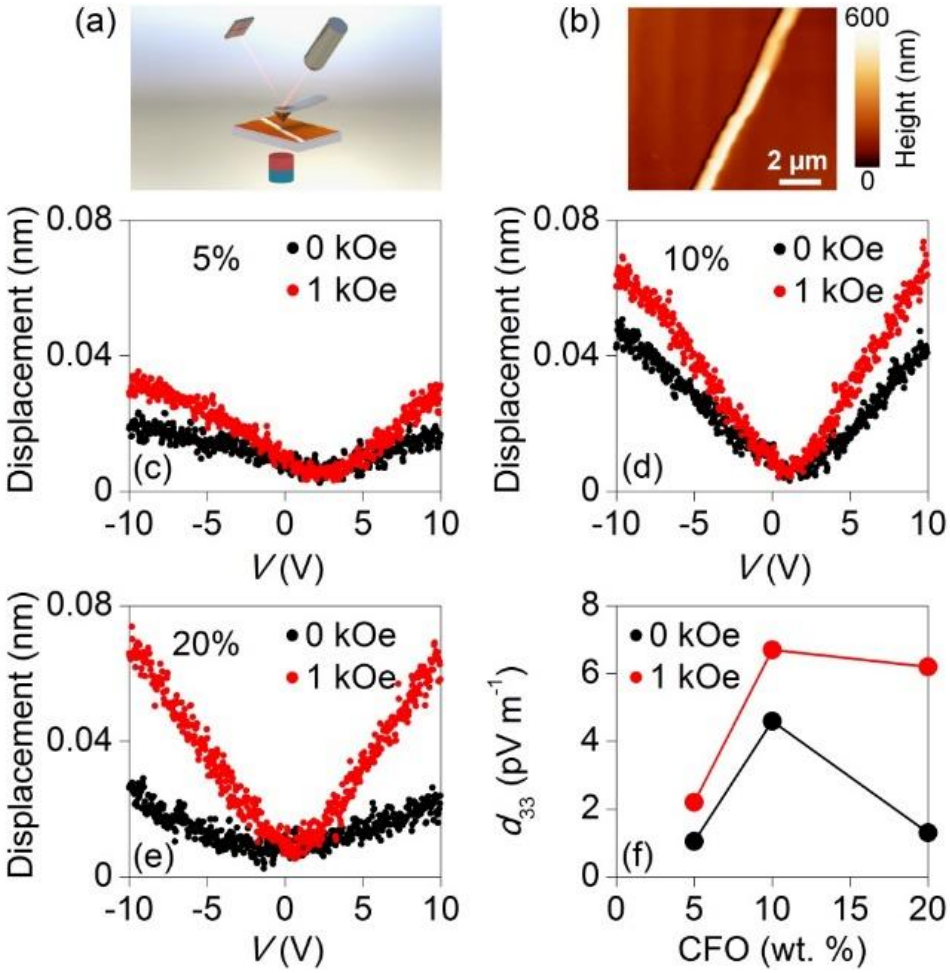

Figure 4.3. a) Schematic representation of the piezoresponse force microscopy setup in the applied magnetic field used to establish the ME character of the CFO/P(VDF) nanofibers. b) One of such nanofibers, as seen via atomic force microscopy. Displacement as a function of voltage, with and without magnetic field, for CFO/P(VDF) nanofibers with c) 5, d) 10 and e) 20 wt.% CFO. The maximum electric field applied was ≈30 MV.m^{-1}, which is smaller than the coercive field of P(VDF) films (≈50-120 MV.m^{-1}) [28]. f) d_{33} as a function of CFO content and magnetic field.

The piezoelectric coefficient increases with the applied magnetic field, due to the strain-mediated coupling between the magnetostrictive CFO nanoparticles and the piezoelectric P(VDF) matrix, which shows reduced piezoelectric coefficients when compared to bulk polymers, possibly due to clamping by the surrounding material, which may reduce significantly the local deformation of the nanofibers [2, 29-32].

4.4. Development of magnetoelectric microspheres

To the best of my knowledge there are no previous reports on polymer-based ME spheres, that can be an innovative and desired solution for applications in which multifunctional active response is needed (either magnetic to electrical or mechanical to electrical responses, due to the ME and piezoelectric effects) such as in non-invasive control of cell growth and differentiation, active drug release and tissue stimulation [7, 9].

For the formation of polymer microspheres several methods have been used such as gas atomization, microdroplet, dispersion polymerization, evaporation and precipitation, emulsion polymerization [6], oil in water (O/W) or water in oil (W/O) emulsions, coacervation and spray drying, among others [33]. Unlike previous methods that require high-energy input devices like sonicators and/or high-cost devices such as high-pressure homogenisers, electrospray technique is a straightforward and versatile technique featuring advantages like ambient condition and single-step processing, high reproducibility, high yield and economical set-up [8, 17, 34].

Thus, novel CFO/P(VDF) MF microspheres have been prepared, with large potential applications in the biomedical, sensing, actuation, catalysis and energy fields [6-8].

VSM technique has proved to be a precise technique able to accurately determine the magnetic nanoparticle content on composites [35-37]. Thus, the hysteresis curves shown in figure 4.4 were first used to evaluate the efficiency of the particle loading process, i.e. the relation between the content of the CFO nanoparticles within the solution and the concentration in the obtained microspheres (figure 4.4).

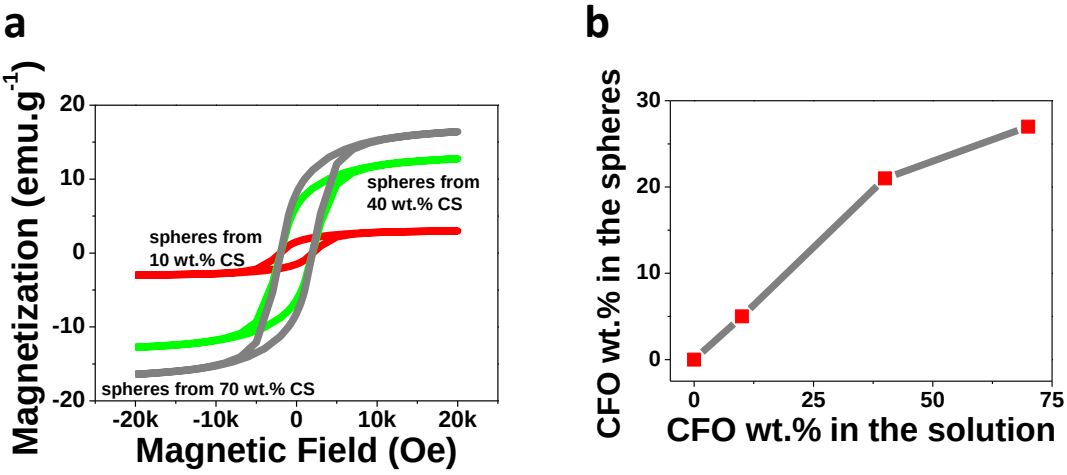

Figure 4.4. a) Room temperature hysteresis loops for the MF CFO/P(VDF) microspheres. b) Relation between the wt.% of CFO nanoparticles within the solution and the wt.% of CFO nanoparticles within the MF microspheres, obtained from the hysteresis loops.

Figure 4.4a reveals the typical ferromagnetic behavior of the CFO/P(VDF) microspheres. For all compositions, the magnetization saturates at ≈2 kOe. As expected, the magnetization saturation increases with increasing nanoparticle filler content. By comparing the M_S value of the pure CFO nanoparticles with the ones from figure 4.4a it is possible to determine, trough equation 4.4, the precise amount of CFO nanoparticles within the MF microsphere (table 4.1).

$$CFO\ wt.\%_{Spheres} = \frac{Saturation\ Magnetization_{Spheres} \times 100}{60} \quad (4.4)$$

Table 4.1. CFO wt.% in the solution, expected spheres M_S, measured spheres M_S and the calculated CFO wt.% in the spheres values.

CFO wt% in the solution	Spheres M_S (expected)	Spheres M_S (measured)	Calculated CFO wt.% in spheres
10	6	3.0	5
40	24	12.8	21
70	42	16.4	27
100*	60	60.0	100

*pure powder

Figure 4.4b and table 4.1 show that with 10, 40 and 70 wt.% CFO contents within the solution leads to microspheres with 5, 21 and 27 wt.% CFO amounts, respectively. Thus, the maximum CFO content allowed in the microspheres starts to saturate at ≈20

wt.%, since an increase of 30 wt.% in the solution wt.% content of CFO (from 40 to 70 %) leads to just an increase of only 6 % of CFO nanoparticles inside the MF microsphere (from 21 to 27 %).

Therefore, the concentrations of CFO nanoparticles in the electrosprayed microspheres is lower than those on the composite solutions, in agreement to previous reports [38], and can be attributed to the higher density of the CFO nanoparticles (when compared to the polymer matrix) that causes the settling of some nanoparticles on the bottom of the syringe during the ES process. Further, some contributions can also come from a partial blockage of the needle hole by agglomeration of nanoparticles, due to the flow funnelling towards the needle. Figure 4.5a-e shows representative SEM images of ME CFO/P(VDF) microspheres with 5-27 wt.% ferrite content.

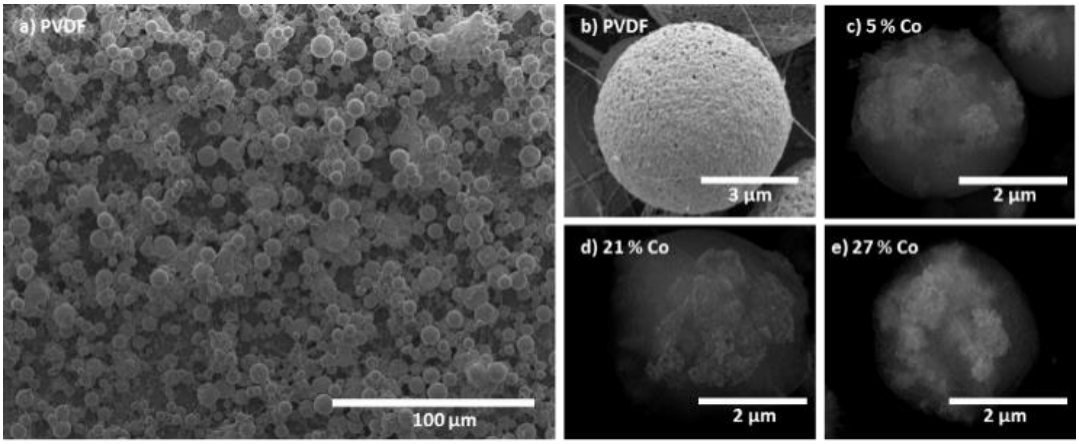

Figure 4.5. Morphology of a) and b) P(VDF) microspheres and the MF CFO/P(VDF) microspheres with CFO wt.% c) 5, d) 21 and e) 27 CFO nanoparticle content.

The low magnification image (figure 4.5a) shows a homogeneous production of MF microspheres, with good dispersion and spherical shape. Microspheres diameters were between 3 and 7 µm, nearly independently of the CFO filler content. The insertion of the CFO magnetic fillers within the P(VDF) polymer microsphere originates just a slight decrease of the average microsphere diameter.

Backscattering images (figures 4.5c-e) reveal that the CFO nanoparticles are effectively inside (white zones of figures 4.5c-e) the polymer microspheres, wrapped by

the polymer matrix (spherical structure of figure 4.5b), giving rise to the desired MF polymer composite structure.

Since the presence of the piezoelectric crystalline β-phase of P(VDF) is an essential requirement to obtain ME response on P(VDF) based ME materials [4], FTIR was used to identify and quantify the β-phase content of P(VDF).

For the pure polymer and the CFO/P(VDF) microspheres, typical FTIR spectra are presented in Figure 4.6a and the calculated F(β), equation 4.1, is represented in Figure 4.6b.

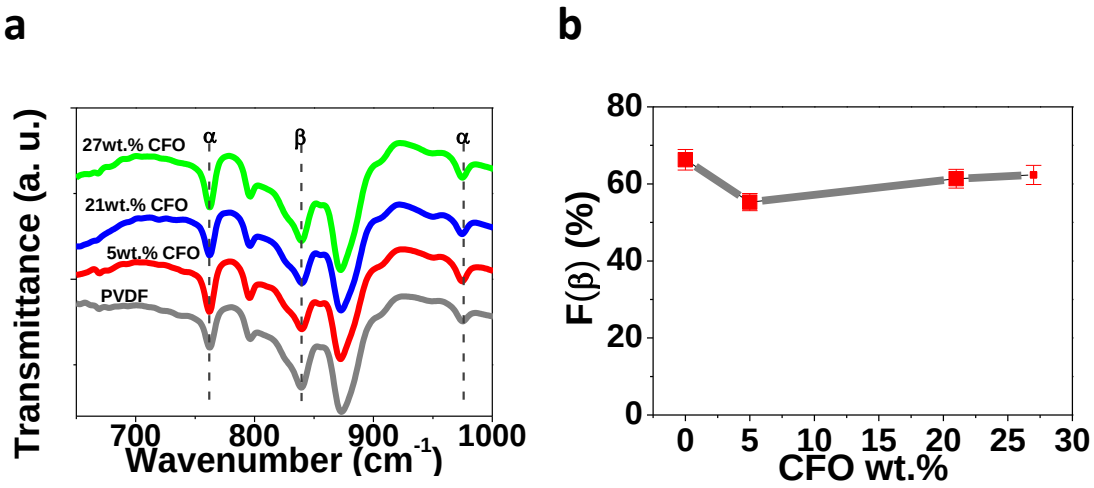

Figure 4.6. FTIR spectra of a) pure P(VDF) microspheres and CFO/P(VDF) composites microspheres with 5, 21 and 27 wt% filler content and b) variation of β-phase content as a function of CFO content.

Figure 4.6a shows that the crystalline phase of the polymer matrix in the microspheres are mainly in the β-phase and no significant differences between the spectra of the different composite microsphere are detected. All microspheres, pure P(VDF) and CFO/P(VDF) composites, show β-phase contents between 65 and 75 % and this value is independent of the CFO content. It is to notice that those β-phase contents are compatible with the maximum piezoelectric response of the polymer, as it has been verified in [38]. In this way, the β-phase formation is mainly attributed to the low solvent evaporation temperature (≤ 60 °C), which mainly leads to the crystallization of the polymer in this phase [8, 25]. Further, electrostatic interaction of the filler nanoparticles with the highly polar polymer chains certainly reinforce this effect, as it has been verified

in samples prepared after melting, that are nucleated in the β-phase, whereas the polymer without fillers remain in the α-phase [8].

Figure 4.7a shows the DSC thermograph of the microspheres of P(VDF) and CFO/P(VDF) composites. From the melting endotherm peak and applying equation 4.2, the degree of crystallinity (X_c) was obtained, as represented in Figure 4.7b.

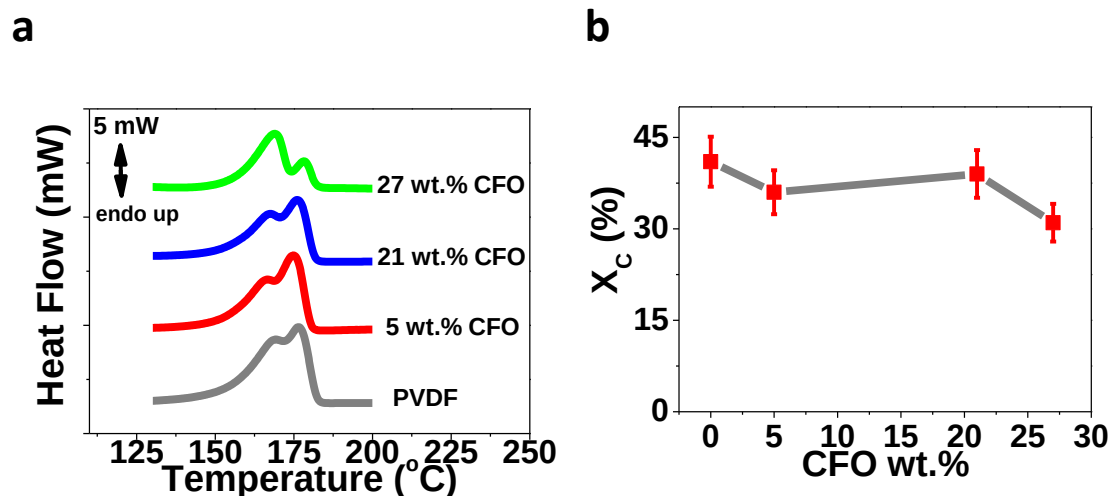

Figure 4.7. a) DSC thermographs and b) degree of crystallinity of the pristine P(VDF) and the CFO/P(VDF) composite microspheres.

The DSC thermographs of all samples are characterized by a double endothermic peak, related to the polymer crystallization in both α and β crystalline structures as confirmed by FTIR (figure 4.6) results [39] and the presence of the nanofillers. In both cases ill-crystallized region arises with lower melting temperature due to the larger energy of the imperfect structures. The degree of crystallinity values (figure 4.7b) are in good agreement with those obtained in P(VDF) processed by similar procedures [40]. Additionally, the overall lower degree of crystallinity is slightly lower when the fillers are present in the polymer matrix, which is attributed to hindered crystallization due to the presence of the fillers, which can act as nucleation centers for crystallization, but also hinder spherulite growth [37, 39].

The interface between magnetostrictive materials and piezoelectric polymers is one of the most sensitive parameters influencing the ME response of the composites. This interface can be determined by the TGA results presented in (figure 4.8) [19, 40].

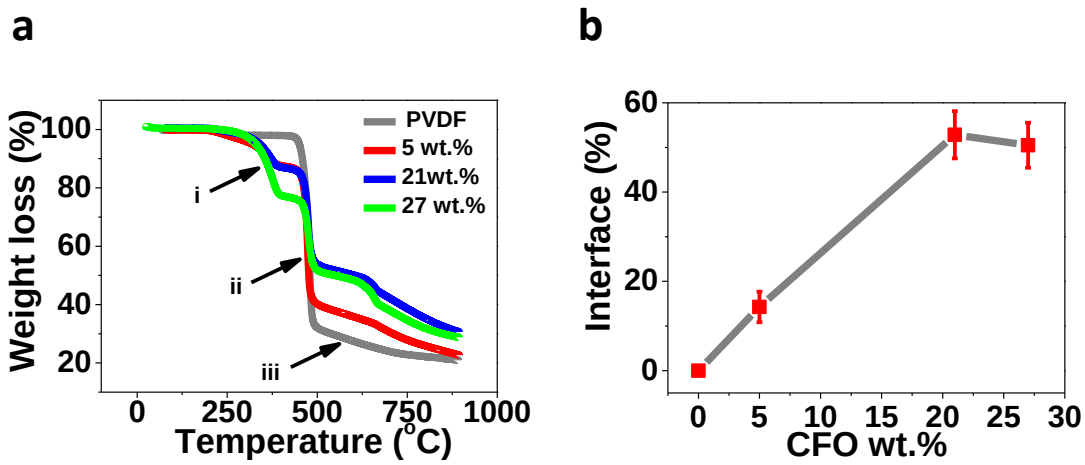

Figure 4.8. a) TGA thermographs for the different samples and b) interface volume between nanoparticles and polymer as a function of CFO nanoparticle concentration.

In all composite microspheres samples, with and without CFO nanoparticles, the typical two step thermal degradation, characteristic of P(VDF), was observed [41]. The onset temperature, defined as the temperature at which the polymer losses 1 % of its weight, was found to be ≈460 °C for the pure P(VDF) microspheres, slightly lower than those obtained for CFO/P(VDF) microspheres that was around ≈465 °C. These results shows that the addition of the CFO nanoparticles into the P(VDF) microspheres slightly improves the thermal stability of the microspheres. Such effect has already been reported in previous studies [19] and can be attributed to two factors: (a) the CFO filler in the composite can hinder the formation and escape of volatile by-products during heating and (b) the thermal motion of P(VDF) segments near the CFO surfaces may be restricted because of the physical interlock and electrostatic interaction [42].

The first degradation step occurs between ≈400 and ≈500 °C (ii), being the polymer maximum degradation temperature not influenced by the CFO content. In this initial degradation step the decomposition mechanism is chain-stripping where carbon-hydrogen and carbon-fluorine scission occurs, the presence of both hydrogen and fluorine radicals leading to the formation of hydrogen fluoride [41, 43].

The second degradation step occurs between ≈500 and ≈850 °C (iii), and the differences observed in the plots relatively to the pure P(VDF) microspheres sample are to be ascribed to the presence of CFO nanoparticles, as the different phases of P(VDF)

show similar thermal degradation behavior [44]. This second step is a complex degradation process resulting in poly(aromatization). The polyenic sequence previously formed on the first degradation step, is unstable and, as a consequence, the macromolecules formed undergo further reactions leading to scission followed by the formation of new aromatic molecules [19, 41, 45]. Previously to these typical two thermal degradation steps, an additionally degradation was observed between ≈290 and ≈400 °C (i) resultant from the degradation of the Triton X-100 [46].

Figure 4.8b shows the mass fraction of the polymer located at the interface as a function of the CFO content, calculated after equation 4.3. The interface value increases with increasing ferrite loading as a result of the increased number of particles interacting with the polymer matrix up to a filler content of ≈20 wt.%, after this value, increasing CFO content has a result a small decrease in the CFO/P(VDF) interface, explained by the fact that a larger filler content can lead to the formation of clusters and agglomerations and therefore a decrease of the overall surface contact area. The highest interface value (55 %) was obtained for the CFO/P(VDF) microspheres with 21 wt.% ferrite content. This interface value is ≈40 % higher than the one reported to CFO/P(VDF) MF composite films [47] and will lead to an increased ME coupling due to the larger contact area between the magnetostrictive and piezoelectric phases.

The ME coupling was measured [48, 49] by evaluating the piezoelectric response of the composites with and without an applied magnetic field of 220 mT (figure 4.9).

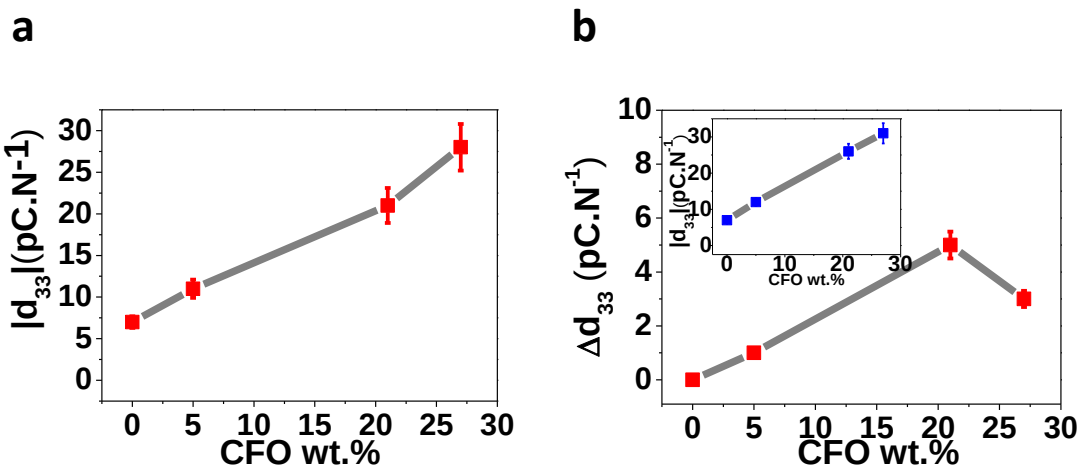

Figure 4.9. a) $|d_{33}|$ as a function of CFO wt.% and b)$|d_{33}|$ (inset) and Δ $|d_{33}|$ as a function of CFO wt.% with the applied 220 mT DC magnetic field.

Figure 4.9a represents the variation of the piezoelectric response of the samples (polymer films made out of microspheres - figure 4.5) as a function of filler content. The presence of the CFO nanoparticles improves the piezoelectric response of composite microspheres due to the strong interfacial interactions between particles and polymer [25, 37, 50]. With higher ferrite contents, the interfacial elastic effect is stronger and leads to higher piezoelectric responses [50].

Once a 220 mT DC magnetic field was applied with two permanent magnets, at the same time that the piezoelectric response is being measured, an increase in the $|d_{33}|$ value is observed in the composite samples (figure 4.9b, inset) but no variation is detected in the pristine polymer samples revealing the ME character of the MF microspheres (figure 4.9b).

Since magnetostrictive CFO induces displacements at the interface between nanoparticles and polymer [51], with increasing interface value, a better coupling [25] and interaction between the piezoelectric P(VDF) and the magnetostrictive CFO ferrites will be promoted, explaining the larger increase of the $\Delta|d_{33}|$ with increasing nanoparticle content until ≈20 wt.%. Such interaction will be hindered for higher CFO concentrations, due to the decrease of the previously shown interface area (figure 4.8b), leading to a lower ME coupling and a decrease in the $|d_{33}|$ variation value.

4.5. Conclusions

The structural, magnetic and piezoelectric properties of low temperature processed nanofiber composites of CFO and P(VDF) were reported. Magnetic field induced changes in the piezoelectric response of the nanofibers demonstrated the ME character of these 0-1 composites, which may be useful for the development of micro and nanoscale ME devices. The average diameter of the electrospun composite fibers is ≈325 nm, independently of nanoparticle content, and the amount of crystalline polar β-phase is strongly enhanced when compared to pure P(VDF) polymer nanofibers. The piezoelectric response of these electroactive nanofibers is modified by an applied magnetic field, thus evidencing the ME character of the CFO/P(VDF) composites.

ME CFO/P(VDF) microspheres have been prepared by an electrospray process. The concentrations of CFO nanoparticles in the microspheres reaches values up to 0-27 wt.%, though their concentration in solution reaches values up to 70 wt.%. Microspheres diameters are between 3 and 7 μm, being the size nearly independent of the CFO filler content.

The addition of CFO nanoparticles into the polymeric microspheres has almost no effect on the β-phase content (≈60 %), crystallinity (40 %) and the onset degradation temperature (460-465 °C) of the polymer matrix.

The interface between CFO nanoparticles and P(VDF) was found to have a strong influence on the ME response of the CFO/P(VDF) microspheres. Increased interface values (from 0 to 55 %) had as result and optimized ME response ($\Delta|d_{33}|$ from 0 to 5 $pC.N^{-1}$) when a 220 mT DC magnetic field was applied to the CFO/P(VDF) microspheres with 21 wt.% of ferrite. Thus, the overall properties of the ME microspheres, the simplicity and scalability of the processing method indicates a large potential of the CFO/P(VDF) multifunctional microspheres for the development of advanced applications.

4.6. References

1. Zhang, J.X., et al., *The effect of magnetic nanoparticles on the morphology, ferroelectric, and magnetoelectric behaviors of CFO/P(VDF-TrFE) 0–3 nanocomposites.* Journal of Applied Physics, 2009. **105**(5): p. 054102.
2. Martins, P., C. Costa, and S. Lanceros-Mendez, *Nucleation of electroactive β-phase poly(vinilidene fluoride) with CoFe2O4and NiFe2O4 nanofillers: a new method for the preparation of multiferroic nanocomposites.* Applied Physics A: Materials Science & Processing, 2011. **103**(1): p. 233-237.
3. Martins, P., et al., *Linear anhysteretic direct magnetoelectric effect in Ni 0.5 Zn 0.5 Fe 2 O 4 /poly(vinylidene fluoride-trifluoroethylene) 0-3 nanocomposites.* Journal of Physics D: Applied Physics, 2011. **44**(48): p. 482001.
4. Martins, P. and S. Lanceros-Méndez, *Polymer-Based Magnetoelectric Materials.* Advanced Functional Materials, 2013. **23**(27): p. 3371-3385.
5. Martins, P., et al., *Correlation between Crystallization Kinetics and Electroactive Polymer Phase Nucleation in Ferrite/Poly(vinylidene fluoride) Magnetoelectric Nanocomposites.* The Journal of Physical Chemistry B, 2012. **116**(2): p. 794-801.
6. Otaigbe, J.U., et al., *Generation, Characterization, and Modeling of Polymer Micro- and Nano-Particles*, in *Polymer Physics and Engineering*. 2001, Springer Berlin Heidelberg: Berlin, Heidelberg. p. 1-86.
7. Yue, K., et al., *Magneto-Electric Nano-Particles for Non-Invasive Brain Stimulation.* PLoS ONE, 2012. **7**(9): p. e44040.
8. Luo, C.J., et al., *Preparation of polymeric nanoparticles by novel electrospray nanoprecipitation.* Polymer International, 2015. **64**(2): p. 183-187.
9. Cao, Y., et al., *Polymer-controlled core-shell nanoparticles: a novel strategy for sequential drug release.* RSC Advances, 2014. **4**(57): p. 30430-30439.
10. Kang, H.B., et al., *(Na,K)NbO3 nanoparticle-embedded piezoelectric nanofiber composites for flexible nanogenerators.* Composites Science and Technology, 2015. **111**: p. 1-8.
11. Banerjee, S., D. Konwar, and A. Kumar, *Polyaniline nanofiber reinforced nanocomposite based highly sensitive piezoelectric sensors for selective*

detection of hydrochloric acid: Analysis of response mechanism. Sensors and Actuators B: Chemical, 2014. **190**: p. 199-207.

12. Baji, A., et al., *Electrospun barium titanate/cobalt ferrite composite fibers with improved magnetoelectric performance.* RSC Advances, 2014. **4**(98): p. 55217-55223.
13. Yanhuai, D., et al., *Preparation of PVdF-based electrospun membranes and their application as separators.* Science and Technology of Advanced Materials, 2008. **9**(1): p. 015005.
14. Zaccaria, M., et al., *Effect of oxide nanoparticles on thermal and mechanical properties of electrospun separators for lithium-ion batteries.* J. Nanomaterials, 2012. **2012**: p. 119-119.
15. Ribeiro, C., et al., *Influence of Processing Conditions on Polymorphism and Nanofiber Morphology of Electroactive Poly(vinylidene fluoride) Electrospun Membranes.* Soft Materials, 2010. **8**(3): p. 274-287.
16. Martins, P., A.C. Lopes, and S. Lanceros-Mendez, *Electroactive phases of poly(vinylidene fluoride): Determination, processing and applications.* Progress in Polymer Science, 2014. **39**(4): p. 683-706.
17. Correia, D.M., et al., *Electrosprayed poly(vinylidene fluoride) microparticles for tissue engineering applications.* RSC Advances, 2014. **4**(62): p. 33013-33021.
18. Sun, L.L., et al., *Achieving very high fraction of β-crystal PVDF and PVDF/CNF composites and their effect on AC conductivity and microstructure through a stretching process.* European Polymer Journal, 2010. **46**(11): p. 2112-2119.
19. Gonçalves, R., et al., *Nucleation of the electroactive β-phase, dielectric and magnetic response of poly(vinylidene fluoride) composites with Fe2O3 nanoparticles.* Journal of Non-Crystalline Solids, 2013. **361**: p. 93-99.
20. Miao, H., et al., *Magnetic-field-induced ferroelectric polarization reversal in magnetoelectric composites revealed by piezoresponse force microscopy.* Nanoscale, 2014. **6**(15): p. 8515-8520.
21. Caruntu, G., et al., *Probing the local strain-mediated magnetoelectric coupling in multiferroic nanocomposites by magnetic field-assisted piezoresponse force microscopy.* Nanoscale, 2012. **4**(10): p. 3218-3227.

22. Martins, P., et al., *Large linear anhysteretic magnetoelectric voltage coefficients in CoFe2O4/polyvinylidene fluoride 0–3 nanocomposites.* Journal of Nanoparticle Research, 2013. **15**(8): p. 1-6.
23. Xie, S., et al., *Multiferroic CoFe2O4-Pb(Zr0.52Ti0.48)O3 core-shell nanofibers and their magnetoelectric coupling.* Nanoscale, 2011. **3**(8): p. 3152-3158.
24. Nair, M., et al., *Externally controlled on-demand release of anti-HIV drug using magneto-electric nanoparticles as carriers.* Nat Commun, 2013. **4**: p. 1707.
25. Martins, P., et al., *On the origin of the electroactive poly(vinylidene fluoride) [small beta]-phase nucleation by ferrite nanoparticles via surface electrostatic interactions.* CrystEngComm, 2012. **14**(8): p. 2807-2811.
26. Bean, C.P., *Hysteresis Loops of Mixtures of Ferromagnetic Micropowders.* Journal of Applied Physics, 1955. **26**(11): p. 1381-1383.
27. Chinnasamy, C.N., et al., *Unusually high coercivity and critical single-domain size of nearly monodispersed CoFe2O4 nanoparticles.* Applied Physics Letters, 2003. **83**(14): p. 2862-2864.
28. Dickens, B., et al., *Hysteresis measurements of remanent polarization and coercive field in polymers.* Journal of Applied Physics, 1992. **72**(9): p. 4258-4264.
29. Baji, A., et al., *Electrospinning induced ferroelectricity in poly(vinylidene fluoride) fibers.* Nanoscale, 2011. **3**(8): p. 3068-3071.
30. Sabolsky, E.M., S. Trolier-McKinstry, and G.L. Messing, *Dielectric and piezoelectric properties of 〈001〉 fiber-textured 0.675Pb(Mg1/3Nb2/3)O3–0.325PbTiO3 ceramics.* Journal of Applied Physics, 2003. **93**(7): p. 4072-4080.
31. Jungk, T., Á. Hoffmann, and E. Soergel, *Influence of the inhomogeneous field at the tip on quantitative piezoresponse force microscopy.* Applied Physics A, 2007. **86**(3): p. 353-355.
32. Jungk, T., Á. Hoffmann, and E. Soergel, *Challenges for the determination of piezoelectric constants with piezoresponse force microscopy.* Applied Physics Letters, 2007. **91**(25): p. 253511.
33. Lee, Y.-H., et al., *Release profile characteristics of biodegradable-polymer-coated drug particles fabricated by dual-capillary electrospray.* Journal of Controlled Release, 2010. **145**(1): p. 58-65.

34. Konermann, L., R.G. McAllister, and H. Metwally, *Molecular Dynamics Simulations of the Electrospray Process: Formation of NaCl Clusters via the Charged Residue Mechanism.* The Journal of Physical Chemistry B, 2014. **118**(41): p. 12025-12033.

35. Lin, W., et al., *Two-Dimensional Magnetic Field Vector Sensor Based on Tilted Fiber Bragg Grating and <newline/>Magnetic Fluid.* Journal of Lightwave Technology, 2013. **31**(15): p. 2599-2605.

36. Valan, M.F., A. Manikandan, and S.A. Antony, *Microwave Combustion Synthesis and Characterization Studies of Magnetic Zn1–x Cd x Fe2O4 (0 ≤ x ≤ 0.5) Nanoparticles.* Journal of Nanoscience and Nanotechnology, 2015. **15**(6): p. 4543-4551.

37. Martins, P., et al., *Optimizing piezoelectric and magnetoelectric responses on CoFe 2 O 4 /P(VDF-TrFE) nanocomposites.* Journal of Physics D: Applied Physics, 2011. **44**(49): p. 495303.

38. Chen, X., et al., *Electrospun Magnetic Fibrillar Polystyrene Nanocomposites Reinforced with Nickel Nanoparticles.* Macromolecular Chemistry and Physics, 2010. **211**(16): p. 1775-1783.

39. Merlini, C., et al., *Electrically pressure sensitive poly(vinylidene fluoride)/polypyrrole electrospun mats.* RSC Advances, 2014. **4**(30): p. 15749-15758.

40. Belouadah, R., et al., *Phase switching phenomenon in magnetoelectric laminate polymer composites: Experiments and modeling.* Physica B: Condensed Matter, 2011. **406**(14): p. 2821-2826.

41. Botelho, G., et al., *Relationship between processing conditions, defects and thermal degradation of poly(vinylidene fluoride) in the β-phase.* Journal of Non-Crystalline Solids, 2008. **354**(1): p. 72-78.

42. Fang, L., et al., *Hydrangea-like zinc oxide superstructures for ferroelectric polymer composites with high thermal conductivity and high dielectric constant.* Composites Science and Technology, 2015. **107**: p. 67-74.

43. Zulfiqar, S., M. Rizvi, and A. Munir, *Thermal degradation of phenyl modified fluorocarbon polymers.* Polymer Degradation and Stability, 1994. **46**(1): p. 19-23.

44. Silva, M.P., et al., *α- and γ-PVDF: Crystallization kinetics, microstructural variations and thermal behaviour.* Materials Chemistry and Physics, 2010. **122**(1): p. 87-92.

45. O'Shea, M.L., C. Morterra, and M.J.D. Low, *Spectroscopic studies of carbons. XVII. Pyrolysis of polyvinylidene fluoride.* Materials Chemistry and Physics, 1990. **26**(2): p. 193-209.

46. Mitsuda, K., H. Kimura, and T. Murahashi, *Evaporation and decomposition of Triton X-100 under various gases and temperatures.* Journal of Materials Science, 1989. **24**(2): p. 413-419.

47. Martins, P., et al., *Interface characterization and thermal degradation of ferrite/poly(vinylidene fluoride) multiferroic nanocomposites.* Journal of Materials Science, 2013. **48**(6): p. 2681-2689.

48. Vopsaroiu, M., et al., *Experimental determination of the magnetoelectric coupling coefficient via piezoelectric measurements.* Measurement Science and Technology, 2008. **19**(4): p. 045106.

49. Xie, S.-H., Y.-Y. Liu, and J.-Y. Li, *Synthesis, microstructures, and magnetoelectric couplings of electrospun multiferroic nanofibers.* Frontiers of Physics, 2011. **7**(4): p. 399-407.

50. Liu, X., et al., *Magnetoelectricity in CoFe2O4 nanocrystal-P(VDF-HFP) thin films.* Nanoscale Research Letters, 2013. **8**(1): p. 1-10.

51. Rondinelli, J.M., M. Stengel, and N.A. Spaldin, *Carrier-mediated magnetoelectricity in complex oxide heterostructures.* Nat Nano, 2008. **3**(1): p. 46-50.

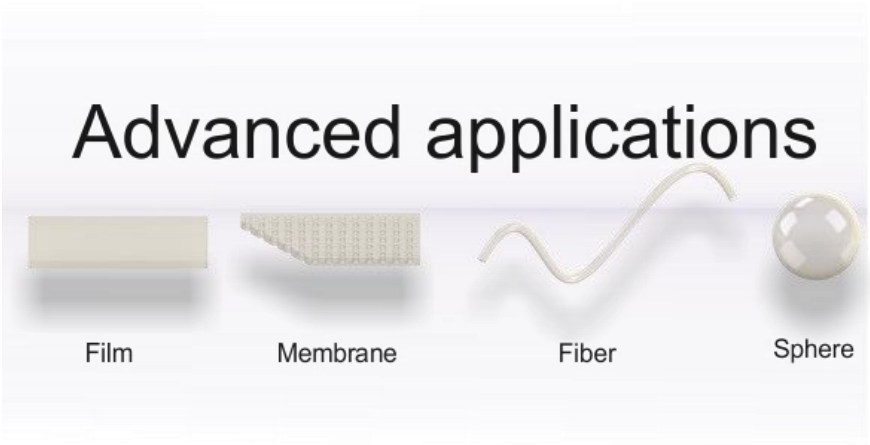

Chapter 5

Conclusions and future work

In this chapter, the main conclusions of the thesis are summarized and some suggestions for future works are provided.

5.1. Conclusions

Polymer-based ME composites proved to be suitable for different applications areas such as sensors, communication, electronics, magnetic recording, microwave absorption-based devices, electrical and automobile industries, as well as for biotechnology and biomedical applications. Different morphologies as film, membrane, fiber and sphere demonstrate to be suitable for the applications mentioned above. The ability to tailor the morphologies and physical-chemical properties of polymer-based ME composites are also critical to understand the ME effect in order to suitably tailor ME response for specific application demands.

In this thesis the possibility of obtaining piezoelectric P(VDF) and/or P(VDF-TrFE) morphologies from film to spheres was demonstrated. Films of both P(VDF) and P(VDF-TrFE) polymers were produced in order to evaluate the effect of filler dispersion on the piezoelectric and ME response, the effect of filler size on the magnetostriction, polymer phase nucleation and ME response of polymer composites. The development of anisotropic ME polymer composites was also studied.

Magnetoelectric films

CFO magnetostrictive filler dispersion methods (surfactation and ultrasound bath) were used to demonstrate that there are no differences in the piezoelectric, magnetic and ME response of the P(VDF-TrFE) nanocomposites when different dispersion levels are achieved. A maximum ME coefficient of 40 $mV.cm^{-1}.Oe^{-1}$ was obtained for samples with 72 wt.% of CFO under a DC magnetic field of 0.25 T. A key parameter in the ME composite preparation was found to be the filler content, more than filler distribution, this fact being of special interest for large industrial scale processing, in which the upscaled feasibility for fabrication of smart structures is one of the main tasks.

Concerning the study of the influence of filler size on the magnetostriction of the fillers and the ME response of P(VDF-TrFE) composites, different Fe_3O_4 sizes were used. The P(VDF-TrFE) was used in order to ensure the total β-phase formation. Fe_3O_4 nanoparticles with three different sizes were synthesized by solvothermal procedures and oxidative hydrolysis methods. The first method lead to nanoparticles with 9 nm

average size and 167 ppm magnetostriction; the second one to nanoparticles with average size of 30 and 50 nm with magnetostriction of 17 and 26 ppm, respectively. Further, Fe_3O_4/P(VDF-TrFE) MF nanocomposites were produced with those nanoparticles, showing ME voltages coefficients (α_{31}) of 920, 100 and 150 $\mu V.cm^{-1}.Oe^{-1}$, for samples fabricated with nanoparticles with 9, 30 and 50 nm average size, respectively. The highest magnetostriction and the ME response is obtained for the nanocomposite with 9 nm nanoparticles. In this material is possible to tailor and optimize the magnetostriction and ME response at the nanoscale, with large potential application in areas of biomedicine, sensors and actuators.

Fe_3O_4 NRs were also synthetized. The effects of surface charge and filler structure on the crystallization behavior of P(VDF) were systematically studied by using two types of nanostructures, Fe_3O_4 NRs and spherical nanoparticles of different sizes. Different Fe_3O_4/P(VDF) composites exhibited distinct β-phase values. Fe_3O_4 nanoparticles with different sizes and distinct zeta potential values failed to induce high fraction values of β-phase within the composites. In contrast, Fe_3O_4 rods with a zeta potential of 30 mV, nucleated ≈70 % of β-P(VDF) within the nanocomposites. The effect of the anisotropy was evaluated with δ-FeO(OH)/P(VDF-TrFE) and CoFeO(OH)/P(VDF-TrFE) ME composites by a simple low-temperature processing method. The nanosheets fillers were introduced in different filler contents and alignment states. The obtained ME voltage coefficient, with a maximum of ≈0.4 $mV.cm^{-1}.Oe^{-1}$, depends on filler content and alignment state, as well as, on both incident magnetic field direction and intensity. Further, a new ME effect is proposed based on the magnetic rotation of the δ-FeO(OH) nanosheets inside the piezoelectric P(VDF-TrFE) polymer matrix that is suitable to be used as magnetic field sensor for advanced applications. New CoFeO(OH) with high magnetostrictive of 507 ppm and anisotropic (nanosheet) nanostructures were synthesized. Flexible CoFeO(OH)/P(VDF-TrFE) composites reveal an interfacial ME coupling strongly dependent on the angle between H_{DC} and CoFeO(OH) length direction. Such composite shows a maximum α_{31} of 5.10 $mV.cm^{-1}.Oe^{-1}$. Anisotropic ME magnetic sensing capability and good linearity value of 0.995 allows the use of CoFeO(OH)/P(VDF-TrFE) composites in polymer-based magnetic sensor devices, actuators and in the biomedical field.

Magnetoelectric membranes

CFO/P(VDF-TrFE) ME membranes were fabricated and characterized. The composites simultaneously respond to external stimuli, such as mechanical, magnetic or electrical signals, showing a piezoelectric response with an effective d_{33} coefficient of -22 $pC.N^{-1}$, a maximum magnetization of 12 $emu.g^{-1}$ and a maximum ME coefficient of 9 $mV.cm^{-1}.Oe^{-1}$.

Magnetoelectric nanofibers and microspheres

Fiber and spherical ME morphologies were studied. In both, structural, magnetic and piezoelectric properties of low temperature processed composites of CFO and P(VDF) were evaluated. The concentrations of CFO nanoparticles in the fibers reached values up to 0-20 wt.%. The CFO/P(VDF) nanofibers show a strong enhancement in the volume fraction of electroactive β-phase when compared to pristine P(VDF) electrospun nanofibers. The magnetization of the nanofibers increases with increasing CFO content reaching to a maximum of 11.5 $emu.g^{-1}$. Magnetic field induced changes in the piezoelectric response of the nanofibers demonstrated the ME character. The concentrations of CFO nanoparticles in the microspheres reaches values up to 0-27 wt.%, though their concentration in solution reached values up to 70 wt.%. The interface between CFO nanoparticles and P(VDF) was found to have a strong influence on the ME response of the CFO/P(VDF) microspheres (3-7 μm average diameter). With the increasing of CFO content, the interface increase from 0 to 55 %. CFO/P(VDF) microspheres ME character was proved once the piezoelectric response differs from 0 to 5 $pC.N^{-1}$ (in case of sample with 21 wt.%), when a 220 mT DC magnetic field was applied.

5.2. Future Work

In the present thesis, it was shown that different polymer-based ME composite morphologies can be achieved and that they could be applied in different applications. In this sense, some interesting studies should be carried out in the future:

- Explore the potential of the different polymer-based ME composites in specific applications, taking advantage of the specificity of the morphological features of the composites;
- Expand the multifunctionality of the composites by using more than one magnetostrictive filler in composite to achieved a composite that react to different magnetic fields;
- Prepare ME composites from biodegradable piezoelectric polymers for biomedical applications;
- Expand the preparation of the composites by addressing novel magnetostrictive geometries, such as magnetostrictive micro and nanowires.